Optimal Geometric Configuration of a Cross Bore in High Pressure Vessels

A thesis submitted in fulfilment of the requirements for the degree Doctorate Technologiae: Mechanical Engineering

in the Faculty of Engineering and Technology

Nziu, P.K.

211128910

Vaal University of Technology

Promoter: Prof. L.M. Masu

April 2018

DECLARATION

I Mr. Patrick Kiola Nziu, declare that this thesis is my original work and that it has not been presented to any other university or institution for similar or any other degree award.

………………………………….. 01/04/2018

Signature Date

ACKNOWLEDGEMENTS

Since the time I commenced working on this project to this final manuscript, I have continuously sought advice, suggestions, data and financial support from numerous sources. For this, I am greatly indebted to a number of people for the success of this project.

First of all I express my thanks and gratitude to God, for giving me the strength and sanity to finish this project report.

My greatest debts are to my family for their encouragement, materials and financial support. I also give thanks to my colleagues for their contribution. Special thanks go to my promoter Prof LM Masu for his brilliant suggestions, guidance and constructive criticism without which the project objectives could not have been achieved.

Lastly the author pays gratitude to Vaal University of Technology for their support during this research.

DEDICATION

To my family, friends and relatives.

ABSTRACT

The purpose of this study was to develop analytical and numerical solutions to be used in the design of thick walled high pressure vessels for optimal location of a cross bore. In addition, the effects of internally applied combined thermo-mechanical loading on Stress Concentration Factor (SCF) on these vessels, was also evaluated.

An analytical solution, to predict principal stresses on radial circular cross bore, was developed. The developed analytical solution was verified using finite element analysis methods. An optimisation process, using finite element analysis, was further done to determine the optimal combination of the major cross bore geometry that affect stress concentration. The cross bore geometries that were studied included the size, shape, location, obliquity and thickness ratio. The geometrically optimised cross bore was then subjected to combined thermo-mechanical loading to determine the resulting stress concentration effects.

A total of 169 finite element part models were created and analysed. Seven thick walled cylinders having either circular or elliptical shaped cross bore positioned at radial, offset or and inclined were investigated.

The analytical solution developed correctly predicted all the radial stresses at the intersection of the cross bore and main bore. However, out of 35 studied models, this analytical solution predicted the magnitude of hoop stresses in 9 models and that of axial stresses in 15 models correctly. The lowest SCF given by the radial circular cross bore was 2.84. Whereas, the SCF

due to offsetting of the same cross bore size reduced to 2.31. Radial elliptical shaped cross bore gave the overall lowest SCF at 1.73. In contrast, offsetting of the same elliptical shaped cross bore resulted in tremendous increase in SCF magnitude exceeding 1.971. Additionally, the magnitudes of SCF were observed to increase whenever the circular offset cross bores were inclined along the RZ axis of the cylinder.

The hoop stress due to internally applied combined thermo-mechanical loading increased gradually with increase in temperature until it reached a maximum value after which it began to fall sharply. In contrast, the corresponding SCF reduced gradually with increase in temperature until it reached a uniform steady state. After which, any further increase in temperature had insignificant change in stress concentration factor. The optimal SCF magnitude due to combined thermo-mechanical loading was 1.43. This SCF magnitude was slightly lower than that due to the pressure load acting alone.

TABLE OF CONTENTS

LIST OF FIGURES

LIST OF TABLES

NOMENCLATURE

a, a_1	Radius of the circular hole
d	Hole or nozzle diameter
σ	The far field uniaxial tension
w	Width of the plate
a	Major axis of the ellipse
b	Minor axis of the ellipse
a_2	Auxiliary hole radius
δ	Optimum centre distance
R_1	Inside radius of the pipe
R_2	Outside radius of the pipe
α, γ	Intensification factors.
D, b	Run pipe outer diameter or vessel
t	Branch pipe or nozzle thickness
r	Vessel mean radius
C	Ratio of major and minor axis of the ellipse (Ellipticity)
α, A	Coefficient of thermal expansion

$T, \Delta t$	Change in temperature
ν , μ	Poisson's ratio
E	Young's modulus of elasticity
ε_θ	Hoop strain
ε_r	Radial strain
ε_z	Axial strain
p_i	Internal pressure.
$\sigma_{\theta_{1,}} \sigma_h$	Hoop stress generated by the pressurised main bore.
σ_{r_1}	Radial stress generated by the pressurised main bore.
σ_z	Longitudinal stress at the surface of the cross bore
$d\theta$	Angle subtended by the small element.
θ	Angle between the vertical axis and the small element.
K	Cylinder thickness ratio
R_i	Internal radius of the main bore.
R_O	External radius of the main bore.
$r_{i,}$ R_C	Cross bore radius.
R	Radius at any point along the wall thickness.

ABBREVIATIONS

SCF	Stress Concentration Factor
TSCF	Thermal Stress Concentration Factor
DSCF	Dynamic Stress Concentration Factor
FEA	Finite Element Analysis
BIE	Boundary Integral Element
LP	Linear Programming

CHAPTER ONE: INTRODUCTION

1.1 BACKGROUND OF THE STUDY

High pressure vessels are air tight containers (Nabhani *et al*., 2012), mostly cylindrical, conical, ellipsoidal or spherically shaped (Hyder and Asif, 2008), that are used to store large amounts of energy (Kihiu and Masu, 1995). They are termed as thick walled when their ratio of thickness and internal radius exceeds $^{1}/_{20}$ (Nabhani *et al*., 2012). The basic pressure vessel design takes into account the vessel failure modes, induced stresses, selection of materials, the surrounding environment and stress concentration (Hyder and Asif, 2008). Pressure vessels are used for various applications in thermal and nuclear power plants, process and chemical industry, space, ocean depth and fluid supply in industries, etc. (Kharat and Kulkarni, 2013; Jeyakumar and Christopher, 2013).

Pressure vessels are usually loaded with working fluid at high pressures and temperatures commonly referred to as thermo-mechanical loading (Nayebi and Sadrabadi, 2013). This loading induces dynamic and thermal stresses on the cylinder wall due to the variation in pressure and temperature, respectively (Choi *et al.,* 2012). However, due to the discontinuities in the cylinder, the stress distribution along the cylinder wall is not uniform. These discontinuities which include geometric, loads and metallurgical factors, etc., create regions of high stresses that are referred to as stress concentrations. The stress concentrations, due to dynamic and thermal stresses, are calculated using dimensionless factors called the Dynamic Stress Concentration Factor (DSCF) and the Thermal Stress Concentration Factor (TSCF), respectively (Babu *et al.*, 2010). High values of these stress concentration factors are some of the sources of pressure vessel failures (Nabhani *et al*., 2012) or reduced operating life (Choi *et* *al.*, 2012). Failures of pressure vessels are usually catastrophic and may lead to loss of life, damage of property or pose a health hazard (Masu, 1997; Kharat and Kulkarni, 2013). However, these catastrophic failures can be avoided when the design and manufacture of pressure vessels is done in accordance with standard pressure vessel design codes (Kihiu and Masu, 1995). Nevertheless, these codes only give sets of wall thickness and their corresponding hoop stresses that are below the allowable working stresses without any detailed stress analysis (Kihiu *et al.*, 2004). This practice has led to the use of high safety factors in pressure vessel design ranging from 2 to 20 (Masu, 1997). This phenomenon results in uneconomical use of material which translates into high manufacturing cost of pressure vessels. Other processes such as autofrettage (a metal fabrication technique in which a pressure vessel is subjected to enormous pressure, causing internal portions of the part to yield plastically, resulting in internal compressive residual stresses once the pressure is released) and shakedown (Li *et al*, 2010) are also performed at the manufacturing stage of pressure vessels to increase their strength (Kihiu *et al.*, 2004). However, it is likely that a more detailed stress analysis will obviate the need for autofrettage, with the accompanying reduction in the manufacturing cost.

In practice, holes or openings are drilled in the wall of plain pressure vessels (Masu, 1998). A single hole in one side of the vessel is known as a side hole. Whereas two transverse holes in both sides of the vessel are known as cross holes or cross bores (Peters, 2003; Makulsawatudom *et al.*, 2004). Cross bores are referred to as radial when they are drilled at the centre axis of the vessel. On the other hand, cross bores are referred to as offset when drilled at any other chord away from the vessel centre axis (Makulsawatudom *et al.*, 2004). Cross bores are of different sizes and shapes. The size ranges from small drain nozzles to large handhole and manholes such as tee junctions (Kharat and Kulkarni, 2013). The most common cross bore shapes are circular and elliptical in shape (Nagpal *et al.*, 2012). These cross bores give provision for fitting relief and safety valves, bursting discs, gas inlets, flow circuit meters, temperature and internal pressure measurement, inspection covers, lubrication, etc. (Kihiu and Masu, 1995). As a result, cross bores are inevitable in pressure vessels design (Kihiu and Masu, 1995).

These openings in the pressure vessels introduce geometric discontinuities that alter the uniform stress distribution in the cylinder walls (Kharat and Kulkarni, 2013). The geometric discontinuities act as stress raisers, thus creating regions of high stress concentration especially near the openings (Masu and Craggs, 1992). Due to these high stress regions, the elemental stress equations in thick walled vessels cease to apply (Kharat and Kulkarni, 2013).

The stress concentration in cross bored high pressure vessels is dependent on the cross bore geometry. The major parameters of the cross bore geometry include the cross bore size, shape, location, obliquity angle and the thickness ratio. However, the optimal combination of these cross bore geometries that give minimum stress concentration factors have not been fully established.

Therefore, this study developed optimal solutions for a cross bore in thick walled high pressure vessels using analytical and numerical methods in respect of radial circular cross bores. Furthermore, it established an optimal geometry of the cross bore that gives a minimum stress concentration factor. In addition, the study evaluated the effects of combined thermo-mechanical loading on stress concentration in high pressure vessels with cross bores.

1.2 Purpose of the study

The purpose of this study was to develop analytical and numerical solutions to be used in the design of thick walled high pressure vessels for optimal location of a cross bore. In addition, the effects of combined thermo-mechanical loading on SCF on these vessels was also evaluated.

1.3 The significance of study

High pressure vessels are some of the essential accessories in industry. They are used for storage, industrial processing and generation of power under high pressures and temperatures (Kihiu and Masu, 1995). Research studies on stresses in high pressure vessels with a view of optimising SCF may provide the much needed information that is required in the design of pressure vessels. This may lead to safer working environments, improved availability of equipment, economic use of materials, lower operating costs and reduction in losses due to catastrophic or disruptive failures (Kihiu *et al*., 2004).

1.4 Problem statement

The majority of industrial processes use various types of high pressure vessels such as boilers, air receivers, heat exchangers, tanks, towers, condensers, reactors, etc., in their operation. Failure of high pressure vessels do occur, being the source of approximately 24.4% of the total industrial accidents in industrial processes (Nabhani *et al*., 2012). These failures have resulted in loss of human life, damage of property, environmental pollution and in some instances led to emergency evacuation of residents living in the surrounding areas (Nabhani *et al*., 2012). Failure of these vessels are caused by induced stresses in the walls of cylinders resulting from varying operating pressures and temperatures. The induced stresses lead to formation of stress related failures in the material such as fatigue, creep, embrittlement and stress corrosion cracking (Nabhani *et al.,* 2012).

To prevent pressure-vessel failures, pressure vessel designers have started to use pressure vessel design codes (Kharat and Kulkarni, 2013). In order to reduce industrial process accidents and hence the loss of human life, damage of property as well as possible environmental pollution, high pressure vessel design should be appropriately done. This can be achieved if a thorough understanding of the stress concentration situations in the pressure vessels can be obtained and optimised. Hence, the need for the present study.

1.5 Objectives

The main objective of this study was to determine the optimal location of a cross bore in thick walled high pressure vessels. In addition, the effects of thermo-mechanical loading on stress concentration factors in high pressure vessels with cross bore were also studied.

The research work entailed the development of optimal solutions of cross bores in thick walled high pressure vessels using analytical and numerical methods in respect of radial circular cross bores. Furthermore, establishing an optimal geometry of a cross bore in thick walled high pressure vessels that gives minimum stress concentration factor. In addition, the study evaluated the effects of combined thermo-mechanical loading on stress concentration in high pressure vessels with cross bores.

CHAPTER TWO: LITERATURE REVIEW

2.1 LITERATURE SURVEY

Stress Concentrations Factor (SCF), also referred to as the Effective Stress Factor (ESF) (Moffat *et al.*, 1991), is determined using the relationship given in Equation (2.1) as detailed by Masu and Craggs (1992) and Kharat and Kulkari (2013);

$$\mathrm{SCF} = \frac{\text{Maximum hoop stress at cross bore}}{\text{Hoop stress at bore of cylinder without cross bore}} \tag{2.1}$$

According to Cole *et al*. (1976), high values of SCF act as points of weakness leading to reduction in the vessel strength as well as its fatigue life. This consequently may reduce the pressure carrying capacity of the pressure vessel by up to 60 % (Masu, 1989) when compared to a plain vessel without cross bores. These findings justify the need for pressure vessel designers to ensure minimum SCF due to cross bore. For instance, in the design and manufacture of components such as shafts, valves seats, forging, etc., blending geometry technology has been extensively used to reduce the SCF (Masu and Craggs, 1992).

Research studies with a view to reducing SCF across the cross bore have been carried out. The following is a general overview of the studies conducted on stress analysis. Mackerle (1996) comprehensively reviewed 632 published journal articles between 1976 and 1996 on "linear and nonlinear, static and dynamic, stress and deflection analyses", but only 9% of the published articles were on stress analysis. Mackerle (1999; 2002; 2005) repeated the same study and published three more articles covering the periods from 1996 to 1998, 1998 to 2001 and 2001 to 2004. In each period mentioned earlier, the number of articles reviewed on the same study was given as 173, 140 and 128, respectively. However, the studies on stress analysis were found to be 15%, 11% and 6%, respectively.

More recently, Kharat and Kulkarni (2013) reviewed 41 published journal articles on stress concentration. Of these, only 27% were on SCF around cross bore openings. 76% of the articles reviewed in this study were on thick walled pressure vessels. Interestingly, the study recommended the need for more research in stress concentration on thin walled cylinders. This recommendation contradicted another study conducted by Diamantoudis and Kermanidis (2005) which concluded that most industrial applications use thick walled high pressure vessels. They argued that, the use of pressure vessel design codes during the manufacture of high pressure vessels advocates for large safety factors, hence the increase in material thickness. In this regard, most of the industrial applications use thick walled cylinders, hence more research ought to be done on them.

The total stress concentration induced in the cylinder wall is due to SCF, TSCF and the DSCF. The SCF depends on the choice of the pressure vessels geometric design parameters. These design parameters include cross bore position, shape, size, angle of inclination and thickness ratio. Numerous studies on the effects of geometric design parameters on SCF in high pressure vessels have been conducted. Nevertheless, there has been less investigation on optimisation of the geometric design parameters (Kharat and Kulkarni, 2013). Studies on optimisation of the TSCF and the DSCF in the high pressure vessels have not been adequately covered, despite this being a common phenomenon in the industry (Kihiu, 2002). Therefore, this literature review focuses on the effects of geometric design parameters and thermo-mechanical loading on stress concentration in high pressure vessels, with a view to investigate the optimum conditions.

2.2 MEASUREMENT OF STRESS DISTRIBUTION

Several techniques namely, experimental, analytical and numerical (also known as computational), are used to conduct the analysis of stress distribution in high pressure vessels. Experimental techniques use various methods such as photo-elasticity, grid, brittle coating, moiré, strain gauge measurements, among others to obtain experimental solutions. In experimental techniques, prototype specimens are mainly used for experimental testing. However, the use of prototype specimens instead of models, together with equipment and labour costs make the experimental techniques more expensive than the other methods (Masu, 1994).

Theories of elasticity, elastoplastic or plasticity are used in analytical methods (Zhang *et al.*, 2012) to analyse stresses of certain simple geometrical shapes. The accuracy of the arising solutions depends on the assumptions of the theory and the boundary conditions used. The solutions obtained from these methods are referred to as exact or analytical or closed form solutions (Nagpal *et al.*, 2012). These closed form solutions are obtained using various mathematical methods (Dharmin *et al.*, 2012) such as complex function theory (Conformal mapping, Boundary collocation, Laurent series expansion, Complex variable approach, etc.) and integral transforms (Fourier, Laplace, Mellin, Hanckel, Eigen function expansion, etc.). Lately, computer software packages such as Matlab and Maple are used to solve the generated simultaneous equations by the analytical methods.

Lastly, numerical methods use packages such as Finite Element Analysis (FEA), Finite Difference, Finite Volume, Boundary Integral Element (BIE) and Mesh Free methods for stress analysis (Masu, 1989: Nagpal *et al.*, 2012). The solutions obtained by these numerical methods are referred to as approximate numerical solutions. Each of these methods is suitable for various applications. For instance, Mesh Free method is used to determine stress distribution in elements with discontinuous or moving boundaries. Whereas, the BIE method is used to determine the stress distribution at the surface of the element (Nagpal *et al.*, 2012).

Some of the FEA commercially based software packages commonly used in stress analysis are ANSYS, COSMOL, DYNA, ABAQUS, PAFEC 75, ADINA, NASTRAN and LUSAS (Nagpal *et al.*, 2012). Other common applications for these FEA software packages are tabulated in Table 1. The choice of a particular software package depends on the availability, the type of stress analysis to be performed, the element to be analysed and the required depth of accuracy, among other factors (Nagpal *et al*., 2012). However, some of the software packages' applications are common, as indicated in Table 1.

FEA numerical method has been more extensively used for stress analysis in the last decade than both experimental and analytical methods (Kharat and Kulkarni, 2013). This is due to its ability to perform simulation and give highly accurate results (Zhang *et al.*, 2012) that are comparable with those from its competitors (experimental and analytical methods). The results given by FEA are independent of the presence of any geometric parameters. The FEA method is also more convenient, faster, cheaper and easy to use (Kharat and Kulkarni, 2013). The speed and convenience of use with results of acceptable level of accuracy makes numerical methods more

Table 1. Applications of some of the common FEA software packages used in stress analysis (Nagpal et al., 2012; Fagan, 1992).

S/No.	Name of the software	General area of preferred applications	Capabilities
1.	ANSYS	Structural, electrical, civil and mechanical engineering.	Stress analysis, heat transfer, fluid flow and electro-magnetic.
2.	COSMOL	Nuclear, electrical, civil and electrical engineering.	Stress analysis, electromagnetic, heat transfer and fluid flow.
3.	DYNA	Automobile, aerospace, civil and biomedical engineering.	Impact, vibration, stress analysis and fluid flow.
4.	ABAQUS	Aerospace, automotive, electrical, hydraulic, mechanical, structural and biomedical engineering.	Stress analysis, buckling, vibration, impacts, heat transfer, fluid flow and electromagnetic.
5.	PAFEC 75	Structural, automotive and mechanical engineering.	Stress analysis, impact, vibration and buckling.
6.	ADINA	Electrical, mechanical and structural engineering.	Structural, heat transfer, fluids flow and electromagnetic.
7.	NASTRAN	Automotive, mechanical and structural engineering.	Vibration, impact and stress analysis.
8.	LUSAS	Aerospace, civil, mechanical and structural engineering.	Stress analysis, fluid flow, buckling and vibration.

preferable when compared to those obtained from experimental and analytical methods (Zhang et al, 2012). However, the accuracy of numerical solutions depends on correct usage of the type of element, mesh density, accurate modelling of the domain, material, loading and boundary conditions (Qadir and Redekop, 2009). Besides, in symmetrical structures, the FEA analysis is performed using only a quarter or an eighth of the entire cross section (Masu, 1991). This technique reduces both the computer memory required and the run time by up to 75% (Kihiu and Masu, 1995).

One of the aims of this study was to develop an analytical solution for determining stress concentration factors in thick walled pressure vessels with a cross bore. The verification of the analytical solution to be developed was to be done by numerical modelling using FEA Abaqus software.

2.3 STRESS CONCENTRATION ANALYTICAL ANALYSES

Various solutions for SCFs have been developed for flat plates with holes, as well as in high pressure vessels having radial, offset and inclined cross bores.

2.3.1 Solutions for SCFs in flat plates with holes

Solutions for SCFs of flat plates with holes under tension as shown in Figure 1, have been developed and are widely used in engineering and machine design. Nagpal *et al.* (2011) cited Kirsch's analytical solutions for radial σ_{rr}, hoop $\sigma_{\theta\theta}$, and shear $\tau_{r\theta}$ stresses for large thin flat plates with a small circular hole at the centre, under uniaxial tension applied at the far field as;

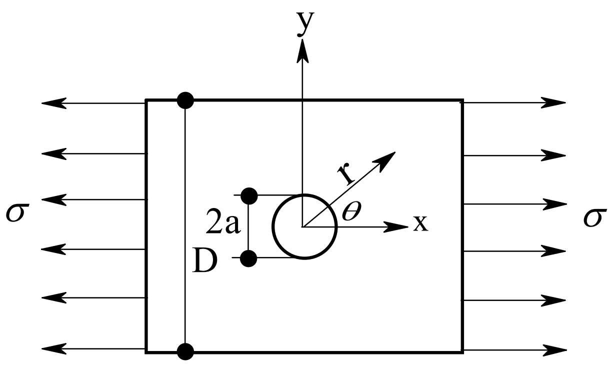

Figure 1. Flat thin plate with a central small circular holes under tension (Dharmin *et al.*, 2012)

$$\sigma_{rr} = \frac{\sigma}{2}\left(1-\frac{a^2}{r^2}\right)+\frac{\sigma}{2}\left(1-\frac{a^2}{r^2}\right)\left(1-\frac{3a^2}{r^2}\right)\cos 2\theta \tag{2.2}$$

$$\sigma_{\theta\theta} = \frac{\sigma}{2}\left(1+\frac{a^2}{r^2}\right)-\frac{\sigma}{2}\left(1+\frac{3a^4}{r^4}\right)\cos 2\theta \tag{2.3}$$

$$\tau_{r\theta} = -\frac{\sigma}{2}\left(1-\frac{a^2}{r^2}\right)-\frac{\sigma}{2}\left(1+\frac{3a^2}{r^2}\right)\sin 2\theta \tag{2.4}$$

Where

σ is the far field uniaxial tension

θ is the subtended angle measured clockwise from X –axis

a is the radius of the circular hole

Equations 2.2 to 2.4 are analytical equations for an infinitely small hole in a plate also referred to as the Kirsch's solutions. At an angle of 90^0 and at the radius of the hole, the SCF is 3. However, in the derivation of these equations 2.2 – 2.4, the ratio of the hole radius, a, and the plate width, b, was neglected ($\frac{a}{b} \sim 0$). Despite the assumption, these equations were found to give sufficiently accurate results when the ratio of $\frac{a}{b} < \frac{1}{10}$ (Ford and Alexander, 1977).

The solution for SCF for a flat plate with the same features as those discussed in the preceding paragraph was presented by Hyder and Asif (2008) using two equations. For $\frac{d}{w} \leq 0.65$ the solution was given as;

$$\mathrm{SCF} = 3.0039 - 3.753\frac{d}{w} + 7.9735\left(\frac{d}{w}\right)^2 - 9.2659\left(\frac{d}{w}\right)^3 + 1.8145\left(\frac{d}{w}\right)^4 + 2.9684\left(\frac{d}{w}\right)^5 \quad (2.5)$$

While, for $\frac{d}{w} > 0.65$ as;

$$\mathrm{SCF} = 2.0 + \left(1 - \frac{d}{w}\right)^3 \quad (2.6)$$

Where

d is the hole diameter

w is the width of the plate

However, the SCF solution curves generated by the two equations had a discontinuity at the point where the ratio of $\frac{d}{w} = 0.65$.

Nagpal *et al.,* (2012) reported that further studies by various researchers based on existing experimental and analytical data for flat plates with holes, led to the development of a single equation for calculating the solution of SCF. This eliminated the discontinuity posed by equations 2.5 and 2.6, earlier discussed. The solution of SCF for a flat plate with a circular cross bore was given as;

$$\mathrm{SCF} = 3.0 - 3.13\left(\frac{2r}{w}\right) + 3.66\left(\frac{2r}{w}\right)^2 - 1.53\left(\frac{2r}{w}\right)^3 \quad (2.7)$$

Where

2r is the hole diameter

w is the width of the plate

It can be seen from equations 2.5, 2.6 and 2.7 that, the SCF is a function of the hole diameter and the width of the plate.

Snowberger (2008) gave the solution for SCF of a flat plate with an elliptical hole as;

$$\mathrm{SCF} = \mathrm{C1} + \mathrm{C2}\left(\frac{2\mathrm{a}}{\mathrm{w}}\right) + \mathrm{C3}\left(\frac{2\mathrm{a}}{\mathrm{w}}\right)^2 + \mathrm{C4}\left(\frac{2\mathrm{a}}{\mathrm{w}}\right)^3 \qquad (2.8)$$

Where

$$C1 = 1.0 + 2\left(\frac{a}{b}\right)$$

$$C2 = -0.351 - 0.021\sqrt{\left(\frac{a}{b}\right)} - 2.483\left(\frac{a}{b}\right)$$

$$C3 = 3.621 - 5.183\sqrt{\left(\frac{a}{b}\right)} + 4.494\left(\frac{a}{b}\right)$$

$$C4 = -2.27 + 5.204\sqrt{\left(\frac{a}{b}\right)} - 4.011\left(\frac{a}{b}\right)$$

a is the major axis of the ellipse

b is the minor axis of the ellipse

w is the plate width

In addition, this study by Snowberger (2008) proved the validity of equation 2.8 from the known exact analytical solution of a circle, as the elliptical bore approached a circular shape.

Reviewed literature by Nagpal *et al.* (2012) indicated that the SCF in flat plates was affected by plate length, thickness, hole size, geometric dimensions of the discontinuities and the elastic constants. In another study by Makulsawatudom *et al.*, (2004), on a simple finite plate with hole under uniaxial loading, it was established that the SCF increases with increasing hole size. The study attributed this occurrence to the effects of through-thickness. However, there was no available information on an optimal solution for a flat plate with a hole.

2.3.2 Methods of reducing SCF in flat plates with holes

Small holes in both sides of the main hole commonly referred to as auxiliary holes, have been introduced in the design of flat plates with holes to reduce SCFs as shown in Figure 2. These auxiliary holes cause stress redistribution around the vicinity of the main hole. These hole arrangements create regions of smooth flow stress trajectories which in turn lead to reduced SCF.

Heywood (1952) studied various methods for the reduction of SCFs. The study reported a reduction of 16% in SCFs after the introduction of a single auxiliary hole in the main hole axis. Erickson and Riley (1978) carried out another study on minimisation of SCFs around circular holes. The optimum centre distance between the hole and the auxiliary hole was found to be

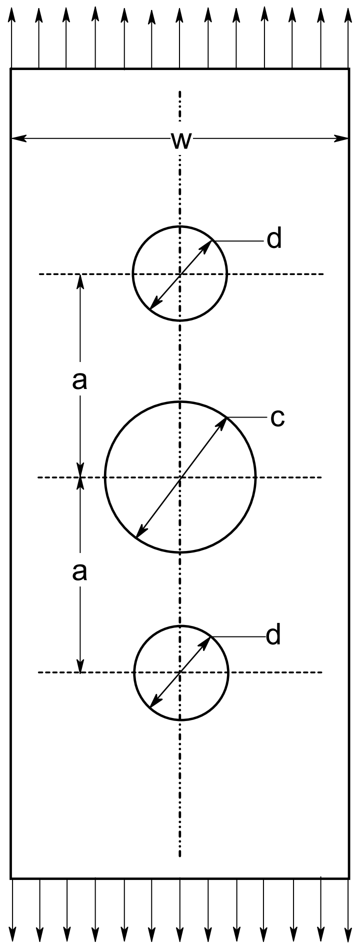

Figure 2. Flat plate with main and auxiliary circular holes **(**Erickson and Riley, 1978).

14.4 mm when the main hole and auxiliary holes' diameters were 42.9 mm and 11.1 mm, respectively. They reported a reduction of SCF ranging from 13 to 21%.

Another similar study by Sanyal and Yadav (2006) developed formulae for calculating the optimum size of the auxiliary hole, and the centre distance between the hole and the auxiliary hole as shown in Figure 3.

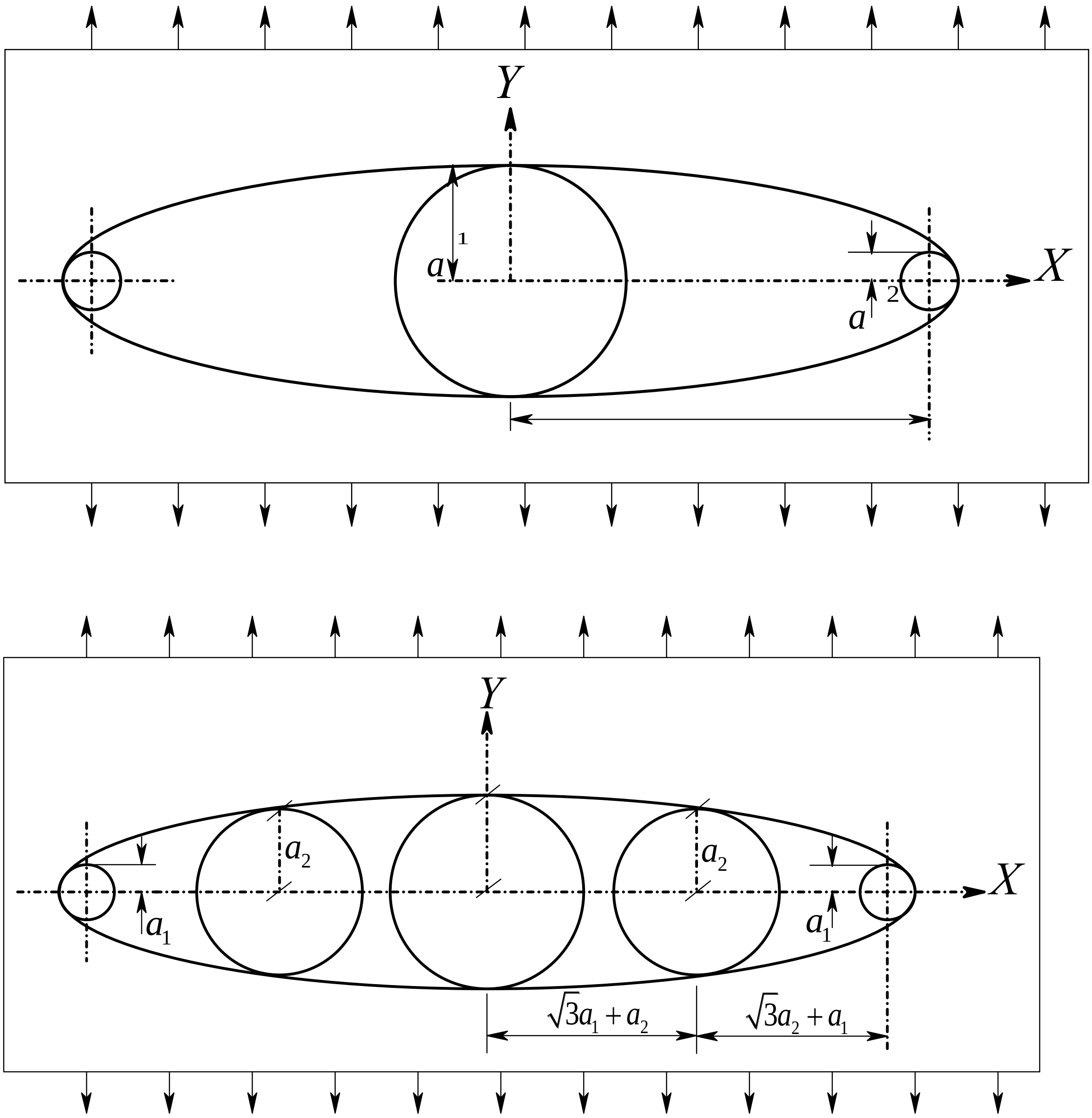

Figure 3. Location of main and auxiliary holes (Sanyal and Yadav, 2006)

The Sanyal and Yadav formulae for optimum conditions are presented as;

$$a_2 = 0.85a_1 \tag{2.9}$$

Where

a_1 is the main hole radius

a_2 is the auxiliary hole radius

and

$$\delta = \sqrt{3}a_1 + a_2 \qquad (2.10)$$

Where

δ is the optimum centre distance

The study reported that the use of the Sanyal and Yadav formulae, the SCF was reduced by 17%. However, a disparity of the results given by the two studies discussed earlier occurred when the optimum values of the auxiliary hole given by Erickson's and Riley's study were tested on Sanyal and Yadav formulae.

Further literature reviewed by Nagpal *et al*. (2012) on flat plates with holes, revealed that introducing 2 or 3 co-axial circular auxiliary holes in the cross bore axis, also termed as defence hole system method, reduce SCFs by 7.5 to 11 %. The authors also reported that SCFs can be reduced by using composite material rings or laminate plates around the cross bore as a form of material reinforcement. The presence of material rings and laminates alter the stress distribution around the cross bore vicinity. Moreover, the study also revealed that gradual increase of the Young's modulus of elasticity away from the cross bore centre had a reducing effect on SCFs. The review concluded that the reduction of SCFs mainly depended on the size and location of the auxiliary hole. However, the study did not consider the effects of various auxiliary hole shapes in stress reduction citing initial design constraints as well as thickness ratios and angles of inclination.

2.4 SOLUTIONS FOR SCF IN CYLINDERS WITH CROSS BORES

Various solutions have been developed to calculate SCF in high pressure vessels with small and large cross bores. According to Steele *et al.* (1986) a cross bore is termed as small when the ratio of the cross bore to main bore diameter is ≤ 0.5. However, when the same bore ratio ranges from ≥ 0.5 to ≤ 1 the cross bore is termed as large.

Earliest researchers developed solutions by considering a cylinder with a cross bore as a flat plate with a small elliptical hole at the centre, under tension. The circumference and the height of the cylinder are considered as the plate width and height, respectively. Timoshenko (1940) cited SCF as;

$$\mathrm{SCF} = 1 + \frac{2\mathrm{a}}{\mathrm{b}} \tag{2.11}$$

Where

a is the ellipse semi-major axis (m)

b is the ellipse semi-minor axis (m)

In this approach it was assumed that the width of the plate is large compared to semi-major axis, a. In the case of a circular hole (where a = b), the SCF was found to be 3. However, the results arising from further experimental and theoretical analysis conducted by Faupel and Harris (1957) on equation 2.11, failed to support this analysis.

Fessler and Lewin (1956) studied stress distribution in a tee junction of thick pipes. They assumed cylindrical thin plate sheets as infinite flat plates each with a circular hole under the action of internal pressure and two perpendicular tensions. These perpendicular tensions are the corresponding hoop and axial stresses that could have acted on the pipe as if the tee junction did not exist. They presented an analytical solution for SCF of closed end pipes as;

$$\mathrm{SCF} = \frac{4\mathrm{R}_2^2+\mathrm{R}_1^2}{\mathrm{R}_2^2+\mathrm{R}_1^2} \qquad (2.12)$$

Where

R_1 is the inside radius of the pipe

R_2 is the outside radius of the pipe

Faupel and Harris (1957) derived the same equation as Fessler and Lewin’s by considering an elliptical hole in an infinite elastic plate subjected to tensile loading. For a circularly shaped cross bore, a SCF equal to 2.5 was obtained; a decrease of 16.7% from that of equation 2.11. The reduction was due to the effects of longitudinal stresses generated by the closed ends of the cylinder. However, the derivation of equation 2.12 did not take into account the shear and compressive stresses which occur within the cross bore vicinity.

The results obtained using equation 2.12 gave an error that was 32% greater than experimental results, performed by photo elastic methods. The photo elastic experiment was performed on a cross bored cylinder with diameter ratios of 3, and the ratio of the cylinder bore to the cross bore as 2. This meant that the size of the cylinder used for the test was too large for equation

2.12 to be applicable (Cheng, 1978). O'Hara (1968) conducted another similar study using the method of photo elasticity. The study considered two cross bored cylinders having diameter ratios of 1.75 and the ratio of main bore to cross bore diameter as 10 and 20. They reported SCFs of 2.95 and 2.75, respectively, which were 14% less that those given by equation 2.11.

Further study of equation 2.12 was carried out by Comlekci *et al.*, (2007). They investigated the elastic stress concentration using FEA on radial cross holes in pressurised thick cylinders with cylinder diameter ratio ranging from 1.4 to 2.5. They concluded that equation 2.12 gave results with an accuracy of up to 99 % for only small holes. These small holes had the ratio of main cylinder bore to that of the cross bore diameter ≤ 100.

Various solutions for determining the SCF in large cross bores have also been developed. Faupel and Harris (1957) presented a solution for the SCF of large circular cross bores using experimental data from Peterson Stress Intensification Factors Charts. The intensifications factors $\propto$ and γ are used to calculate SCF as shown in equation 2.13. The values of intensification factors for various side hole ratios as compiled by Faupel and Harris (1957) are tabulated in Table 2.

The solution of SCF proposed by Faupel and Harris (1957), using intensification factors, is presented as;

$$\mathrm{SCF} = \frac{\alpha\sigma_h + \gamma\sigma_z}{\sigma_h} \qquad (2.13)$$

Table 2 : Peterson stress intensification factors (Faupel and Harris, 1957)

Side Hole Ratio $\left(\frac{\text{Cylinder bore radius}}{\text{Cross bore radius}}\right)$	α	γ
10	3	-0.92
9	3	-0.90
8	3	-0.88
7	2.96	-0.86
6	2.95	-0.84
5	2.92	-0.81
4	2.88	-0.77
3	2.82	-0.70
2	2.71	-0.58
1	2.57	-0.33

Where

σ_h is the hoop stress at the surface of the cross bore

σ_z is the longitudinal stress at the surface of the cross bore

α and γ is the intensification factors.

However, there was no information given on intensification factors for other cross bore profiles such as elliptical.

Gerdeen (1972) presented lengthy analytical solutions for calculating SCFs for large cross bores, which were referred to as side holes. The coordinates and dimensions used for the SCF analysis are shown in Figure 4.

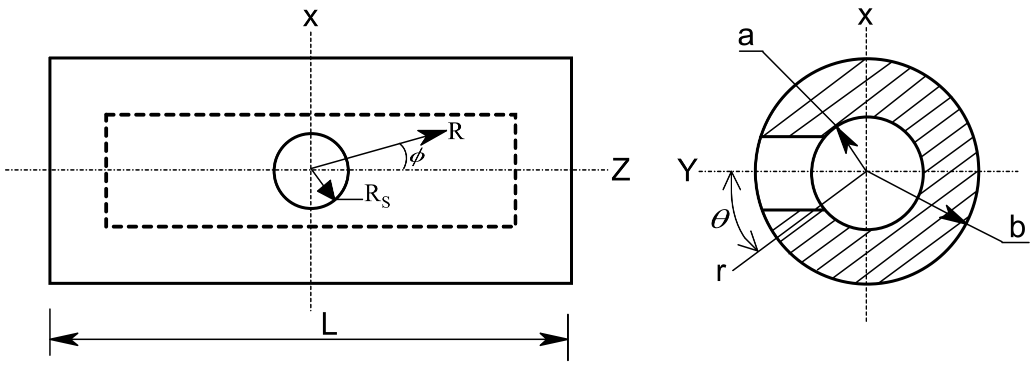

Figure 4. Coordinates and dimensions of the cylinder with a cross bore (Gerdeen, 1972).

A simplified technique to be followed for calculating the SCF using Gerdeen's method is summarised hereunder;

i. Determination of hoop stress for a cylinder without a hole using Lame's theory.
ii. Determination of the total surface stresses at the cylinder bore necessary to keep internal pressure constant. The surface stresses at the cross bore are the sum of radial σ_{RR} and shear stresses $\tau_{R\Phi}$ and τ_{RY} in the transverse plane required to keep the internal stresses constant as in a cylinder without cross bore. The two components of shear stresses were calculated in polar coordinates at the Y axis and at a subtended angle θ from the Y axis

iii. Determination of hoop stress, $\sigma_{\Phi\Phi}$ at the intersection. This was obtained by subtracting the results of (ii) from (i).

iv. Determination of the internal pressure, P in the cylinder.

The maximum hoop stress at the cross bore intersection is obtained by summing the results of (i), (iii) and (iv). The SCF at the intersection is then calculated using equation 2.1.

However, this study did not take into consideration the stresses in the longitudinal plane. Despite Gerdeen's method giving an approximate solution, it considered the effects of shear stress which had been previously neglected by other researchers.

In another study by Xie and Lu, (1985) it was reported that most solutions developed using theoretical methods were limited to thin walled cylinders with the ratio of cross bore to main bore $\leq \frac{1}{3}$. This limitation was associated with difficulties in mathematical analysis. A review by Moffat *et al.*, (1999), compiled SCFs for 36 different geometric sizes at the pipe branch junction under internal pressure loading carried out by different studies. The stress analysis in these studies were performed using experimental and numerical (FEA) methods. The SCFs and their respective geometric dimensions are summarised in Tables 3 and 4.

Table 3: SCFs at the pipe branch junction performed by experimental method (Moffat *et al.*, 1999)

S/No.	d/D	D/T	t/T	SCF
1	0.20	8.00	0.20	3.25
2	0.22	15.80	0.43	3.20
3	0.24	19.50	0.54	2.80
4	0.25	16.50	0.57	3.40
5	0.29	12.90	0.49	4.60
6	0.31	17.90	0.40	3.40
7	0.55	21.00	1.82	2.70
8	0.55	57.60	0.91	4.90
9	0.62	9.98	0.62	4.75
10	0.62	15.08	1.00	3.70
11	0.64	19.00	0.69	5.00
12	0.66	18.87	0.64	4.53
13	0.69	156.00	0.63	8.00
14	0.76	10.30	1.50	3.50
15	1.00	19.00	1.00	5.40
16	1.00	24.70	1.00	4.18

Table 4: SCFs at the pipe branch junction performed by FEA method (Moffat *et al*., 1999)

S/No.	d/D	D/T	t/T	SCF
1	0.09	36.06	1.13	2.55
2	0.12	49.00	0.84	2.52
3	0.16	10.30	0.22	3.14
4	0.20	8.00	0.20	3.25
5	0.22	9.00	0.30	3.01
6	0.22	16.65	0.45	3.20
7	0.39	10.84	0.41	3.87
8	0.46	5.50	1.00	2.44
9	0.50	2.33	0.50	3.62
10	0.50	3.50	0.50	3.63
11	0.50	7.67	0.50	4.17
12	0.50	11.00	0.50	4.23
13	0.62	9.98	0.62	4.24
14	0.62	15.08	1.00	3.60
15	0.64	7.00	0.70	4.10
16	0.70	16.00	0.75	4.67
17	0.80	20.00	1.00	4.08
18	0.91	7.00	0.96	4.35
19	1.00	4.70	1.00	2.80
20	1.00	17.94	1.00	4.03

Where

d is the branch pipe diameter

D is the run pipe diameter

t is the branch pipe thickness

T is the run pipe thickness

Most of the SCF analysis reviewed in tables 3 and 4 were performed on thick walled cylinders with large openings. Actually, the experimental work was done using full scale models. Generally, the data presented in these two tables were found to be consistent and has been used in other previous studies (Qadir and Redekop, 2009) as a reference. The term “reference standard” will be used to refer to the data in tables 3 and 4.

Lind (1967) studied stress concentration in pressurised pipe connection branches and developed two solutions for calculating SCFs using area replacement mathematical techniques. The solution for SCF was taken to be the maximum value obtained from these two equations as shown by equation 2.14.

$$SCF = \text{Max}\begin{cases} \dfrac{\left[1+1.77\left(\frac{d}{D}\right)\sqrt{\frac{D}{T}}+\left(\frac{d}{D}\right)^{2}\sqrt{\frac{s}{S}}\right]\left[1+\dfrac{T/D}{\sqrt{s/S}}\right]}{1+\dfrac{\left(\frac{d}{D}\right)^{2}}{\frac{s}{S}\sqrt{\frac{s}{S}}}} \ldots\ldots\ldots\ldots (2.14\text{ a}) \\ \dfrac{\left[1.67\sqrt{s/S}\cdot\sqrt{D/T}+0.565\left(\frac{d}{D}\right)\right]\left[1+\dfrac{(T/D)}{\sqrt{s/S}}\right]}{0.67\sqrt{s/S}\sqrt{D/T}+0.565\,\dfrac{(d/D)}{s/S}} \ldots\ldots. (2.14\ b) \end{cases} \qquad (2.14)$$

Where

$s = {}^{d}/_{2t}$

$S = {}^{D}/_{2T}$

t is the nozzle thickness

d is the nozzle mean diameter

D is the vessel main diameter

T is the vessel thickness

Qadir and Redekop (2009) studied SCFs at the nozzle intersection in a pressurised vessel using the FEA. They compared the results obtained by Lind’s equation at the intersection with those from the reference standard given by Moffat *et al.* (1999). The study reported that the results given by Lind’s equation had a standard deviation of 1.77 from the reference standard and classified them as being conservative.

Money (1968) developed two other solutions for SCF analysis using linear regression analysis based on several experimental data on tee joints, performed using the method of photo elasticity. The solutions of SCF developed by Money are presented here as;

$$\mathrm{SCF} = 2.5\left[\left(\frac{\mathrm{r}}{\mathrm{t}}\right)\frac{2\mathrm{T}}{\mathrm{R}}\right]^{0.2042} \quad \text{for} \quad 0 < \ {}^{r}\!/_{R} \leq 0.7 \tag{2.15}$$

$$\mathrm{SCF} = 2.5\ \left[\left(\frac{\mathrm{r}}{\mathrm{t}}\right)\frac{2\mathrm{T}}{\mathrm{R}}\right]^{0.24145} \quad \text{for} \quad 0.7\ \leq {}^{r}\!/_{R} \leq 1.0 \tag{2.16}$$

Where

r is the vessel mean radius

R is the nozzle mean radius

t is the nozzle thickness

T is the vessel thickness

The two equations are seen to be dependent on the ratio of cross bore and cylinder bore diameters. However, the solutions present two separate curves with a discontinuity when the ratio of $\left({}^{r}\!/_{R}\right) = 0.7$. Hence there was no definite solution when the ratio of $\left({}^{r}\!/_{R}\right) = 0.7$.

Qadir and Redekop (2009) and Moffat *et al.*, (1991) further studied the two Money's equations and reported a standard deviation of 0.811 from the reference standard. They termed the results obtained from the two equations as accurate.

Decock (1975) developed another solution for SCFs based on experimental data conducted on a pipe branch using strain gauges and the method of photo elasticity. The solution for SCF was given as;

$$\mathrm{SCF} = \frac{\left[2 + 2\frac{d}{D}\sqrt{\left(\frac{d}{D}\times\frac{t}{T}\right)} + 1.25\frac{d}{D}\sqrt{\frac{D}{T}}\right]}{\left[1 + \frac{t}{T}\sqrt{\left(\frac{d}{D}\times\frac{t}{T}\right)}\right]} \qquad (2.17)$$

Where

t is the nozzle thickness

d is the nozzle mean diameter

D is the vessel main diameter

T is the vessel thickness

The Decock equation was further studied by Moffat *et al.*, (1991) who reported that the equation gave accurate results when the ratio of cylinder diameter and thickness was equal to 20. However, they reported erroneous results when the ratio was above or below 20. Consequently, Qadir and Redekop (2009) reported a standard deviation of 1.482 from the reference standard and recommended the use of Decock's equation in determining SCFs at the crotch corner of a tee joint. They termed the results given by the equation as being conservative.

Xie and Lu (1985) developed a three term polynomial solution for predicting SCFs in cylindrical pressure vessels with nozzles using the least squares method. The three term polynomial solution was fitted using experimental data. The solution for SCFs is given as

$$\mathrm{SCF} = 2.87 + \left[1.38 - 0.72\left(\frac{\mathrm{t}}{\mathrm{T}}\right)^{0.5}\right]\left(\frac{\mathrm{D}}{\mathrm{T}}\right)^{0.43}\left(\frac{\mathrm{d}}{\mathrm{D}}\right)^{0.9} - \left(\frac{\mathrm{t}}{\mathrm{T}}\right)^{0.5} \tag{2.18}$$

Where

D is the mean diameter of vessel

D is the mean diameter of nozzle

T is the wall thickness of vessel

t is the wall thickness of nozzle

The accuracy of the Xie and Lu's solution was validated using Money's, Decock's and Lind's solutions at the tee pipe junction. The study reported that Xie and Lu's equation had the best accuracy of 87%, in comparison to Decock's (83.2%), Lind's (72.3%) and Money's (70.7%). Further, the authors recommended the use of the Xie and Lu's solution in the determination of SCFs for both small and large openings.

Moffat *et al*. (1999) derived a lengthy polynomial function using several geometric parameters to determine the SCF on a tee junction using 3D FEA. Their solution is presented here as;

$$\mathrm{SCF} = \left[a_1 + a_2\left(d/_D\right) + a_3\left(d/_D\right)^2 + a_4\left(d/_D\right)^3\right] + \left[a_5 + a_6\left(d/_D\right) + a_7\left(d/_D\right)^2 + a_8\left(\frac{d}{D}\right)^3\right]\left(t/_T\right) + \left[a_9 + a_{10}\left(d/_D\right) + a_{11}\left(d/_D\right)^2 + a_{12}\left(d/_D\right)^3\right]\left(D/_T\right)^P + \left[a_{13} + a_{14}\left(d/_D\right) + a_{15}\left(d/_D\right)^2 + a_{16}\left(d/_D\right)^3\right]\left(t/_T\right)\left(d/_T\right)^P \tag{2.19}$$

Where

t is the nozzle thickness

d is the nozzle mean diameter

D is the vessel main diameter

T is the vessel thickness

P = 1.2

The constants a_1 to a_{16} were obtained from the 3D FEA and given as 2.5, 2.715, 8.125, -6.877, -0.5, -1.193, -5.416, 5.2, 0.0, 0.078, -0.195, 0.11, 0.0, -0.043, 0.152 and -0.097.

Later, Qadir and Redekop (2009) studied the Moffat *et al.* equation and reported a standard deviation of 0.903 from the reference standard. They termed the results given by the equation as being accurate.

Gurumurthy *et al.,* (2001) following a similar procedure as Moffat *et al*. (1991), developed a simplified solution for SCF at the nozzle shell junction based on shell theory using FEA. The solution for SCFs obtained was given as;

$$\mathrm{SCF} = 1.75\left({}^{\mathrm{T}}/_{\mathrm{t}}\right)^{0.4}\left({}^{\mathrm{d}}/_{\mathrm{D}}\right)^{-0.08}(\lambda)^{0.6} \tag{2.20}$$

Where

$\lambda = {}^{\mathrm{d}}/_{(\mathrm{DT})^{0.5}}$ (Pipe factor)

t is the nozzle thickness

d is the nozzle mean diameter

D is the vessel main diameter

T is the vessel thickness

The authors compared the solution of this equation with those of Money (1967), Decock (1975) and Moffat *et al.* (1999) and reported some discrepancies in the SCF values obtained. However, despite the discrepancies, the authors recommended the use of Gurumurthy's equation for stress intensity approximation. In the same study, conducted by Qadir and Redekop (2009), they reported that solutions obtained from the Gurumurthy's equation had a standard deviation of 1.721 from the reference standard. They termed the results as being more conservative, with greater fluctuations than those from other methods discussed earlier.

From the preceding paragraphs, it is evident that reliable and correct results are given by equations 2.15, 2.16 and 2.19 which had an approximate standard deviation of 0.9 from the reference standard. Despite solution validation of equation 18, the reviewed literature did not show any extensive application on other studies. The solutions for SCFs at the tee junction depend on geometric parameters such as the ratio of diameter, thickness, and other physical characteristics at the junction such as sharp corners, chamfers and blades. Interestingly, there is no universally accepted solution for determining SCFs at the tee junction.

Of all the solutions for SCFs in circular cross bore cylinders reviewed here, none gave optimal location of the cross bore. Besides, equations 2.11 and 2.12 being derived analytically, the authors did not take into consideration the analysis of hoop, radial and shear stresses arising from the cross bore cross section when viewed from the longitudinal plane.

2.5 FACTORS AFFECTING STRESS CONCENTRATION FACTORS IN HIGH PRESSURE VESSELS

Hyder and Asif (2008) reported that SCFs depended on the material physical property, nature of loading, the stress distribution pattern and the type of discontinuity such as holes, fillets, grooves and notches. However, the effects of Poison's ratio and Young's modulus of elasticity on SCFs have not been fully investigated (Nagpal *et al.*, 2012).

Some of the geometric design parameters that affect SCFs in high pressure vessels are the cross bore size, shape, location, obliquity and thickness ratio. The following is a brief discussion of these design parameters.

2.5.1 Cross bore size

Gerdeen (1972) studied the relationship between SCFs and different ratios of cross bore to main cylinder bore size in thick cylinders having thickness ratios of 1.5, 2, 3, 4 and 6. The results showed an increase in SCFs as the ratio of cross bore to main cylinder bore increases. These findings compared well to other findings by Masu (1997) and Makulsawatudom *et al.*, (2004). Masu (1997) studied the effects of cross bore size on stress distribution in thick walled cylinders with a thickness ratio of 2. The study reported that for a particular thickness ratio, the SCF increases with increasing cross bore size.

Further extrapolation of the results presented by Gerdeen's equation revealed that the minimum SCF occurred when the ratio of cross bore to cylinder bore size was equal to 1. The Gerdeens' findings were also contradicted by another similar study conducted by Comlekci *et al.* (2007). Comlekci *et al.* (2007) studied thick cylinders with thickness ratio of 1.4, 1.5, 1.6, 1.75, 2.0, 2.25 and 2.50, and cross bore to cylinder bore size ratios ranging from 0 to 0.25. They reported the minimum SCF to occur between the size ratio of 0.1 and 0.2.

Hyder and Asif (2008) conducted another similar study using the Von Mises theory on thick cylinders with a thickness ratio of 2.0. They reported optimal cross bore sizes of 8 mm and 10 mm for cylinders with internal diameter of 200 mm, and 300 mm, respectively. This meant that, the optimal size ratio occurred when the cross bore to cylinder bore ratios were at 0.03 and 0.04.

2.5.2 Cross bore shape

Nagpal *et al*. (2012) identified the common shapes of cross bores used in high pressure vessels as circular and elliptical. Kihiu and Masu (1995) studied the effect of chamfers on the distribution of stress in cross bored thick walled cylinders under internal pressure. They reported that incorporating chamfers, blend or radius entry on cross bore, cause stress redistribution that lead to a reduction in SCF. A SCF reduction of up to 34.2% was noted at the main bore due to the introduction of chamfers in comparison with plain cross bores. A further reduction in SCF can be achieved by either varying the chamfer angle or the length or combinations thereof. However, the study concluded that the percentage reduction in SCF due to the introduction of chamfers depended on cylinder thickness, cross bore radius, chamfer length and angle. For instance, the optimal SCF for a cylinder ratio of 2, was found to be 2.17 at the cross bore radius of 1 mm and chamfer angle of 50^0. Masu (1989) studied the effect of varying chamfer depths on stress distribution. The study concluded that stress magnitude decreases with decreasing chamber depth.

Kihiu (2002) carried out another study on stress characterisation in cross bored thick walled cylinders. The study investigated the effects of introduction of chamfers and radiused entry in plain cross bores. The study reported that the radiused entry had lower SCF than chamfers. This was in line with an earlier study conducted by Masu (1989) on the effects of varying blending radii on stress distribution. The study concluded that stress distribution along blended radiused cross bore was almost the same as that of plain cross bore, particularly when the blend radius size is small.

As reported by Kihiu and Masu (1995), the stress redistribution in the vicinity of the cross bore due to the introduction of chamfers and blends, also gives rise to other points of peak stresses along the chamfer, especially at the crotch corner. The values of the peak stresses occurred at 12.5 mm from the cross bore and were 140 % greater than those at the cross bore intersection. These high peak stresses are some of the causes of reduced fatigue life in high pressure vessels (Comlekci *et al.*, 2007). These findings are in line with another latter study done by Makulsawatudom *et al.* (2004).

Makulsawatudom *et al.* (2004) studied peak stress due to the introduction of blend radius and chamfers for radial circular and elliptical cross bores. The study compared their results with those obtained from a plain cross bore. They reported that introduction of chamfers generated high peak stresses for both circular and elliptical cross bores, with plain cross bores having the lowest peak stresses.

Generally, for all the three cases studied (Masu, (1989); Kihiu and Masu, (1995) and Makulsawatudom *et al.,* (2004)) the peak stresses for elliptical radial cross bore were lower than those of circular cross bore. Moreover, the three studies established that carefully polished chamfers at the intersection of the main cylinder and the cross bore also reduces SCF further. The polished chamfers at the intersection are usually carried out using spark erosion techniques (Masu, 1989).

Cole *et al.* (1976) and Makulswatudom *et al*. (2004) reported that SCFs can be reduced by making elliptically shaped cross bores positioned along the cylinder radial line instead of round shaped cross bores. The two studies also reported that SCFs are reduced when round shaped cross bores are offset by an appropriate distance from the cylinder radial lines. According to Cole (1976) offsetting the position of the cross bore from the radial line also improves the fatigue life of the cylinder by up to 170%.

Makulswatudom *et al.* (2004) pointed out that there was a relatively small difference of up to 5% in the values of SCFs obtained, when elliptically shaped cross bores were drilled in the offset position from the radial line instead of circular ones. They recommended the use of circularly shaped holes at the offset position instead of elliptical ones, due to their low manufacturing cost.

Carvalho (2005) studied the effects of U-shaped notches on SCFs in internally pressurised cylinders using FEA. The study concluded that, regardless of the size, notches alter the stress distribution curves in the whole cross section, creating high regions of stress concentration. In this regard the study recommended that the introduction of notches in any pressure vessel should be avoided.

2.5.3 Cross bore location

Masu (1998) studied the effects of offsetting circular cross bores in thick walled cylinders. SCF reductions of 17 % and 42% were reported, when the cross bore was offset by 6 mm and 11.2 mm, respectively, from the radial line. Makulsawatudom *et al.* (2004) studied two small circular and elliptical openings having cross bore to main bore ratios of 0.01 and 0.05. The study investigated the effects of SCFs when the openings were located at the centre of the cylinder axis and in an optimally offset position. The minimum SCF occurred with a cross bore ratio of 0.05 when the elliptical plain cross bore was positioned radially. Further comparison between authors on SCFs at the vessel intersection with cylinder thickness ratio of 2 is shown in table 5.

Hyder and Asif (2008) also studied stress concentration along the height of the cross bored cylinder under internal pressure. Stress concentration was investigated at five different segments along the cylinder height from the top. The location of these segments were at $1/16$, $1/8$, $2/8$, $3/8$ and $4/8$ (centre of the cylinder). The optimum and maximum SCFs occurred at $1/8$ and $4/8$, respectively.

The SCF at $1/16$ was considerably high due to the effects of the closed ends of the cylinder (Saint Venant's principle). According to this study, for optimum conditions, the cross bore should be positioned away from the cylinder centre and its closed ends.

Table 5: SCF values at the vessel intersection (Masu, 1998; Makulsawatudom *et al.*, 2004)

SCF at the main cylinder bore cross-bore intersection with cylinder thickness ratio of 2								
	Circular radial cross bore		Elliptical radial cross bore		Circular optimally offset (0.112b) cross bore		Elliptical optimally offset (0.112b) cross bore	
Cross bore shape	Plain	Chamfer	Plain	Chamfer	Plain	Chamfer	Plain	Chamfer
Cole *et al.* (1976)	-	-	1.80	-	1.80 (1.4 -1.5 near the outlet plane)	-	-	-
Masu (1998)	2.30	-	1.52	-	1.33	-	-	-
Makulsawatudom *et al.*, (2004). Hole size ratio $\frac{R_C}{b} = 0.01$	3.04	3.7	3.0	2.25	3.00	3.55	2.10	2.5
Makulsawatudom *et al.*, (2004) Hole size ratio $\frac{R_C}{b} = 0.05$	2.89	3.4	2.00	2.25	2.80	3.3	2.3	2.6

Where

R_C is the cross bore radius

b is the outer diameter of the cylinder

2.5.4 Cross bore obliquity

As reported by Little and Bagci (1965), small inclined cross bores in the transverse plane generate positions of major and minor axes on the main bore of the cylinder. Whenever, the major axis is perpendicular to the Z direction (see Figure 4), the maximum SCF occurs at both ends of the major and minor axes. The same study by Little and Bagci (1965), also reported that small, inclined cross bore in the longitudinal plane have their major axis parallel to the Z direction. Therefore, maximum SCF occurs only at the ends of the major axis, and was given by;

$$\mathrm{SCF} = \frac{4\mathrm{C}\mathrm{R}_2^2+\mathrm{R}_1^2}{\mathrm{R}_2^2+\mathrm{R}_1^2} \qquad (2.21)$$

Cheng (1978) gave the analytical solution of SCF for closed end cylinder at the ends of the major axis as;

$$\mathrm{SCF} = \frac{2(\mathrm{C}-1)\mathrm{R}_2^2+\mathrm{R}_1^2}{\mathrm{R}_2^2+\mathrm{R}_1^2} \qquad (2.22)$$

While at the end of minor axis as;

$$\mathrm{SCF} = \frac{\left({4\mathrm{R}_2^2}/{\mathrm{C}}\right)+\mathrm{R}_1^2}{\mathrm{R}_2^2+\mathrm{R}_1^2} \qquad (2.23)$$

Where

C is the ratio of major and minor axis of the ellipse (Ellipticity)

R_1 is the cylinder inside radius

R_2 is the cylinder outside radius

Comparing the two equations, it was evident that the SCF at the major axis is higher than that of the minor axis.

The symbol notations remain the same as those in equations 2.21 and 2.22.

Adenya and Kihiu (2010) studied stress concentration factors in high pressure vessel with elliptical cross bores. They reported a reducing effect on SCF, when an elliptical shaped cross bore whose major axis was perpendicular to the cylinder axis, was rotated clockwise with respect to the longitudinal plane by 90^0. At this position, the minimum SCF was found to be $<$ 2 (a decrease of up to 33% compared to that given by a circular cross bore in equation 2.11). The study concluded that, the maximum SCFs occurred when the major axis of elliptical cross bore lay in the longitudinal plane. Whereas, the minimum SCFs occurred when the major axis of elliptical cross bore lay in transverse plane.

2.5.5 Thickness ratio

Masu (1991) studied SCFs at the intersection of the cylinder bore and plain circular cross bore, on cylinders with thickness ratios of 1.4 and 2.0. The specimens tested had ratios of cylinder length to outside diameter ≥ 2 and cylinder bore radius to cross bore radius ≥ 7.5. The study reported that SCFs decreased with decreasing thickness ratio. Further, tabulation of some of the SCF results obtained at the intersection of cross bore and main cylinder bore using various techniques with different thickness ratios (K) are shown in Table 6.

The data in Table 6 revealed that, the highest and the lowest SCFs values occurred in the cylinder with a thickness ratio of 3. The highest SCF of 3.78 was obtained by Chaban and Burns (1986) using 3D FEA while the lowest SCF of 2.51 was reported by Faupel & Harris (1957) using experimental methods, at K=3.0.

Kihiu (2002) studied cross bored thick walled cylinder under internal pressure posessing thickness ratios ranging from 1.75 to 3. The study reported a constant SCF of 2.753 over the thickness ratio when the cross bore to main bore radius ratio was at 0.2. However, when the ratio of cross bore to main bore was < 0.2, the SCF increased with increasing thickness ratio, whereas when the ratio was > 0.2 the SCF decreased with increasing thickness ratio. In another study, Kihiu *et al*. (2003) developed a 3D FEA computer program to determine the SCF and geometric constants in thick walled cylinders with a plain cross bore subjected to internal pressure. The study reported that when the thickness ratio was < 1.75 the geometric constant was 0.11 and the SCF was 2.67, whereas, when the thickness ratio was > 1.75 the geometric constant was 0.2 and the SCF was 2.734.

Table 6: Comparison of SCF of radial circular cross bore at the vessel intersection (Masu, 1991; Makulsawatudom et al., 2004)

K	Gerdeen (1972) (Photo elasticity)	Fessler & Lewin (1956) (Analytical)	Faupel & Harris (1957) (Strain gauge & Photoelasticity 2D & 3D)	Peterson (1974) (Strain gauge)	Tan & Fenner (1980) (Boundary Integral Element (BIE))	Abdul-mihsein & Fenner (1983) (BIE)	Masu (1991) (3D FEA)	Chaaban & Burns (1986) (3D FEA)	Makulsawatudom *et al.*, (2004) (3D FEA) Hole size ratio $\frac{R_C}{b} = 0.01$	Makulsawatudom *et al.*, (2004) (3D FEA) Hole size ratio $\frac{R_C}{b} = 0.05$
1.4	-	2.99	-	-	-	-	2.84	-	-	-
1.5	3.19	3.08	-	-	-	-	-	3.40	2.82	2.73
1.75	-	3.26	-	-	-	-	-	-	2.93	2.83
2.0	3.32	3.4	3.02	3.44	2.98	2.97 - 3.0	3.03	3.58	3.04	2.89
2.25	-	3.51	2.53	-	-	-	-	-	3.13	2.91
2.5	-	3.59	2.54	-	-	-	-	3.69	3.20	2.94
3	-	3.70	2.51	-	-	-	-	3.78	-	-

Later, Kihiu *et al*. (2007) studied universal SCF in chamfered cross bored cylinders with thickness ratios between 2.25 and 3 under internal pressure. The study reported that SCFs increased with decrease of thickness ratio, contradicting the earlier findings by Masu (1991). The study also reported that thick walled cylinders were more suitable for chamfering than thin walled cylinders.

From the preceding paragraphs, it is evident that the three studies conducted by Kihiu *et al*. led to the development of a quick design tool for cross bored thick walled cylinders based on the thickness ratio.

2.6 THERMAL STRESSES

Thermal stresses occur whenever a part of any solid body is prevented from attaining the size and shape that it could freely attain due to change of temperature. Thermal stresses are classified under localised stresses such as fatigue, since they cause minimal distortion on the overall shape of the body (Radu *et al.*, 2008). Harvey (1985) cited thermal stress distribution σ of a bar restricted to expand freely upon temperature change as;

$$\sigma = \mathrm{E}\,\alpha\,\Delta\mathrm{t} \tag{2.24}$$

Where

E is the Young's modulus of elasticity

α is the coefficient of thermal expansion

Δt is the change in temperature

Thus, thermal stress is a function of the material property (Young's modulus of elasticity and Coefficient of thermal expansion), together with change in temperature across the thickness of the bar.

Rapid increase of the working fluid temperature in the pressure vessel induces thermal and dynamic stresses on the walls of cylinders. Thermal stress is induced in the wall of the pressure vessel, whenever there is any temperature gradient or non- uniform temperature distribution across the wall (Choudhury *et al.*, 2014). Large thermal stresses may cause susceptible component failure, reduce their operating life (Choi *et al.*, 2012) or limit their operational flexibility. The temperature gradient in the pressure vessel is usually oscillating and, therefore, the need for accurate thermal stress analysis.

The thermal stress distribution in thick pressure vessels made of a single material layer is determined by (Timoshenko and Goodier, 1951) as;

Hoop stress $\sigma_{\theta} = \frac{\alpha E}{(1-\nu)} \frac{1}{r^2} \left[\frac{r^2 + r_i^2}{r_0^2 - r_i^2} \int_{r_i}^{r_o} \mathrm{Trdr} - \int_{ri}^{r} \mathrm{rdr} \right]$ (2.25)

Radial stress $\sigma_{r} = \frac{\alpha E}{(1-\nu)} \frac{1}{r^2} \left[\frac{r^2 - r_i^2}{r_0^2 - r_i^2} \int_{r_i}^{r_o} \mathrm{Trdr} - \int_{r_i}^{r} \mathrm{Trdr} \right]$ (2.26)

Longitudinal stress $\sigma_{Z} = \frac{E \alpha}{1-\nu} \left[\frac{2}{r_0^2 - r_i^2} \int_{r_i}^{r_0} \mathrm{Trdr} - \mathrm{T} \right]$ (2.27)

Where

α is the coefficient of thermal expansion

E is the Young's modulus of elasticity

ν is the Poisson's ratio

r is the radius

r_i is the inside radius

r_o is the outside radius

T is the temperature change

From these three stress equations, it can be seen that thermal stress is a function of the material properties (Poisson's ratio, Young's Modulus of elasticity and coefficient of thermal expansions), the cylinder size and the temperature gradient across the wall of the cylinder.

Majority of thermal stress analyses in pressure vessels have been investigated under steady state conditions using Von-Mises theory to determine thermal stress (Gonyea, 1973). Kandil *et al.* (1994) studied the effect of thermal stresses on thick walled cylinders and reported that the maximum thermal stress occurred at the inside surface of the cylinder. The peak of the thermal stress occurred at the beginning of the operating temperature. The study recommended gradual preheating of the cylinder wall up to the operating temperature, since it reduces thermal stress by 50 – 60%, for a short period of time, when the normalising heating time was equal to 1.0. Moreover, the study also reported that long term heating, that is, when the normalising heating time was ≥ 3.0, had insignificant effects on reduction of thermal effective stress. The study concluded that the time required for a thick walled cylinder to attain steady state operating conditions depended on the time of heating and the diameter ratio.

Segall (2003) derived a lengthy analytical polynomial equation expressing temperature as a function of radius and time for an arbitrary internal thermal boundary in a hollow cylinder. The study recommended the use of Segall's polynomial equation in the design and manufacturing processes of pressure vessels. In addition, the authors recommended the use of Segall's polynomial equation as a calibration tool in FEA modelling. However, it was noted that for the equation to give accurate results, the input data was limited to a particular sequence.

Marie (2004) developed another solution for determining hoop, radial and axial thermal stresses in high pressure vessels due to temperature variation. Marie's solution took into consideration the effects of the inner surface layer of the cylinder. However, the solution ignored other thermal parameters such as material conduction, thermal diffusivities and the coefficient of heat exchange. Despite these assumptions, the study recommended the use of Marie's equations in solving thermal shock and fatigue problems in pressure vessels and piping elements.

Radu *et al.*, (2008) derived another analytical solution for determining radial, hoop and axial elastic thermal stresses in the wall of a long hollow cylinder under sinusoidal transient thermal loading. The equations were developed using finite Hankel transform and their subsequent solutions solved by MATLAB software package. The Radu's equation was found to be independent of any temperature field and more so applicable to both steady and transient conditions. However, to obtain a stable response using Radu's equations, the authors recommended the use of at least a total of 100 transcendental roots having radial steps in order of thousands.

2.7 THERMO-MECHANICAL LOADING

Pressure vessels operate at extreme conditions such as high temperature, pressure and corrosive environment. Therefore, it is difficult to have one single material satisfy all the requirements. To overcome this problem, multi-layered composites materials and more recently Functionally Graded Materials (FGMs) are being used in the design of high pressure vessels. Multi-layered composites consist of different layers of material with the inner layer being of higher performance alloy than the outer layer (Choudhhury *et al.*, 2014). FGMs consists of two or more different materials having their material volume fraction varying smoothly along the desired directions. The most common examples of FGMs materials being the combination of Ceramics and Metals (Choudhhury *et al.*, 2014).

Choudhhury *et al.,* (2014) researched on the rate of the heat flow across the wall of a multi-layered pressure vessel consisting of Titanium and Steel layers under thermo-mechanical loading. The study considered two different experimental setups with the aim of investigating the effects of centrifugal and centripetal thermal flux in the cylinder wall. The latter being where the temperature at the inner surface of the cylinder is higher than the outside ambient temperature. Whereas, the former was vice versa. It was found that the rate of centripetal flux was higher than centrifugal flux. Okrajni and Twardawa (2014) performed heat transfer modelling of a super heater in a steam power plant, operating under thermo-mechanical loading using FEA. The study established that the use of time dependent heat transfer coefficients in heat transfer problems eliminates disparities in temperature measurements.

Zhang *et al.*, (2012) derived analytical solutions for determining hoop σ_θ, radial σ_r and axial σ_z stresses in a multi-layered composite pressure vessel under thermo-mechanical loading. The analysis took into consideration the effects of the closed ends of the cylinder. The three Zhang's equations are presented here as follows;

$$\sigma_\theta = \frac{E}{(1+\mu)(1-2\mu)}[(1-\mu)\varepsilon_\theta + \mu(\varepsilon_r + \varepsilon_z)] - \frac{E\alpha T}{1-2\mu} \quad (2.28)$$

$$\sigma_r = \frac{E}{(1+\mu)(1-2\mu)}[(1-\mu)\varepsilon_r + \mu(\varepsilon_\theta + \varepsilon_z)] - \frac{E\alpha T}{1-2\mu} \quad (2.29)$$

$$\sigma_z = \frac{E}{(1+\mu)(1-2\mu)}[(1-\mu)\varepsilon_z + \mu(\varepsilon_\theta + \varepsilon_r)] - \frac{E\alpha T}{1-2\mu} \quad (2.30)$$

Where

E is the Young's modulus of elasticity

μ is the Poisson's ratio

ε_θ is the hoop strain

ε_r is the radial strain

ε_z is the axial strain

A is the coefficient of thermal expansion

T is the temperature change

The stresses due to thermo-mechanical loading were shown to depend on the vessel size and length, the variation of pressure and temperature and the material properties of the cylinder wall. Moreover, the authors validated the three equations using 3D FEA on a six-layered composite pressure vessel. Geometric and materials' properties considered for each composite layer in this FEA modelling include wall thickness, Young's modulus of elasticity, Poisson's ratio, thermal conductivity, coefficient of thermal expansion, density and specific heat. The study reported good correlations between the analytical and the 3D FEA solution. In addition, the authors recommended the use of these equations in the design of multi-layered pressure vessels to be subjected to thermal and mechanical loading.

Chaudhry *et al.*, (2014) studied the behaviour of hoop stress across the wall of multi-layered pressure vessels during normal start-up and shutdown condition subjected under thermo-mechanical loading. They reported that at the inner surface of the pressure vessel wall, the hoop stress was found to be compressive during normal start-up and tensile during normal shutdown. However, the study did not investigate the effects of hoop stress in pressure vessels during emergency shutdown, under thermo-mechanical loading conditions. Emergency shutdown occurs when pressure is suddenly cut off.

2.8 Summary

From the literature reviewed, it is evident that there is no universally known and accepted method for determining optimum stress concentration factors in thick walled pressure vessels, considering the effects of the various geometric design parameters identified. In fact, the existing solutions addressed the optimum conditions based on each design parameter separately, despite most of the parameters being closely interrelated. Other authors compared magnitudes of stress concentrations without taking into consideration the size of the cross bore. In addition, studies carried out so far have failed to determine the optimal conditions in high pressure vessels with a cross bore under the combination of static, thermal and dynamic stresses, arising from the geometric configuration, working fluids, at high pressures and temperature, despite this being a common phenomenon in the industry. Moreover, the analytical solutions reviewed here did not take into consideration the analysis of hoop, radial and shear stresses arising from the cross bore when the cross section is viewed from the longitudinal plane.

Thus, this study developed optimal solutions for a cross bore in thick walled high pressure vessels using analytical and numerical methods in respect of radial circular cross bore. Besides, an optimal geometry of the cross bore that give minimum stress concentration factor in regards to, the cross bore size, location, shape, obliquity and thickness ratio was established. In addition, the study evaluated the effects of combined thermo-mechanical loading on stress concentration in high pressure vessels with cross bores.

CHAPTER THREE: RESEARCH METHODOLOGY

3.1 OVERVIEW OF THE STUDY

This study covers two broad sections. The first section dealt with the development of an analytical solution of elastic stresses along a radial circular cross bore in a thick walled cylinder. In addition, this section contains the validation of the developed analytical solution using finite element analysis.

Whereas, the second part of the study dealt with numerical optimisation of the cross bore geometry using finite element analysis. The optimisation process was based on selected geometric design parameters of the cross bore which have a major effect on stress concentration. These cross bore geometric parameters include the cross bore size, shape, location, obliquity angle and the thickness ratio. In addition, the effects of varying fluid temperature on stress concentration in a geometrically optimised cross bore were studied.

In this study, a total of 169 finite element analysis part models were created and analysed for various numerical investigations.

3.2 STRESS CONCENTRATION IN A RADIAL CIRCULAR CROSS BORE ALONG TRANSVERSE XY PLANE

3.2.1 Introduction

This section deals with the determination of the elastic stress concentration in a radial circular cross bore along transverse XY plane in a thick walled pressure vessel subjected to internal pressure. The solutions for stress concentration were obtained using analytical and the numerical methods. The analytical solutions were derived from first principles using elastic stress equations, whereas, the numerical solutions were obtained using a three dimensional finite element modelling. For these analyses, Abaqus Version 6.16 computer software was used.

The solutions obtained from these two methods were compared for the purposes of authentication. In addition, these solutions were also compared with other solutions presented in the reviewed literature to establish any correlation thereof.

3.2.2 Study cases

Seven cylinders with various wall thickness ratios and cross bore sizes were studied. The wall thickness ratio of the cylinders (K) was selected to coincide with those discussed in the reviewed literature by Masu (1991); Makulsawatudom *et al.,* (2004) and Nihous *et al.,* 2008. These included K values of 1.4, 1.5, 1.75, 2.0, 2.25, 2.5 and 3.0. In all of the analyses carried out, the main bore diameter of the cylinder was taken as 0.05 m. A total of five different cross bores, comprising of both small and large cross bores were investigated. The cross bore size ratios (cross bore to main bore ratio) of 0.1, 0.3 and 0.5 were classified as small cross bores (Steele *et al.*, 1986). Whereas, the cross bore size ratios of 0.7 and 1.0 (pipe junction) were categorised as large cross bores. The results were analysed along the cross bore transverse edge where $\theta = \frac{\pi}{2}$. Generally, the stresses along the cross bore transverse edge are presumed to be maximum (Ford and Alexander, 1977).

3.2.3 Analytical derivation of elastic stresses along a radial circular cross bore in a thick walled cylinder.

3.2.3.1 Introduction

This section of the study dealt with the analytical derivation of hoop, radial, axial and shear elastic stresses together with the stress concentration factor along a radial circular cross bore in a thick walled cylinder with closed ends. Figure 5 illustrates the main bore and the cross bore configuration including the associated stresses. The global coordinates of the configuration are indicated by the direction of the principal stresses in the main cylinder. Whereas, the local coordinates are indicated by the direction of stresses in the cross bore.

The derivation took into account four states of stresses acting in a closed cylinder when both the main bore and the cross bore are subjected to internal pressure. These various states of the stresses are listed below;

1. Stresses in an internally pressurized thick walled cylinder without a cross bore.
2. Stresses induced by the introduction of pressurized radial circular cross bore.
3. Stresses induced by the uniform axial tensile stresses due the closed end caps on the main cylinder bore due to internal pressure.
4. Stresses due to the internal pressure at the cross bore.

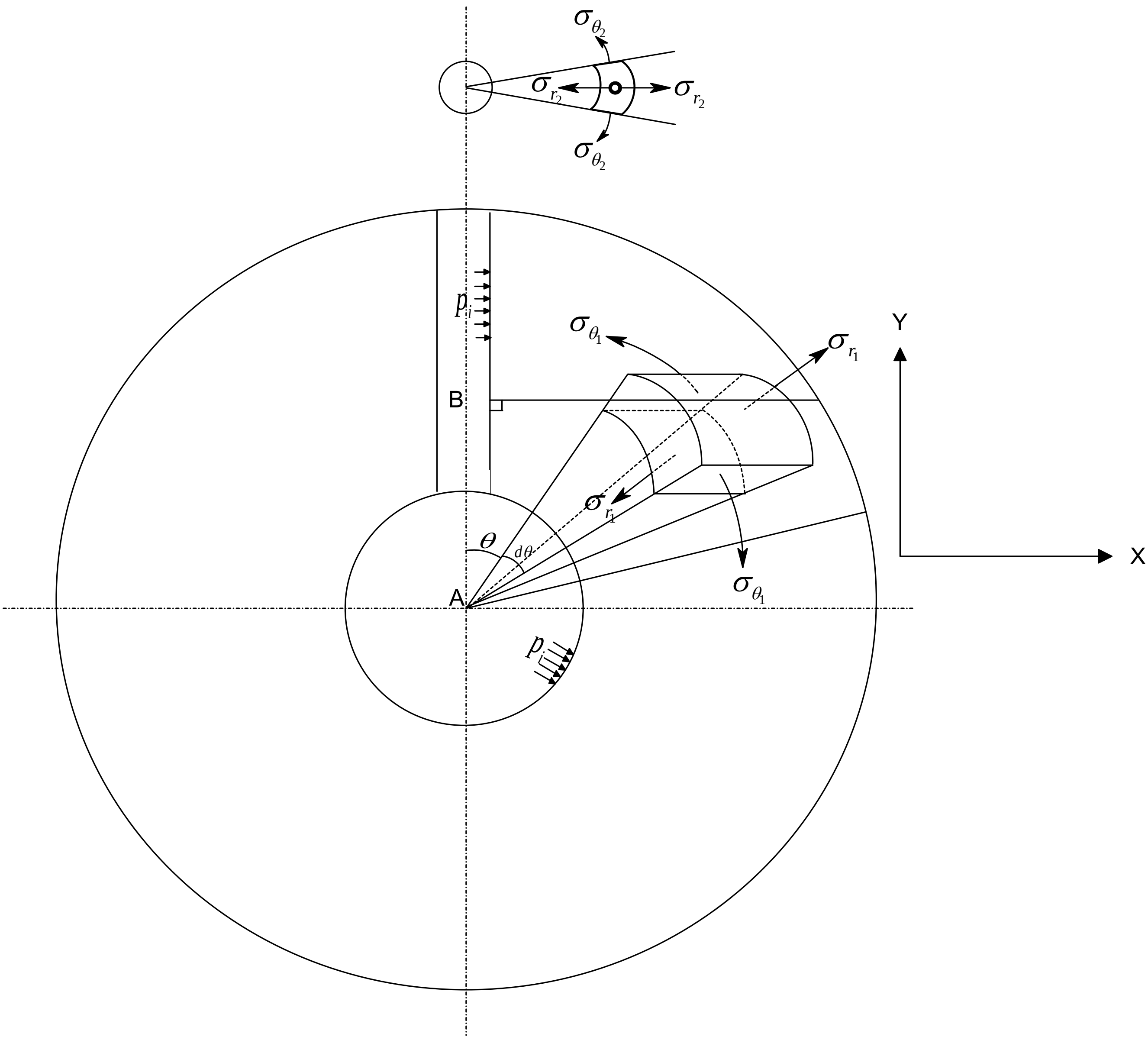

Figure 5: Main bore – cross bore configuration

Where;

p_i is the internal pressure.

σ_{θ_1} is the hoop stress generated by the pressurised main bore.

σ_{r_1} is the radial stress generated by the pressurised main bore.

$d\theta$ is the angle subtended by the small element.

θ is the angle between the vertical axis and the small element.

Each of these four states of stresses contribute independently to the total stress being experienced in the vessel. As a result, the stresses were analysed independently and their results superimposed together, in reference to their global plane of action. The four states of stresses are discussed briefly in the sections that follow.

3.2.3.2 Stresses in a thick walled cylinder without a cross bore (Step 1)

In this step, the stresses that exist in a thick walled cylinder without a cross bore were calculated. From Lame's theory, the hoop σ_{θ_1} and radial σ_{r_1} stresses in a thick walled cylinder without a cross bore subjected to an internal pressure p_i are given by;

$\sigma_{\theta_1} = A + \frac{B}{R^2}$; and $\sigma_{r_1} = A - \frac{B}{R^2}$; respectively.

Applying the boundary conditions to obtain the constants A and B. The expression of radial stress was used to calculate the constants, since its magnitude at the inner and outside surface are known. Thus, at the inside surface of the main bore, $r = R_i$, the corresponding radial stress $\sigma_{r_1} = -p_i$. Whereas, at the outside surface of the cylinder, $r = R_0$, the radial stress $\sigma_{r_1} = 0$, hence,

$$\sigma_{\theta_1} = \frac{p_i}{K^2 - 1}\left(1 + \left(\frac{R_0}{R}\right)^2\right), \text{ and} \tag{3.1}$$

$$\sigma_{r_1} = \frac{p_i}{K^2 - 1}\left(1 - \left(\frac{R_0}{R}\right)^2\right) \tag{3.2}$$

Where

K is the cylinder thickness ratio

R is the arbitrary radius measured from the main bore centre

The axial stress σ_z also referred to as longitudinal stress of the cylinder depends on the end fixing conditions. The end fixing conditions are dependent on whether the cylinder is open ended or closed. In an open ended cylinder, there is no axial stress generated. However, in a closed ended cylinder, a uniform axial stress across the thickness is generated, which is given by the following expression;

$$\sigma_z = \frac{p_i}{K^2 - 1} \tag{3.3}$$

3.2.3.3 Stresses induced by the introduction of radial cross bore (Step 2)

The configuration showing the introduction of a radial cross bore in the thick walled cylinder is illustrated in Figure 4. The stresses induced by the cross bore were calculated by assuming the cross bore as an open ended cylinder. In addition, it was assumed that, the curvature of the cylinder had no effect on the stress concentration. The internal radius of the cross bore was denoted as r_i. Whereas, the external radius which was defined as the horizontal distance between the transverse plane of the cross bore and the outside surface of the main cylinder was denoted as b, as shown in Figure 6. Along the outside surface of the cylinder, the external radius b is given by $R_0 \sin\theta$.

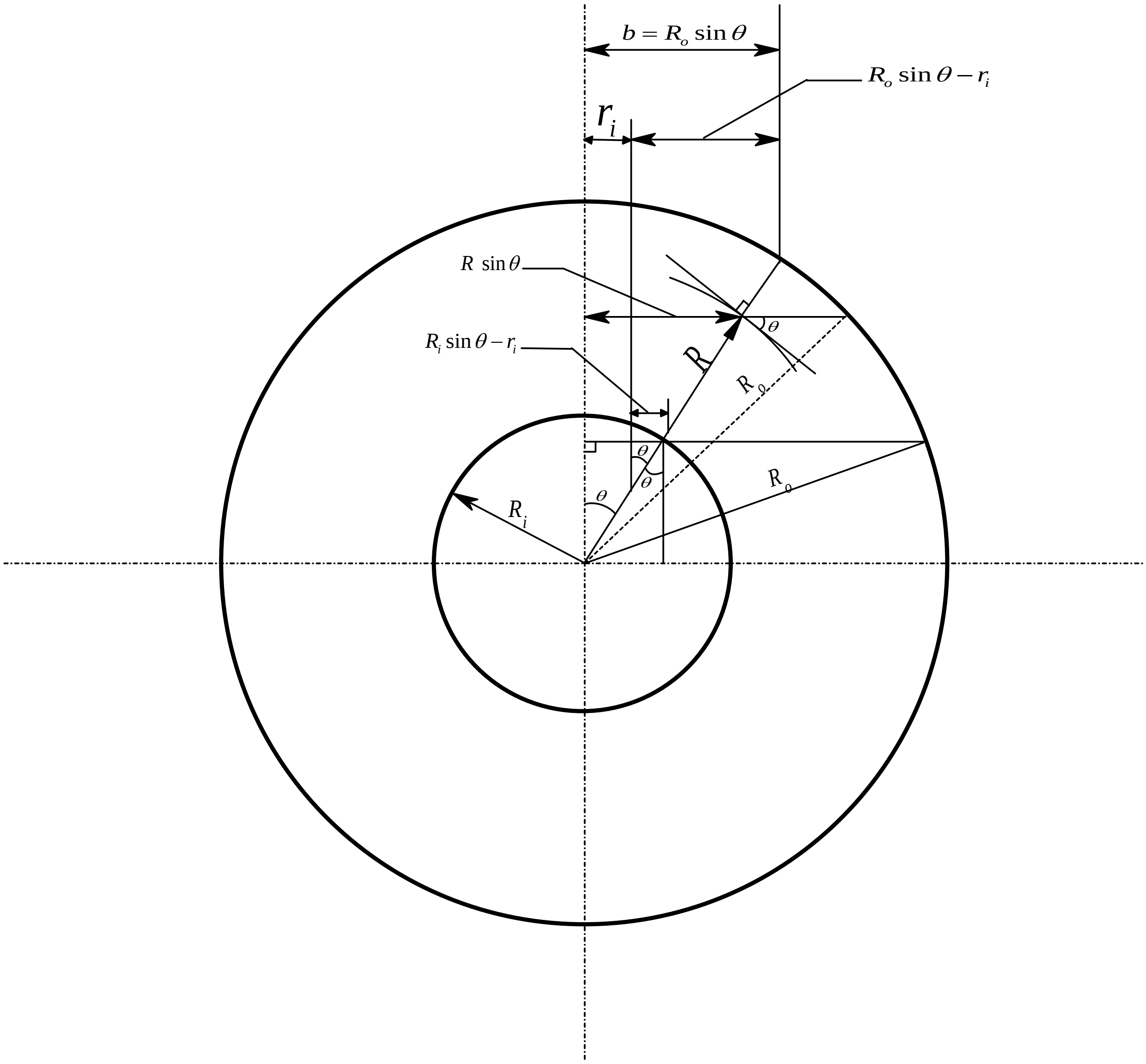

Figure 6 : Cross bore configuration

Where

R_i is the internal radius of the main bore.

R_O is the external radius of the main bore.

r_i is the cross bore radius.

R is the radius at any point along the wall thickness.

The corresponding hoop, σ_{θ_2} and the radial, σ_{r_2} stresses were obtained by assuming the Lame's theory along the pressurised cross bore, as shown in the proceeding expressions;

$$\sigma_{\theta_2} = C + \frac{D}{r^2}; \quad \text{and} \quad \sigma_{r_2} = C - \frac{D}{r^2};$$

Similarly, to obtain the constants C and D, the following boundary conditions were applied. At the inside surface of the cross bore $r = r_i$, the corresponding radial stress $\sigma_{r_2} = -p_i$. Whereas, at the outside surface of the vessel, $r = R_0 \sin\theta$, the corresponding radial stress $\sigma_{r_2} = 0$. From which, the constants were obtained as;

$$C = \frac{P_i r_i^2}{R_0^2 \sin^2\theta - r_i^2}, \text{ and}$$

$$D = \frac{P_i r_i^2 R_0^2 \sin^2\theta}{R_0^2 \sin^2\theta - r_i^2}, \text{ therefore,}$$

$$\sigma_{\theta_2} = \frac{P_i r_i^2}{R_0^2 \sin^2\theta - r_i^2}\left(1 + \left(\frac{R_0 \sin\theta}{r}\right)^2\right) \tag{3.4}$$

$$\sigma_{r_2} = \frac{P_i r_i^2}{R_0^2 \sin^2\theta - r_i^2}\left(1 - \left(\frac{R_0 \sin\theta}{r}\right)^2\right) \tag{3.5}$$

But from the cross bore configuration shown in Figure 4, it can be seen that, at any arbitrary radius along the wall thickness $r = R\sin\theta$. Thus, substituting for $r = R\sin\theta$ in equations 3.4 and 3.5, the above equations became,

$$\sigma_{\theta_2} = \frac{p_i r_i^2}{R_0^2 \sin^2\theta - r_i^2}\left(1 + \left(\frac{R_0}{R}\right)^2\right) \qquad (3.6)$$

$$\sigma_{r_2} = \frac{p_i r_i^2}{R_0^2 \sin^2\theta - r_i^2}\left(1 - \left(\frac{R_0}{R}\right)^2\right) \qquad (3.7)$$

By letting $K = \frac{R_0}{R_i}$ and $m = \frac{R_i}{r_i}$

Therefore, from these two expressions, r_i can be written as $r_i = \frac{R_0}{Km}$

Substituting the expression of r_i in equations 3.6 and 3.7 and solving;

$$\sigma_{\theta_2} = \frac{k^2 m^2 p_i}{k^4 m^4 \sin^2\theta - 1}\left(1 + \frac{R_0^2}{R^2}\right) \qquad (3.8)$$

$$\sigma_{r_2} = \frac{k^2 m^2 p_i}{k^4 m^4 \sin^2\theta - 1}\left(1 - \frac{R_0^2}{R^2}\right) \qquad (3.9)$$

3.2.3.4 Stresses induced by the axial tensile stress due to the closed ends on the main bore cylinder (Step 3).

Axial tensile stress is generated uniformly across the thickness of the cylinder due to the closed ends. Figure 7 shows the configuration of the axial tensile stress in a cross bore thick walled cylinder. The local coordinates are indicated by the direction of stress as shown in Figure 7.

The solution for this configuration was aided by considering an imaginary cylinder of radius R_i, which is represented by the dotted ring as shown in Figure 7. Assuming an elastic system, the total radial stress around the cross bore was found to be composed of two parts (Faupel and Harris, 1957; Gerdeen, 1972; Hearn, 1999).

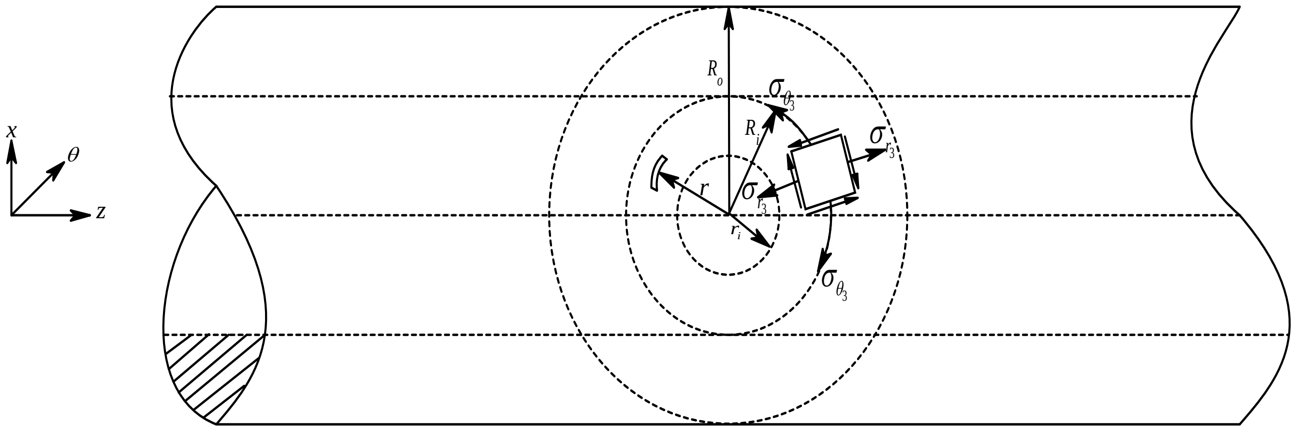

Figure 7: Configuration of the axial tensile stress in a cross bore vessel

The first part entailed stress due to the internal pressure which was considered as a constant radial stress. While, the second part comprised of sinusoidal stress variation, signifying the variation of radial stress across the wall thickness. This form of stress variation represented the required surface stresses at the cross bore, to give the same internal stresses that are present in a similar cylinder without a cross bore (Gerdeen, 1972). Thus, the second part was considered as consisting of a varying radial stress. As a result, the two parts were solved independently as shown in the following section, Step 3a and 3b.

3.2.3.4.1 Stresses induced by a constant radial stress at the cross bore (Step 3a)

The stresses induced by a constant radial stress at the cross bore were calculated by considering the region between the two circular rings, of radii r_i and R_i, as illustrated in Figure 7. Ignoring the effects of the curvature in the main cylinder, the stresses within the two rings correspond to those existing in a thick walled cylinder (Ford and Alexander, 1977). Thus, the Lame's equations was applied within the two rings, formed by radii r_i and R_i. The corresponding hoop $\sigma_{\theta_{3a}}$ and radial $\sigma_{r_{3a}}$ stresses were obtained using the following expressions;

$$\sigma_{\theta_{3a}} = A + \frac{B}{r^2}, \qquad \text{and} \qquad \sigma_{r_{3a}} = A - \frac{B}{r^2}$$

To solve for the constants A and B, the following boundary conditions were applied on the radial stress. At the inner surface of the cross bore $r = r_i$, the corresponding radial stress $\sigma_{r_{3a}} = -p_i$. Whereas, on the outer ring, $r = R_i$ (which also coincides with the inner surface of the main bore), the corresponding radial stress $\sigma_{r_{3a}} = \sigma_z$. Hence, the contributions to the hoop and radial stresses are shown by equations 3.10 and 3.11.

$$\sigma_{\theta_{3a}} = \frac{1}{m^2 - 1}\left[m^2\sigma_z + p_i + m^2\frac{R_i^2}{r^2}(\sigma_z + p_i)\right], \text{ and} \tag{3.10}$$

$$\sigma_{r_{3a}} = \frac{1}{m^2 - 1}\left[m^2\sigma_z + p_i - m^2\frac{R_i^2}{r^2}(\sigma_z + p_i)\right] \tag{3.11}$$

Since $\sigma_{\theta_{3a}}$ and $\sigma_{r_{3a}}$ are principal stresses, there is no shearing stress in the cylinder. Therefore, the maximum shear stress $\tau_{r\theta_{max}}$ at any point along the cross bore was calculated by use of Tresca's theory;

$$\tau_{r\theta_{max}} = \frac{\sigma_{\theta_{3a}} - \sigma_{r_{3a}}}{2}$$

Hence,

$$\tau_{r\theta_{max}} = \frac{R_i^2}{r^2}\left(\frac{m^2}{m^2-1}\right)\left(\sigma_z + p_i\right) \tag{3.12}$$

3.2.3.4.2 Stress induced by the varying radial stress (Step 3b)

The stress distribution induced by the sinusoidal stress variation was solved using the theory of elasticity and stress functions methods (Gerdeen, 1972; Faupel and Fisher, 1981). The trend of the radial and shear stress variation that simulates the stress behaviour present in a similar cylinder without a cross bore was established in the form of polar coordinates (Hearn (1999). At the outer ring, $r = R_i$, which also coincides with the surface of the cylinder bore, the radial stress $\sigma_{r_{3b}}$ is $\frac{1}{2}\sigma_z \cos 2\theta$. Whereas, the corresponding shear stress $\tau_{r\theta_{3b}}$at the same position is $-\sigma_z \sin 2\theta$. Several authors (Timoshenko and Goodier (1951); Geerden (1972); Ford and Alexander (1977); Faupel and Fisher (1981) and Hearn (1999)) have classified the stress function formed under these condition as an axisymmetric biharmonic order. Because the harmonic order denoted the solution as n is equal to 2. This trend, therefore, satisfied the use of the following biharmonic stress function equation φ

$$\varphi = (Cr^2 + D/r^2 + Er^4 + F)\cos 2\theta. \qquad (3.13)$$

The three corresponding stress components generated from this biharmonic stress function, as cited by the authors mentioned in the preceding paragraph were calculated as follows;

$$\sigma_{r_{3b}} = -\left(2C + \frac{6E}{r^4} + \frac{4F}{r^2}\right)\cos 2\theta \qquad (3.14)$$

$$\sigma_{\theta_{3b}} = \left(2C + 12Dr^2 + \frac{6E}{r^4}\right)\cos 2\theta \qquad (3.15)$$

$$\tau_{r\theta_{3b}} = \left(2C + 6Dr^2 - \frac{6E}{r^4} - \frac{2F}{r^2}\right)\sin 2\theta \qquad (3.16)$$

The four constants C, D, E and F, were evaluated by considering the following boundary conditions obtained using radial and shear stresses.

a) With reference to Figure 7, at the surface of the cross bore, $r = r_{i,}$ the corresponding radial stress $\sigma_{r_{3b}} = -p_i$. Specifically, the radial stress on the cross bore surface is equal to the gauge pressure and acts in the opposite direction. Substituting these boundary conditions into equation 3.14,

$$-p_i = -\left(2C + \frac{6E}{r_i^4} + \frac{4F}{r_i^2}\right)\cos 2\theta$$

Which can be re-written as

$$p_i \sec 2\theta = 2C + \frac{6E}{r_i^4} + \frac{4F}{r_i^2} \qquad (3.17)$$

b) With reference to Figure 6, the magnitude of both the radial and the shear stress at the outer surface of the cylinder when the radius $r = b$, is zero. Thus, the expressions for radial and shear stress can be formulated. Using equation 3.14, the following radial stress equation was formulated;

$$0 = -\left(2C + \frac{6E}{b^4} + \frac{4F}{b^2}\right)\cos 2\theta$$

As seen from the preceding expression, the product of the two terms in the right hand side is equal to zero. However, the magnitude of $\cos 2\theta$ varies along the outer surface of the cylinder. Thus, its magnitude is not equal to zero at all points along the surface. Therefore, the first term is equal to zero. Hence,

$$0 = -\left(2C + \frac{6E}{b^4} + \frac{4F}{b^2}\right) \qquad (3.18)$$

Using the same analogy as discussed in the preceding paragraph, the expression for the shear stress was formulated using equation 3.16 as follows;

$$0 = \left(2C + 6Db^2 - \frac{6E}{b^4} - \frac{2F}{b^2}\right)\sin 2\theta$$

Similarly, the magnitude of $\sin 2\theta$ varies along the outer surface of the cylinder. Therefore, the term $\sin 2\theta \neq 0$ at all the points on the cylinder surface. Hence,

$$0 = \left(2C + 6Db^2 - \frac{6E}{b^4} - \frac{2F}{b^2}\right) \qquad (3.19)$$

c) With reference to Figure 7, at the outer ring, the radius $r = R_i$, (which also coincides with the inner surface of the cylinder bore), the corresponding shear stress $\tau_{r\theta_{3b}} = -\sigma_z \sin 2\theta$. Substituting these boundary conditions into equation 3.16;

$$-\sigma_z = 2C + 6DR_i^{\,2} - \frac{6E}{R_i^4} - \frac{2F}{R_i^2} \qquad (3.20)$$

The four equations formed from the boundary conditions are sufficient to solve for the unknown constants C, D, E and F. They are presented inform of a matrix as shown in equation 3.21 hereafter;

$$\begin{bmatrix} 2 & 0 & \frac{6}{r_i^4} & \frac{4}{r_i^2} \\ -2 & 0 & -\frac{6}{b^4} & -\frac{4}{b^2} \\ 2 & 6b^2 & -\frac{6}{b^4} & -\frac{2}{b^2} \\ 2 & 6R_i^2 & -\frac{6}{R_i^4} & -\frac{2}{R_i^2} \end{bmatrix} \begin{bmatrix} C \\ D \\ E \\ F \end{bmatrix} = \begin{bmatrix} P_i \sec 2\theta \\ 0 \\ 0 \\ -\sigma_z \end{bmatrix} \qquad (3.21)$$

The constants from this matrix expression were solved using Cramer's rule with the aid of computer mathematical software, Mathcad Version 15. The iterations of the solutions of the constants are as follows;

$$C = |C| = \frac{\begin{vmatrix} P_i \sec 2\theta & 0 & \frac{6}{r_i^4} & \frac{4}{r_i^2} \\ 0 & 0 & -\frac{6}{b^4} & -\frac{4}{b^2} \\ 0 & 6b^2 & -\frac{6}{b^4} & -\frac{2}{b^2} \\ -\sigma_z & 6R_i^2 & -\frac{6}{R_i^4} & -\frac{2}{R_i^2} \end{vmatrix}}{\begin{vmatrix} 2 & 0 & \frac{6}{r_i^4} & \frac{4}{r_i^2} \\ -2 & 0 & -\frac{6}{b^4} & -\frac{4}{b^2} \\ 2 & 6b^2 & -\frac{6}{b^4} & -\frac{2}{b^2} \\ 2 & 6R_i^2 & -\frac{6}{R_i^4} & -\frac{2}{R_i^2} \end{vmatrix}}$$

$$\mathrm{C} = \frac{P_i R_i^6 r_i^4 + 2\sigma_z \cos 2\theta R_i^4 b^6 - 2\sigma_z \cos 2\theta R_i^4 b^4 r_i^2 + P_i R_i^2 b^4 r_i^4 - 2P_i b^6 r_i^4}{2\cos 2\theta (R_i - b)(R_i + b)(b - r_i)(b + r_i)\left(3R_i^4 b^2 - R_i^4 r_i^2 + R_i^2 b^4 - R_i^2 b^2 r_i^2 - 2b^4 r_i^2\right)} \tag{3.22}$$

$$D = |D| = \frac{\begin{vmatrix} 2 & P_i \sec 2\theta & \frac{6}{r_i^4} & \frac{4}{r_i^2} \\ -2 & 0 & -\frac{6}{b^4} & -\frac{4}{b^2} \\ 2 & 0 & -\frac{6}{b^4} & -\frac{2}{b^2} \\ 2 & -\sigma_z & -\frac{6}{R_i^4} & -\frac{2}{R_i^2} \end{vmatrix}}{\begin{vmatrix} 2 & 0 & \frac{6}{r_i^4} & \frac{4}{r_i^2} \\ -2 & 0 & -\frac{6}{b^4} & -\frac{4}{b^2} \\ 2 & 6b^2 & -\frac{6}{b^4} & -\frac{2}{b^2} \\ 2 & 6R_i^2 & -\frac{6}{R_i^4} & -\frac{2}{R_i^2} \end{vmatrix}}$$

$$\mathrm{D} = \frac{-2\mathrm{P_I}\mathrm{R_i^4}\mathrm{r_i^4} - 3\mathrm{P_i}\mathrm{b^4}\mathrm{r_i^4} + 2\mathrm{P_i}\mathrm{R_i^2}\mathrm{b^2}\mathrm{r_i^4} + 3\mathrm{R_i^4}\mathrm{b^4}\sigma_\mathrm{z}\cos 2\theta - 4\mathrm{R_i^4}\mathrm{b^2}\mathrm{r_i^2}\sigma_\mathrm{Z}\cos 2\theta + R_i^4 r_i^4 \sigma_z \cos 2\theta}{6\cos 2\theta(\mathrm{R_i}-\mathrm{b})(\mathrm{R_i}+\mathrm{b})(\mathrm{b}-\mathrm{r_i})(\mathrm{b}+\mathrm{r_i})\left(3\mathrm{R_i^4}\mathrm{b^2} - \mathrm{R_i^4}\mathrm{r_i^2} + \mathrm{R_i^2}\mathrm{b^4} - \mathrm{R_i^2}\mathrm{b^2}\mathrm{r_i^2} - 2\mathrm{b^4}\mathrm{r_i^2}\right)} \qquad (3.23)$$

$$E = |E| = \frac{\begin{vmatrix} 2 & 0 & P_i \sec 2\theta & \frac{4}{r_i^2} \\ -2 & 0 & 0 & -\frac{4}{b^2} \\ 2 & 6b^2 & 0 & -\frac{2}{b^2} \\ 2 & 6R_i^2 & -\sigma_z & -\frac{2}{R_i^2} \end{vmatrix}}{\begin{vmatrix} 2 & 0 & \frac{6}{r_i^4} & \frac{4}{r_i^2} \\ -2 & 0 & -\frac{6}{b^4} & -\frac{4}{b^2} \\ 2 & 6b^2 & -\frac{6}{b^4} & -\frac{2}{b^2} \\ 2 & 6R_i^2 & -\frac{6}{R_i^4} & -\frac{2}{R_i^2} \end{vmatrix}}$$

$$E = \frac{R_i^2 b^4 r_i^2 \left(3P_i R_i^4 r_i^2 - P_i b^4 r_i^2 - 2P_i R_i^2 b^2 r_i^2 + 2R_i^2 b^4 \sigma_z \cos 2\theta - 2R_i^2 b^2 r_i^2 \sigma_z \cos 2\theta\right)}{6 \cos 2\theta (\mathrm{R_i} - \mathrm{b})(\mathrm{R_i} + \mathrm{b})(\mathrm{b} - \mathrm{r_i})(\mathrm{b} + \mathrm{r_i})\left(3\mathrm{R_i^4 b^2} - \mathrm{R_i^4 r_i^2} + \mathrm{R_i^2 b^4} - \mathrm{R_i^2 b^2 r_i^2} - 2\mathrm{b^4 r_i^2}\right)} \qquad (3.24)$$

$$F = |F| = \frac{\begin{vmatrix} 2 & 0 & \frac{6}{r_i^4} & P_i \sec 2\theta \\ -2 & 0 & -\frac{6}{b^4} & 0 \\ 2 & 6b^2 & -\frac{6}{b^4} & 0 \\ 2 & 6R_i^2 & -\frac{6}{R_i^4} & -\sigma_z \end{vmatrix}}{\begin{vmatrix} 2 & 0 & \frac{6}{r_i^4} & \frac{4}{r_i^2} \\ -2 & 0 & -\frac{6}{b^4} & -\frac{4}{b^2} \\ 2 & 6b^2 & -\frac{6}{b^4} & -\frac{2}{b^2} \\ 2 & 6R_i^2 & -\frac{6}{R_i^4} & -\frac{2}{R_i^2} \end{vmatrix}}$$

$$F = \frac{b^2\left(72P_i b^6 r_i^4 - 144P_i R_i^6 r_i^4 + 72P_i R_i^4 b^2 r_i^4 - 72R_i^4 b^6 \sigma_z \cos 2\theta + 72{R_i}^4 b^2 r_i^4 \sigma_z \cos 2\theta\right)}{\cos 2\theta\left(432R_i^6 b^4 - 576R_i^6 b^2 r_i^{23} + 144R_i^6 r_i^4 - 288R_i^4 b^6 + 288R_i^4 b^4 r_i^2 - 144R_i^2 b^8 + 144R_i^2 b^4 r_i^4 + 288b^8 r_i^2 - 288b^6 r_i^4\right)} \qquad (3.25)$$

3.2.3.5 Stresses due to the internal pressure at the cross bore (Step 4)

Stress distribution due to the internal pressure at the cross bore was considered to be acting inside a thick walled cylinder with an infinite external radius, since the cylinder wall is “joined on itself” (Fessler and Lewin, 1956; Geerden , 1972; Ford and Alexander, 1977). Applying the Lame equation on the configuration shown in Figure 6 and assuming an infinite external radius that is $b \rightarrow \infty$

$$\sigma_{\theta_4} = \frac{p_i}{\left(1 - \frac{r_i^2}{b^2}\right)}\left(1 + \frac{r_i^2}{b^2}\right) \rightarrow p_i, \text{ and} \tag{3.26}$$

$$\sigma_{r_4} = -\frac{p_i}{\left(1 - \frac{r_i^2}{b^2}\right)}\left(1 - \frac{r_i^2}{b^2}\right) \rightarrow -p_i \tag{3.27}$$

3.2.3.6 Superposition of stresses at the cross bore surface

The direction of stress components produced by the four cases considered in the preceding sections was established before superimposing the results. It was noted that the hoop stress component produced by the main cylinder and that which was induced by the cross bore acted in the same direction. However, the radial stress component induced by the cross bore was found to act in the axial direction of the main cylinder. However, there was no axial component produced by cross bore, i.e., in the radial direction of the main cylinder, as it was considered an open ended cylinder.

The summation of the stress distribution along the cross bore was done with reference to the direction of the global coordinates of the three principal stresses, as shown in Figure 3. They are briefly discussed below;

3.2.3.6.1 Stress component in the hoop direction of the main cylinder

The total hoop stress $\sigma_{\theta_{Total}}$ along the cross bore, which can also be taken as the maximum principal stress, was obtained by the summation of the corresponding hoop equations, in all the four cases considered,

$$\sigma_{\theta_{Total}} = \sigma_{\theta_1} + \sigma_{\theta_2} + \sigma_{\theta_{3a}} + \sigma_{\theta_{3b}} + \sigma_{\theta_4}$$

$$\sigma_{\theta_{Total}} = \frac{p_i}{k^2 - 1}\left(1 + \left(\frac{R_0}{R}\right)^2\right) + \frac{k^2 m^2 p_i}{k^4 m^4 \sin^2 \theta - 1}\left(1 + \frac{R_0^2}{R^2}\right) + \frac{1}{m^2 - 1}\left[m^2 \sigma_z + p_i + m^2 \frac{R_i^2}{r^2}\left(\sigma_z + p_i\right)\right] +$$

$$\left(2C + 12Dr^2 + \frac{6E}{r^4}\right)\cos 2\theta + p_i \qquad (3.28)$$

3.2.3.6.2 Stress component in radial direction of the main cylinder

The radial stress, $\sigma_{r_{Total}}$, at the inside surface of the cross bore as well as that at the main bore was found to be equal and opposite to the internal pressure (gauge pressure)

$$\sigma_{r_{Total}} = \sigma_r = -p_i \tag{3.29}$$

3.2.3.6.3 Stress component in axial direction of the main cylinder

The total stress distribution for this component was obtained by adding all the stresses acting in the axial direction. However, it was noted that the axial stress generated by the main cylinder at the cross bore surface was zero, as it was being relieved by the cross bore. Hence;

$$\sigma_{z_{Total}} = \sigma_{r_2} + \sigma_{r_{3a}} + \sigma_{\theta_{3b}}$$

$$\sigma_{z_{Total}} = \frac{k^2 m^2 p_i}{k^4 m^4 \sin^2\theta - 1}\left(1 - \frac{R_0^2}{R^2}\right) + \frac{1}{m^2 - 1}\left[m^2\sigma_z + p_i - m^2\frac{R_i^2}{r^2}\left(\sigma_z + p_i\right)\right] - \left(2C + \frac{6E}{r^4} + \frac{4F}{r^2}\right)\cos 2\theta \tag{3.30}$$

The maximum shear stress in the cylinder as well as the shear stress, $\tau_{r\theta_{max}}$, in the $r\theta$ direction, can also be calculated using equations 3.12 and 3.16, as discussed in the preceding sections.

3.2.3.7 Determination of the stress concentration factor

The stress concentration factor (SCF) was defined as the ratio of localised critical stresses in a cross bore cylinder to the corresponding stresses in a similar cylinder without a bore (Ford and Alexander, 1977). The definition exemplifies the intensity of stress concentration at each particular point of interest. SCFs can be determined for various stress criteria such as maximum tensile stress (hoop) , Von Mises or Tresca. The choice to use a particular criterion depends on the working conditions of the vessel.

The hoop stress concentration factor SCF_{Hoop} is given by the following expression;

$$SCF_{Hoop} = \frac{\sigma_{\theta_1} + \sigma_{\theta_2} + \sigma_{\theta_{3a}} + \sigma_{\theta_{3b}} + \sigma_{\theta_4}}{\sigma_{\theta_1}}$$

$$SCF_{Hoop} = \frac{\frac{p_i}{k^2-1}\left(1+\left(\frac{R_0}{R}\right)^2\right) + \frac{k^2 m^2 p_i}{k^4 m^4 \sin^2\theta - 1}\left(1+\frac{R_0^2}{R^2}\right) + \frac{1}{m^2-1}\left[m^2\sigma_z + p_i + m^2\frac{R_i^2}{r^2}(\sigma_z + p_i)\right] + \left(2C + 12Dr^2 + \frac{6E}{r^4}\right)\cos 2\theta + p_i}{\frac{p_i}{k^2-1}\left(1+\left(\frac{R_0}{R}\right)^2\right)}$$

(3.31)

The SCFs for Von Mises and Tresca's theories can also be calculated analytically using their respective formulae based on the same definition as in equation 3.31. Their corresponding SCFs expressions are shown hereunder;

$$\mathrm{SCF}_{\mathrm{Vonmises}} = \frac{\left(\sigma_{\theta_T} - \sigma_{Z_T}\right)^2 + \left(\sigma_{Z_T} - \sigma_{r_T}\right)^2 + \left(\sigma_{r_T} - \sigma_{\theta_T}\right)^2}{\left(\sigma_{\theta_1} - \sigma_{Z_1}\right)^2 + \left(\sigma_{Z_1} - \sigma_{r_1}\right)^2 + \left(\sigma_{r_1} - \sigma_{\theta_1}\right)^2} \tag{3.32}$$

$$\mathrm{SCF}_{\mathrm{Tresca}} = \frac{\sigma_{\theta_T} - \sigma_{r_T}}{\sigma_{\theta_1} - \sigma_{r_1}} \tag{3.33}$$

These Von Mises and Tresca's stress concentration factors enable comparison between working stresses in cylinders with different sizes subjected to varying loading magnitudes.

3.2.4 Three dimensional finite element analysis of radial circular cross bore

Finite element analyses were performed on the high pressure vessels with the same dimensions as those studied analytically in section 3.2.2, for the purpose of verifying the results. The cross bored high pressure vessel was analysed using a commercial software program called Abaqus version 6.16. The Abaqus software was chosen for this study due to its availability as well as the capability to perform axisymmetric modelling in pressure vessels. Owing to the symmetrical configuration of the pressure vessel, only an eighth of the structure was analysed. In this modelling section, a total of 35 different part models were created and analysed.

3.2.4.1 Modelling using Abaqus software

The following standard procedure used in Abaqus modelling software was followed;

3.2.4.1.1 Creation of a model

A three dimensional deformable solid body was created by sketching an eighth profile of the pressure vessel face. The face of the pressure vessel was then extruded to form the depth of the cylinder. The depth of the cylinder was equal to three times the cylinder's external diameter. As stated by the Saint-Venant's principle, the depth of cylinder should be 2.5 times longer than the outside diameter. This restricts the effects of the closed ends' closures of the cylinder vessels from being transmitted to the other far end of the cylinder.

The cross bore was then created at the other far end of the cylinder. The cross bore was created using a cut-extrude tool at the radial position of the vessel. One of the model profiles created at this stage is shown in Figure 8;

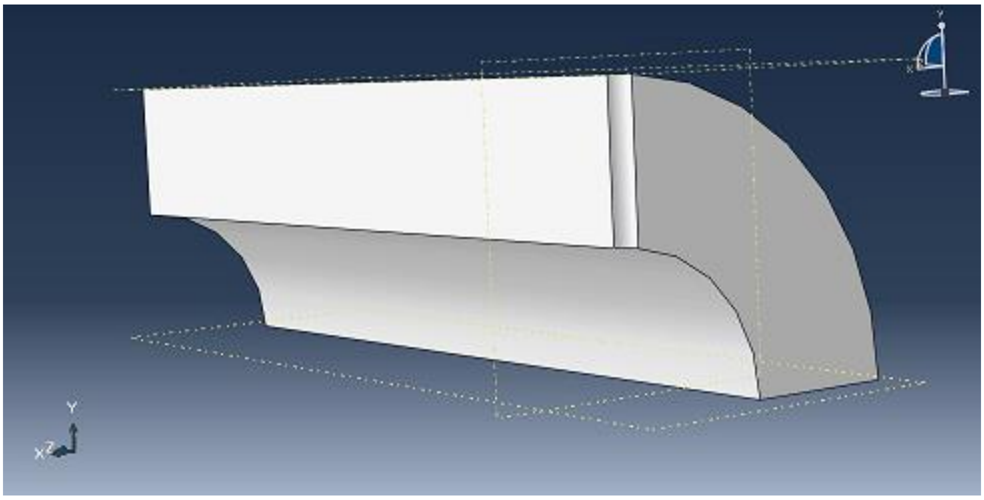

Figure 8: Part profile for K= 2 having cross bore-main bore ratio of 0.1

3.2.4.1.2 Creation of material definition

For this stress analysis problem, a linear elastic model with material properties as indicated in Table 7 was assumed throughout in the modelling process. The material properties chosen for this simulation were similar to those commonly used in the technical literature of high pressure vessels (Chaudhry *et al.*, 2014; Choudhury *et al.*, 2014).

Table 7: Material properties for the static analysis (Chaudhry *et al.,* (2014))

Parameter	Value
Young's Modulus of Elasticity	190 GPa
Poisson's ratio	0.29
Density	7800 Kg/m^3

3.2.4.1.3 Assigning of section properties and model assembly

The section properties of the model were defined as being solid and assigned to the entire profile previously created in Figure 8. This action was then followed by creation of a single assembly. A single assembly usually contains all the geometry in the finite element model. This procedure allowed the creation of a part instance that is independent of the mesh. The model was then oriented in line with the global Cartesian co-ordinates axes that is X, Y and Z axes.

3.2.4.1.4 Analysis configuration

The analysis to be used for this simulation was configured by creating a static pressure step. It is worthwhile to mention that the application of different types of loads and boundary conditions depend on the total number of analysis steps created. Moreover, the creation of a set out point, which defines the history output, was done. The set out point was positioned at the intersection of the main bore and the cross bore and this was followed by the selection of stress, as the required field output request.

3.2.4.1.5 Application of boundary conditions

To prevent any rigid movement of the model, symmetry conditions were applied at the cut section of the cylinder. The symmetry conditions were applied at cut regions in X, Y and Z axes. The careful application of these boundary conditions ensured that no errors occurred due to the Poisson's effect. According to Adams and Askenazi (1999) the Poisson's effect occurs due to incorrect positioning of boundary conditions. The incorrect boundary conditions restrict the material deformation causing a couple strain, hence the occurrence of the Poisson's effect. Note that, the Poisson's effect error is given as 5% (Adams and Askenazi, 1999).

3.2.4.1.6 Applying the load

The pressure vessel was loaded with an internal pressure at both the main bore and the cross bore. The internal pressure was taken as 1Pa, being the most common pressure used in pressure vessels (Gerdeen, 1972). In addition, a uniform axial stress, calculated by using equation 3.3 for each thickness ratio, was applied at the far end of the vessels. This axial stress simulated the end effects generated by the closed end closures in the pressure vessels. The axial stress calculated for each thickness ratio is tabulated in Table 8, respectively;

Table 8: Axial Stresses

K	1.4	1.5	1.75	2.0	2.25	2.5	3.0
σ_z (MN/m^2)	1.04166	0.80	0.485	0.333	0.246	0.190	0.111

3.2.4.1.7 Meshing the model

The local mesh refinement of the model was done using a combination of both the H-element and the P-element techniques. The H-element refinement technique was achieved through two stages. In the first stage, the model was divided into small geometrical sections. In the second stage, the mesh around the cross bore region was biased by increasing the number of elements, commonly referred to as mesh density. In fact, the size of element chosen for this study ranged from 0.003 m to 0.004 m. This high mesh density around the cross bore region increased the capture of the localised stress concentration. This approach gives results with a high level of accuracy without significantly increasing the computer run time.

Alternatively, the P-refinement technique approach which depends on the degree of polynomial was achieved by use of the second order differential equations with reduced integration.

The mesh verification was carried out to establish the element quality and identify any distorted elements. The degree of element distortion depends on the capability of the software and its tolerances, element shape and size, among other factors. The guidelines used to determine the nature of distortions and inform the user on warnings and errors occurring due to the shape and size of the element, are tabulated in Table 9.

Table 9: Guidelines for element distortion

Characteristics	Parameter	Element failure criteria
Shape	Quad-face corner angle	$< 10^0$ and $> 160^0$
	Aspect ratio	> 10
Size	Geometric deviation factor	> 0.2 m
	Shorter edge	> 0.01 m
	Longer edge	> 1 m

Generally, element distortion leads to erroneous results. Thus, to eliminate the occurrence of element distortion, the percentage tolerance for both the element warnings and errors were kept at zero. In addition, the choice of element used for this modelling, was made carefully so as not to introduce element distortions. According to Abaqus 6.16 software documentation guidelines, only second order hexahedral and tetrahedral elements are recommended for stress concentration problems. The elements used were 20-noded second order, C3D20R hexahedral (brick) isoparametric in cylinders with the following cross bore to main bore ratios; 0.1, 0.3, 0.5, and 0.7. Hexahedral elements usually give results with a high degree of accuracy (Fagan, 1992) compared to other elements.

On the other hand, second order C3D10 tetrahedral elements with 10 nodes were used for pipe junction models. Tetrahedral elements are less sensitive to the initial shape of the element, therefore, their vulnerability to distortion is low. A meshed profile of the model part is shown in Figure 9.

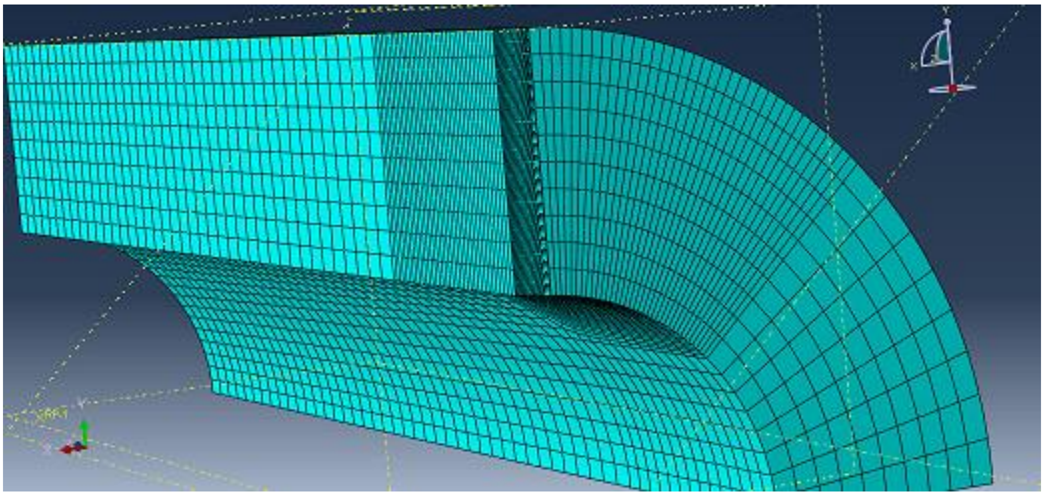

Figure 9: Meshed profile for K = 2 having cross bore- main bore ratio of 0.1

3.2.4.1.8 Creation and submission of the job for analysis

At this stage, the job for each model was created and submitted for analysis. Usually, Abaqus software computes stresses directly at the interior locations of the element known as Gauss points. The calculated stresses at the Gauss points are then extrapolated to the nodes on the element boundary. Thus, different stresses are calculated at each adjacent element. The stress at each node is given by the average stress between the two adjacent elements. Principally, the accuracy of the results depends on the quality of the mesh and its density. In this study, the degree of the accuracy of the results as well as the mesh convergence, were confirmed by comparing the obtained FEA results, with their corresponding analytical results in areas far away from the cross bore. It was assumed that the effects of the cross bore are limited only to the area surrounding it, usually about 2.5 cross bore diameters.

3.2.4.1.9 Viewing the results

The results of this modelling were presented in the form of filled contour plots. These contour plots show the variation of stress along the surface of the model. The stress pattern given by these contour plots usually give a general overview of stress distribution. This stress distribution can also be compared with the expected results for convergence. An example of a stress contour plot showing the position and magnitude of maximum stress of one of the part models created in Figure 8 is shown in Figure 10.

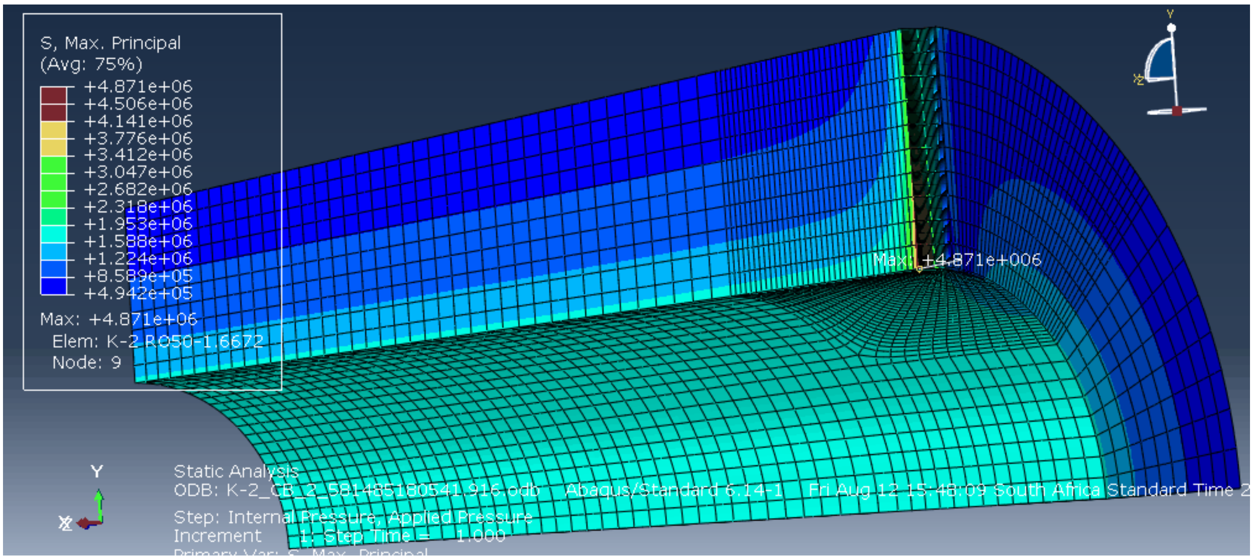

Figure 10: Contour plot of the part model for K=2 with cross bore-main bore ratio of 0.1

The nodes along the transverse edge of the cross bore edge were probed for different types of stress. In this modelling section, only the maximum-, mid- and minimum principal stresses were investigated. The results were presented per unit pressure for ease of the comparisons, since the analysis was performed under elastic conditions.

3.3 OPTIMISATION OF THE CROSS BORE

3.3.1 Introduction

Most of the fatigue failures that occur in high pressure vessels are mainly due to the high magnitude of the hoop stress concentration factor (Masu, 1997), among other factors. It is, therefore, necessary to design for an optimal minimum hoop stress concentration in order to reduce the occurrence of fatigue failures. Stress concentrations in cross bored high pressure vessels depend on the geometric design of the cross bore (Kharat and Kulkarni, 2013). The major geometric parameters in the design of the cross bore are size ratio (cross bore to main bore ratio), location, shape, obliquity angle and thickness ratio. The combination of these geometric design parameters determines the magnitude of the stress concentration. Therefore, one of the aims of this study was to establish an optimal combination of the major geometric design parameters that gives the minimum hoop stress concentration factor.

Optimisation design procedure of the cross bore was undertaken to establish the optimal combination of the major geometric parameters. The analysis was performed using a finite element analysis computer software, called Abaqus version 6.16. Optimisation of each geometric design parameter was performed independently. This mode of analysis is referred to as one factor at a time.

At each optimisation stage, the model solution with minimum hoop stress concentration was selected for the next geometric optimisation analysis. The order used for the geometric optimisation for each thickness ratio was as follows;

1. Selection of the radial circular cross bore size which gives minimum SCF. The cross bore size with minimum SCF is hereafter referred to as optimum sized circular cross bore.

2. Offsetting of the optimum sized circular cross bore to establish an offset position which gives minimum SCF. The offset position with minimum SCF is hereafter referred to as optimum offset position.
3. Determining the optimal elliptical cross bore diameter ratio.
4. Offsetting of the optimum sized elliptical cross bore to establish an offset position which gives minimum SCF
5. Inclination of the optimum sized circular hole at the optimum offset position to determine an oblique angle that gives minimum SCF.

The optimisation design procedure discussed in the preceding paragraphs established a geometrically optimised cross bore. The geometrically optimised cross bore had the minimum SCF after considering the major geometric design parameters. The geometrically optimised cross bore was then subjected to varying fluid temperature to determine its effects on the thermo-mechanical stress concentration.

The optimisation design procedure adopted in this study is briefly described as follows:

3.3.2 Size of the cross bore

With reference to section 3.1, a three dimensional finite element analysis was performed on cylinders with seven different thickness ratios of 1.4, 1.5, 1.75, 2.0, 2.25, 2.5 and 3.0, respectively. Throughout the analysis the diameter of the main bore was taken as 0.05 m. On each of these thickness ratios, five different circular radial cross bores, having cross bore to main bore ratios of 0.1, 0.3, 0.5, 0.7 and 1.0 were investigated.

The results from 35 part models analysed, revealed that the lowest stress concentration factors occurred on the smallest cross bore with a cross bore to main bore ratio of 0.1. Therefore, the cross bore with size ratio of 0.1 was selected as the optimised circular cross bore size. Therefore, only the optimised circular cross bore was considered for further geometric optimisation analysis.

3.3.3 Location of the cross bore

In this section, the modelling procedure of the circular and elliptical shaped cross bores is briefly described:

3.3.3.1 Optimal offset of a circular shaped cross bore

The optimum location was obtained by offsetting optimum sized cross bore with a cross bore to main bore ratio of 0.1, at four different positions along the longitudinal X axis of the cylinder. Throughout this study, the main bore radius was taken as 25 mm. The four offset distances which were investigated were 6.0, 12.0, 17.125 and 22.5 mm. The offset distance was measured from the central axis of the main cylinder to the transverse axis of the cross bore.

The chosen offset distances at 12.0 mm and 22.5 mm were relatively similar to those suggested in the technical literature by Cole *et al.* (1976) and Masu (1998). Whereas, the 6.0 mm and 17.125 mm offset distances were chosen arbitrarily at the mid location to investigate the stress behaviour at those points.

In this modelling section, a total of 28 part models were created and analysed. A similar modelling procedure to the one detailed in section 3.2.4.1 was performed, with slight differences in part creation and meshing steps only. In the part creation step, the cross bore was formed by using cut revolve tool, while applying full boundary constraints on the cross bore. One of the part models created in this section is shown in Figure 11.

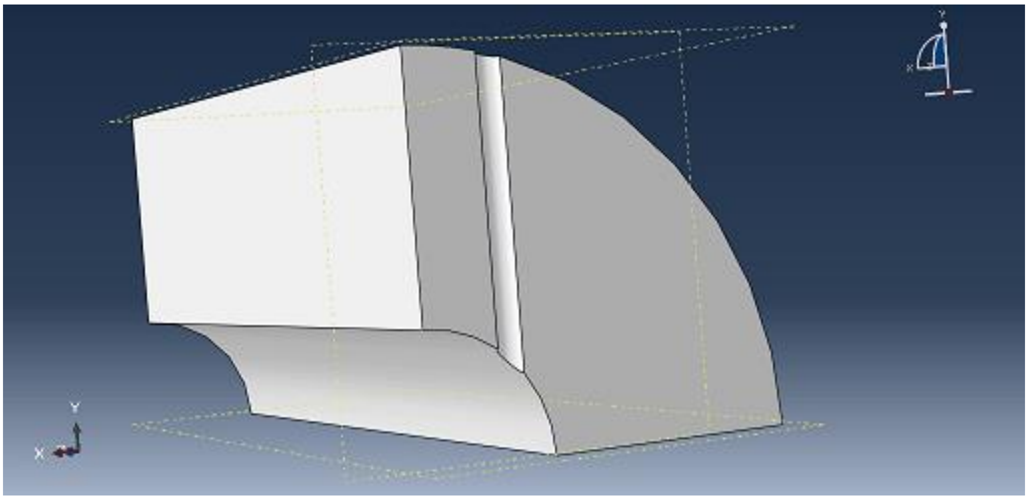

Figure 11: Part model for K = 3.0 having a cross bore-main bore ratio 0.1, offset at 17.125 mm.

Similarly, the meshing of the model was done by dividing the part model into small regions. Second order tetrahedral elements having 10 sided nodes were used for meshing. The meshing was biased around the cross bore region. The corresponding meshed profile of the part model shown in Figure 11 is shown in Figure 12.

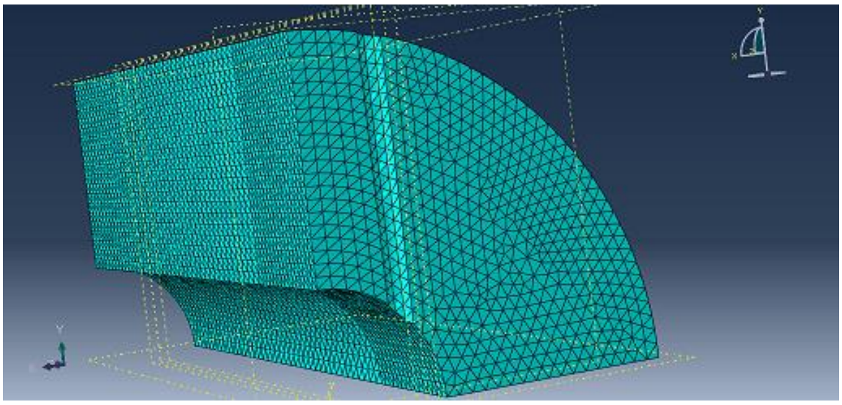

Figure 12: Meshed model for K = 3.0 having cross bore-main bore ratio of 0.1, offset at 17.125 mm

3.3.3.2 Optimal diameter ratio of an elliptical cross bore

The major diameter of the elliptically shaped cross bore was chosen to coincide with the diameter of the optimum sized circular cross bore as cited in reviewed literature by Masu (1997) study. Preliminary investigations were then carried out to establish the optimal diameter ratio. A cylinder with thickness ratio of 2.0 was arbitrarily chosen. Cross bores with major to minor diameter ratios of 1.33, 2.0, 2.5 and 5.0 were investigated. The magnitudes of hoop stress concentration factor obtained in this preliminary investigation are tabulated in Table 10.

Table 10: Maximum hoop stress for various cross bore diameter ratios for K = 2.0

Major to minor diameter ratio	1.33	2.0	2.5	5.0
Stress concentration factor	2.30	1.89	2.14	2.48

The diameter size ratio of 2.0 gave the lowest SCF at 1.89. Therefore, this size ratio was selected as the optimal diameter size ratio in elliptically shaped cross bores. This finding was in agreement with other previous studies done by Harvey (1985) and Makulsawatudom *et al.*, (2004). Harvey (1985) had studied similar elliptical cross bores in thin walled cylinders. The study had reported an optimal SCF of 1.50 when the elliptical diameter ratio was 2.

3.3.3.3 Optimal offset of an optimal elliptical cross bore

The optimised elliptically shaped cross bore was modelled at the same offset position with those of the circularly shaped cross bore discussed earlier. Similar to the circularly shaped cross bores, the offset positions studied were 0, 6.0, 12.0, 17.125 and 22.5 mm. This approach enabled effective comparison of output stresses from both the elliptical and circular cross bore models. The cross bore was positioned such that the minor diameter of the cross bore was parallel with the axial direction of the cylinder, since this cross bore arrangement gives the lowest stress concentration, as suggested by previous studies done by Faupel and Fisher, (1981) and Makulsawatudom *et al.,* (2004).

A total of 35 different part models were created and analysed in this section. The same Abaqus modelling procedure described in section 3.2.4.1 was followed. One of the created part profiles, together with its corresponding mesh, is shown in Figure 13. The mesh was created using tetrahedral elements.

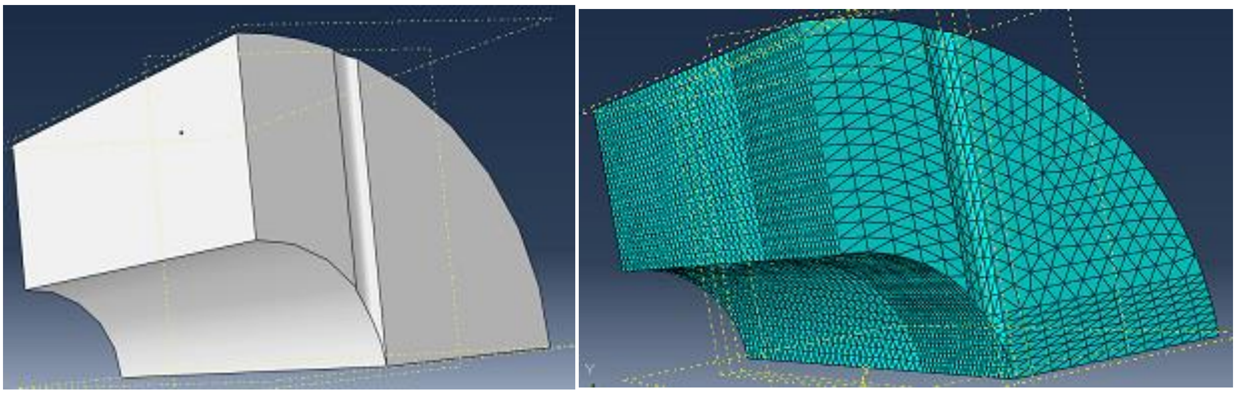

Figure 13: Part profile together with its corresponding mesh for K= 2.5 having elliptical cross bore offset at 17.125 mm.

3.3.4 Oblique angle of a cross bore

The modelling results obtained by offsetting both the circular and elliptically shaped cross bores in the previous sections, revealed that the lowest hoop stress concentration occurred at the circular cross bore, offset at 22.5 mm. Thus, the offset position of 22.5 mm was chosen as the optimised offset position.

At this optimised offset position, the optimised circular cross bore was inclined at 6 different angles. The inclination angles studied were 15^0, 30^0, 45^0, 60^0, 75^0 and 90^0. The first four inclination angles, were chosen to coincide with those investigated by Cheng (1978) and Nihous *et al* (2008) on radially positioned cross bores for comparison. The inclined circular cross bores were created using the cut revolve tool technique. The axis of the cross bore axis was fully constrained at each angle of inclination.

The Abaqus modelling procedure described in section 3.2.4.1 was adopted. In this modelling section of oblique cross bores, a total of 42 part models were created and analysed. One of the created part profiles, together with its corresponding tetrahedral element mesh, is shown in Figure 12.

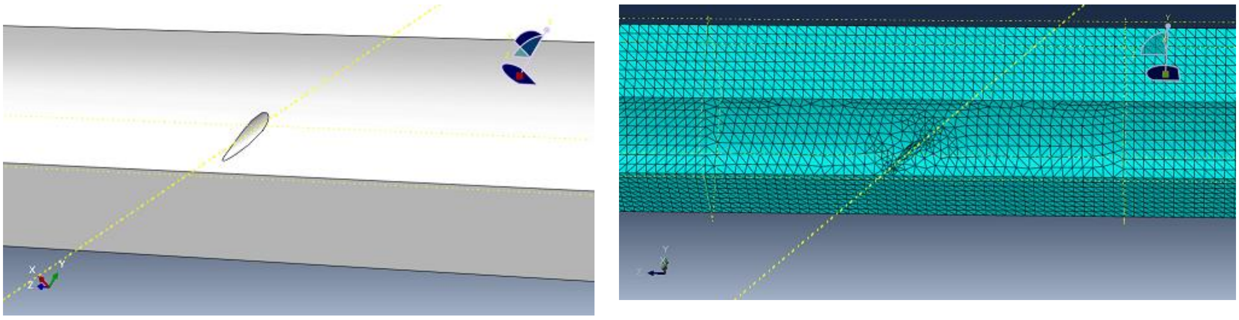

Figure 14: A view at the inside surface of the main bore cylinder of the chosen part profile together with its corresponding mesh, for a circular cross bore having cross bore-main bore ratio of 0.1, inclined at 45^0 from an offset position of 22.5 mm.

3.4 COMBINED THERMO-MECHANICAL STRESS ANALYSIS

Combined thermo-mechanical stresses on the geometrically optimised cross bore for each vessel thickness was determined using thermo-couple analysis. The internal fluid pressure and temperature was taken as $1\mathrm{MN/m^2}$ and 300 ^{o}C, respectively, as recommended in technical literature by Zhang *et al.*, (2012), Chaudhry *et al.*, (2014) and Choudhury *et al.*, (2014) . The ambient temperature was taken as 20 ^{o}C. The properties of the material used are listed in Table 11.

Table 11: Material property for the thermal analysis (Chaudhry *et al.*, (2014))

Parameter	Value
Thermal conductivity	17 W/m K
Thermal expansion coefficient	11E-6 mm/mm/^{o} C
Specific heat	0.48 KJ/kg K

A linear transient condition was assumed throughout the modelling to simulate the starting-up conditions. The stresses due to thermo-mechanical loading were recorded at 17 different nodal temperatures ranging from 20 ^{o}C to 300 ^{o}C for each thickness ratio. A total of 14 different part models were created and analysed in this section.

The results generated by these research methods are presented and discussed in Chapter Four.

CHAPTER FOUR: RESULTS AND DISCUSSION

4.1 INTRODUCTION

In this Chapter, the results obtained by the methods described in the preceding Chapter are presented in the form of graphs and tables. These results and their implications are further discussed in relation to the existing literature.

4.2 CORRELATION OF ANALYTICAL AND NUMERICAL SOLUTIONS IN RADIAL CIRCULAR CROSS BORE

The results obtained by the analytical solution developed in Chapter 3 were compared with their corresponding ones generated by finite element modelling. The numerical solution was selected as the reference method, since it had been authenticated. This reference method selection aided the calculation of error percentages between the two methods. Hence, the solution validation was computed based on the percentage error. In most practical engineering applications, a percentage error less than 5% is regarded to be within the acceptable error margin (Ford and Alexander, 1977). Thus, this standard practice was adopted in this study to determine the degree of correlation between the two methods.

The analytical and numerical results presented in this section are those of hoop, radial and axial stresses along the transverse edge AA of the radial cross bore as shown in Figure 15.

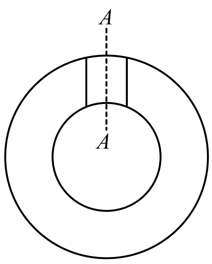

Figure 15: Configuration of the radial cross bore

The analytical results for hoop, radial and axial stresses were computed using equations 3.28, 3.29 and 3.30, respectively. Since all the analyses were performed under elastic conditions, the results were presented per unit pressure for ease of comparison.

4.2.1 Hoop stress component in the direction of the main cylinder

The results generated from the hoop stress along the transverse edge of the radial cross bore for all the pressure vessels studied in section 3.2.2 are presented under the following subheadings;

4.2.1.1 Cross bore to main bore ratio of 0.1

In this section, results of a high pressure vessel with main bore to cross bore size ratio of 0.1 are presented in figures 16 - 22; for thickness ratios, K = 1.4, 1.5, 1.75, 2.0, 2.25, 2.5 and 3.0:

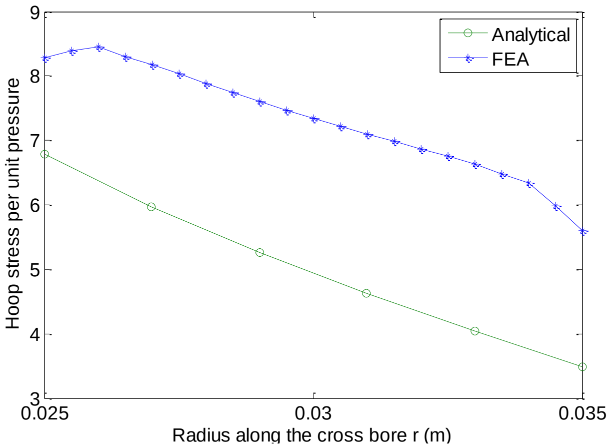

Figure 16: K = 1.4 CB = 0.1

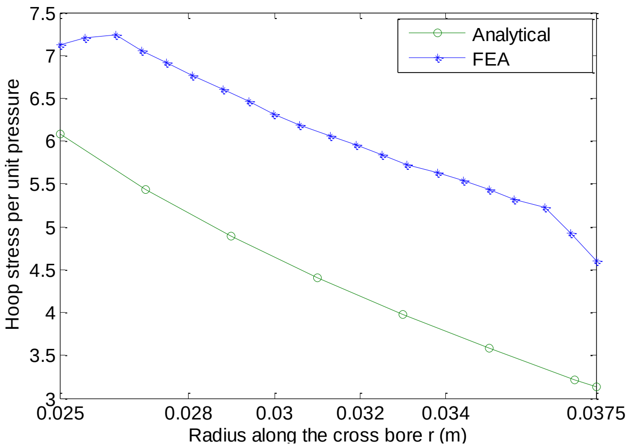

Figure 17: K = 1.5 CB = 0.1

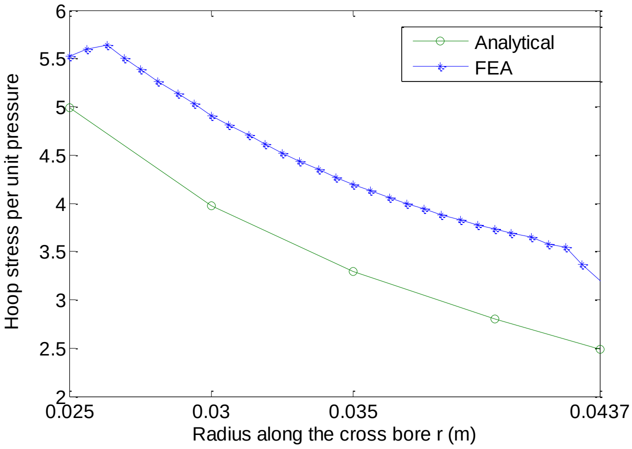

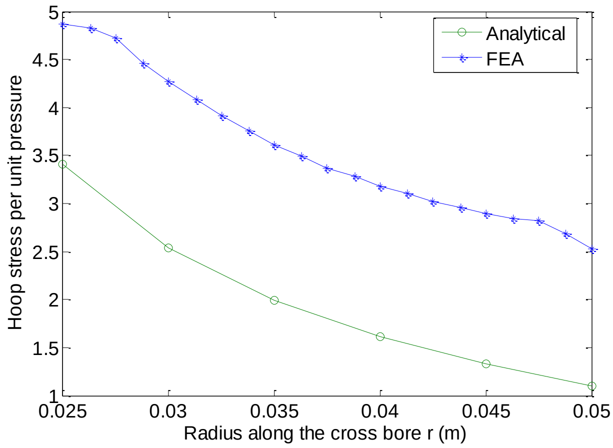

Figure 18 : K = 1.75 CB = 0.1

Figure 19 : K = 2.0 CB = 0.1

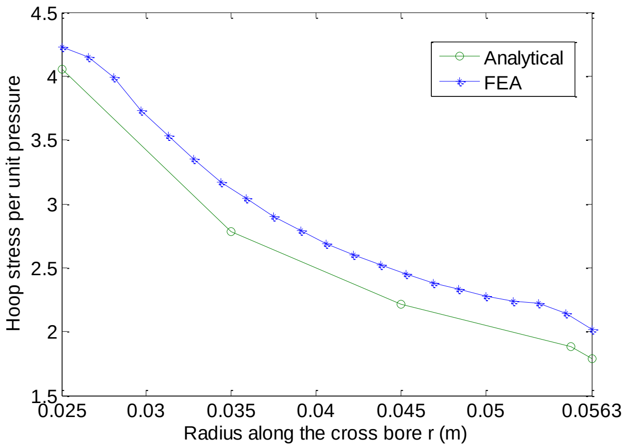

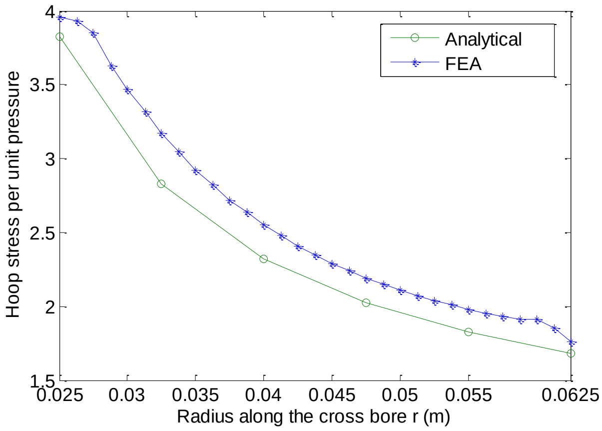

Figure 20: K = 2.25 CB = 0.1

Figure 21: K = 2.5 CB = 0.1

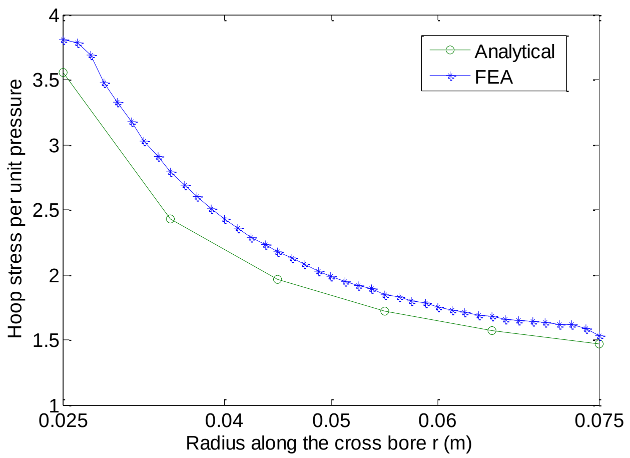

Figure 22 : K = 3.0 CB = 0.1

Figures 16 - 22: Hoop stress distribution per unit pressure for various thickness ratios along a radial circular Cross Bore (CB), having cross bore to main bore size ratio of 0.1.

From Figures 16 to 22, it can be seen that the analytical method predicted lower stress values in comparison to those obtained by FEA. Notable disparity of the results given by analytical and numerical methods were seen in Figures 16 and 18. However, as the thickness ratio is increased, the solution given by the two methods began to converge, as illustrated by Figures 20 to 22.

With the exception of thickness ratios 1.4, 1.5 and 1.75, the magnitude of hoop stress was highest at the intersection between the cross bore and the main bore. However, the hoop stress reduced gradually along the cross bore depth. For K=1.4, 1.5 and 1.75, the maximum hoop stress occurred slightly away from the intersection at approximately 1.25 mm. Respectively, these peaks were slightly higher by a margin of 2.13%, 1.63% and 3.96%, in comparison to those present at the intersection. This occurrence was attributed to redistribution of stress due to change in state of stress from plane stress to plane strain. Similar occurrence had previously been noted by Masu (1989) study.

A structure is termed to be under plane stress conditions whenever the magnitude of one of the three principal stress is small in comparison to the other two stresses (Spyrakos, 1996). Usually, the magnitude of the small principal stress is approximated as zero. On the other hand, a structure is said to be under plane strain conditions whenever the strain developed along one of the principal axes is zero (Spyrakos, 1996). This phenomenon occurs as a result of one of the three sections of the structure being large in comparison to the other two sections.

The maximum value of hoop stress occurred in the pressure vessels with the smallest thickness ratio of K = 1.4. The peak values of the hoop stresses per unit pressure were at 6.783 and 8.460 for analytical and FEA methods, respectively. Whereas, the smallest magnitude of the hoop stress occurred in the cylinder with the highest thickness ratio, K = 3.0. This trend implied that the magnitude of hoop stress reduces with increase in the thickness ratio. Usually, as the thickness ratio increase the structural stiffness of the cylinder also increase, leading to lower hoop stresses and vice versa.

Comparing the results obtained through the analytical and FEA methods at the cross bore intersection, the lowest error was at 3.4% for K = 2.5. While the errors calculated from K = 2.25 and 3.0 were 4.1% and 6.4%, respectively. The other thickness ratios studied had errors above 9%.

A similar study conducted by Comleki *et al.* (2007) using FEA on thick cylinders having the same thickness ratio gave results that compared favourably to those obtained by the numerical solution, as tabulated in Table 12.

The margin of error was computed by comparing the two FEA solutions and taking the results from the present study as the reference. The errors for K = 1.4, 1.5, 1.75 and 2.0 were found to be 2.6%, 2.6%, 4.4% and 3.7%, respectively. Interestingly, only the errors given by K = 2.25 and 2.5 were slightly higher at 9.6% and 10.1%. A condition attributed to the degree of mesh refinement during

Table 12: Hoop stress per unit pressure at the intersection of cross bore size ratio of 0.1

K	1.4	1.5	1.75	2.0	2.25	2.5
Comleki *et al*. (2007) (FEA)	8.50	7.31	5.77	5.05	4.64	4.39
Present study (FEA)	8.29	7.12	5.52	4.87	4.23	3.96

modelling. Usually, the Abaqus commercial software used in this study has better capability in control of element meshing than ANSYS software used in the Comleki *et al.* (2007) study. The good results correlation between the two studies further authenticated the modelling procedures adopted in this study.

Geerden (1972) performed analytical studies on pressure vessels with a cross bore size ratio of 0.1, having thickness ratios of K=1.5, 2 and 3. The Geerden study predicted much higher hoop stresses at the cross bore intersection than those from the analytical and numerical results presented in this study. Errors exceeding 16% were noted. Probably, this was due to the inclusion of shear stresses in Geerden's solution during the computation of the hoop stress.

4.2.1.2 Cross bore to main bore ratio of 0.3

Results of a high pressure vessel with main bore to cross bore size ratio of 0.3 are presented in figures 23 - 29 for K = 1.4, 1.5, 1.75, 2.0, 2.25, 2.5 and 3.0.

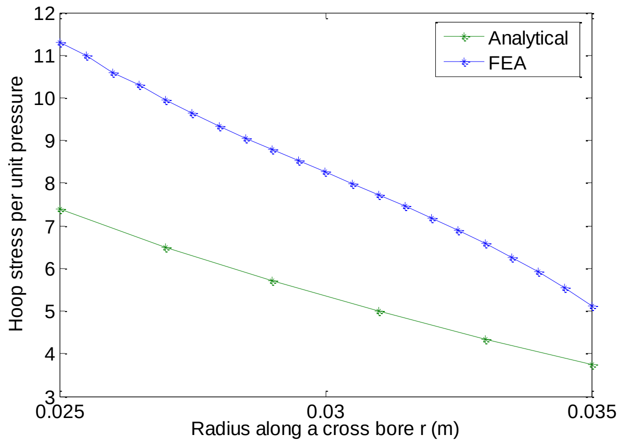

Figure 23: K = 1.4 CB = 0.3

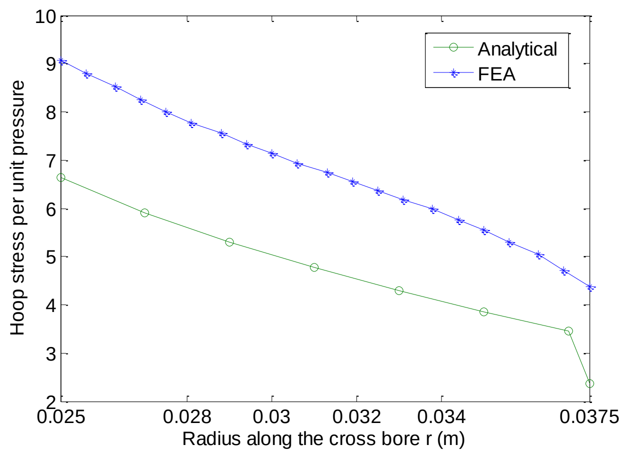

Figure 24: K = 1.5 CB = 0.3

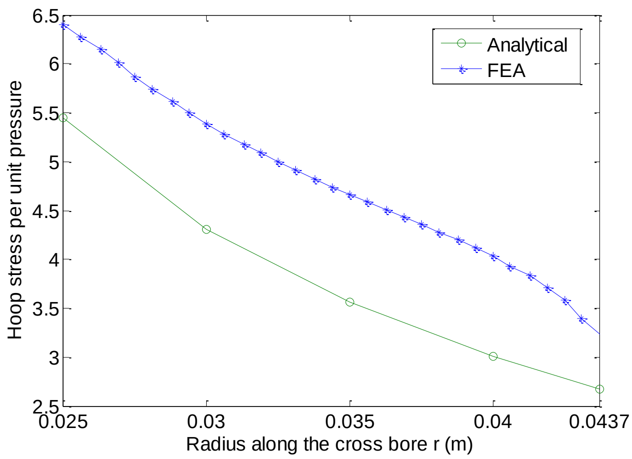

Figure 25: K = 1.75 CB = 0.3

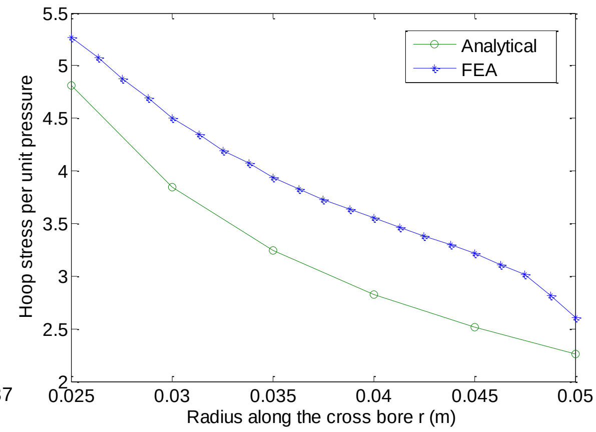

Figure 26: K = 2.0 CB = 0.3

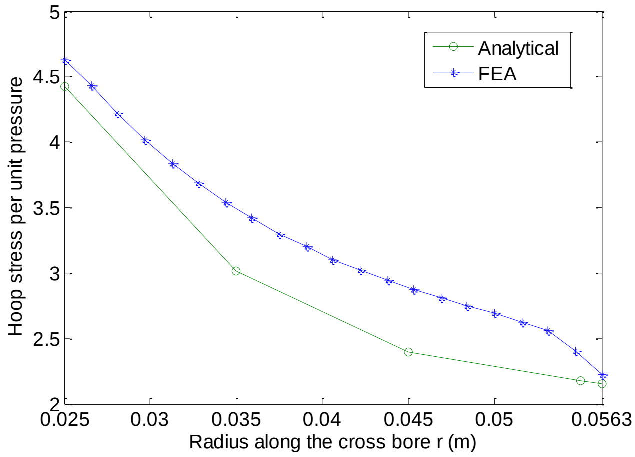

Figure 27: K = 2.25 CB = 0.3

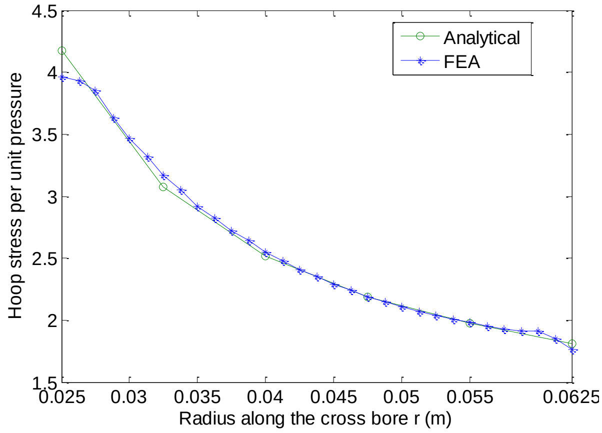

Figure 28: K = 2.5 CB = 0.3

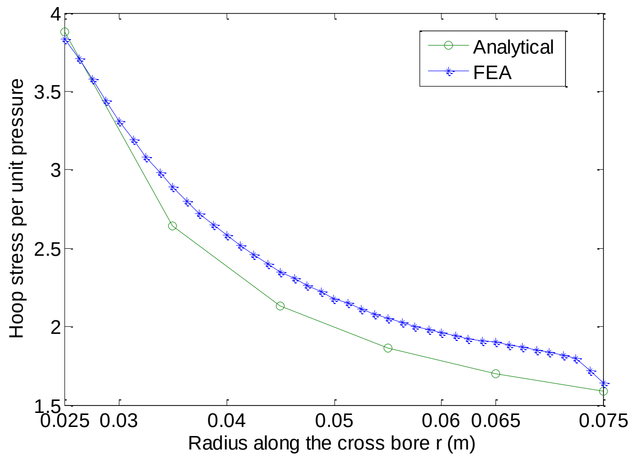

Figure 29: K = 3.0 CB = 0.3

Figures 23- 29: Hoop stress distribution per unit pressure for various thickness ratios along a radial circular cross bore, having cross bore to main bore size ratio of 0.3.

In this section, a similar stress distribution pattern as previously exhibited in the section 4.2.1.1 was observed. The magnitudes of hoop stresses were high at the cross bore intersection and reduced gradually towards the outside surface of the cylinder.

A general comparison between hoop stresses due to the introduction of the cross bore size ratio of 0.3 and those of 0.1, as illustrated in figures 16 -22 and 23 -29, showed an increase in magnitude of hoop stress as the cross bore size increased. For instance, in the case of K = 1.4, the hoop stress per unit pressure at the intersection was found to be 7.405 and 11.34, for analytical and FEA, respectively. Resulting to an increase of 9.17% and 36.9% when compared with similar stresses obtained in pressure vessels with a cross bore size ratio of 0.1 presented earlier in section 4.2.1.1. The structural stiffness of the cylinder reduce with the increase of the cross bore size leading to higher hoop stresses.

The disparities in hoop stress distribution predicted by the analytical and FEA were more pronounced in K = 1.4, 1.5 and 1.75 as shown in Figures 22 to 25. However, as the thickness ratio increased, the hoop stress distribution curves generated by both the analytical and numerical methods tended to converge.

Comparing the results given by the two methods, the minimal error was at 1.15% for K = 3.0, while, the thickness ratios of K = 2.0, 2.25 and 2.5 gave errors of 1.97%, 4.37% and 8.62%, respectively. The margin of error presented by other thickness ratios exceeded 15%. It was noted that the margin of error increased tremendously with reduction in thickness ratio.

Geerden (1972) carried out similar studies on pressure vessels with a radial cross bore size ratio of 0.3. The results by Geerden (1972) at the cross bore intersection are compared in Table 13 with corresponding ones obtained in the present study.

Errors of 20.3%, 12.7% and 7.35%, for K = 1.5, 2.0 and 3.0 respectively were obtained upon comparison with the analytical solution presented in this study. Correspondingly, errors calculated upon comparison with FEA data were 12%, 3% and 8.58% for K = 1.5, 2.0 and 3.0, respectively.

Thus, only the FEA results for K = 2 were within the acceptable margin of error.

Table 13 : Hoop stress per unit pressure at the intersection of cross bore size ratio of 0.3

K	1.5	2.0	3.0
Geerden, 1972 (Analytical)	7.98	5.43	4.16
Present study (Analytical)	6.63	4.81	3.88
Present study (FEA)	9.07	5.27	3.83

4.2.1.3 Cross bore to main bore ratio of 0.5

Results of a high pressure vessel with main bore to cross bore size ratio of 0.5 are presented in figures 30 - 36 for K = 1.4, 1.5, 1.75, 2.0, 2.25, 2.5 and 3.0.

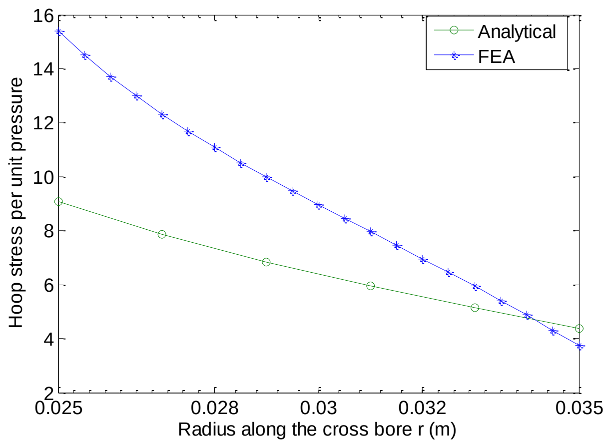

Figure 30: K =1.4 CB = 0.5

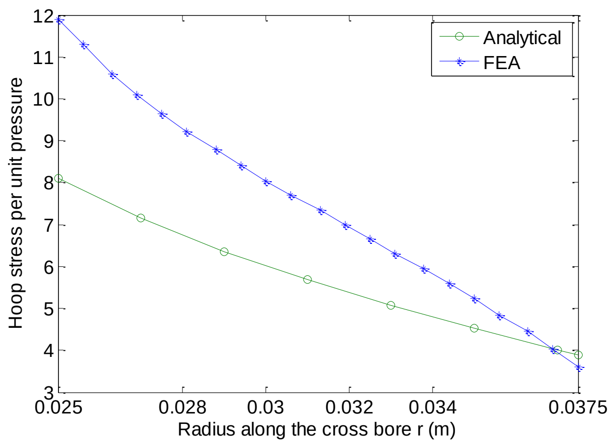

Figure 31: K = 1.5 CB = 0.5

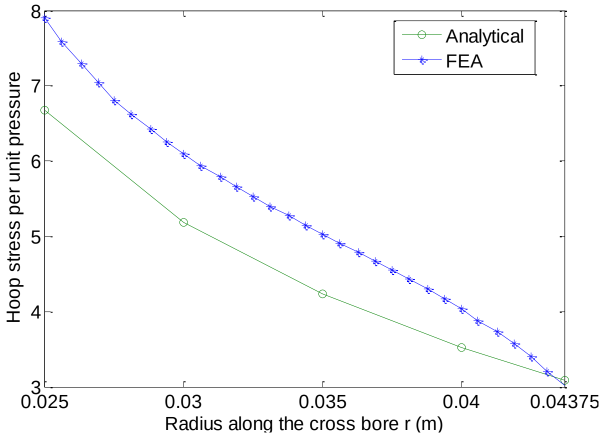

Figure 32: K = 1.75 CB = 0.5

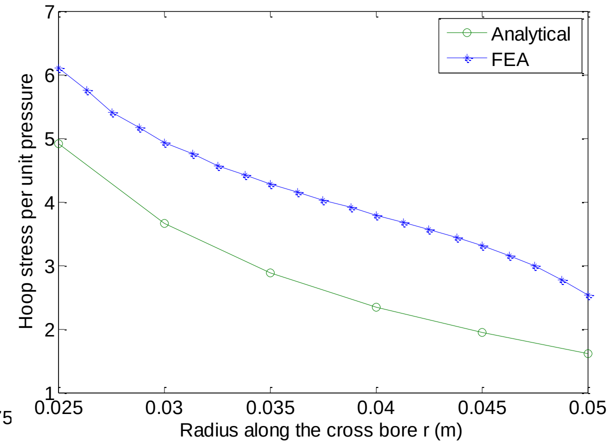

Figure 33: K = 2.0 CB = 0.5

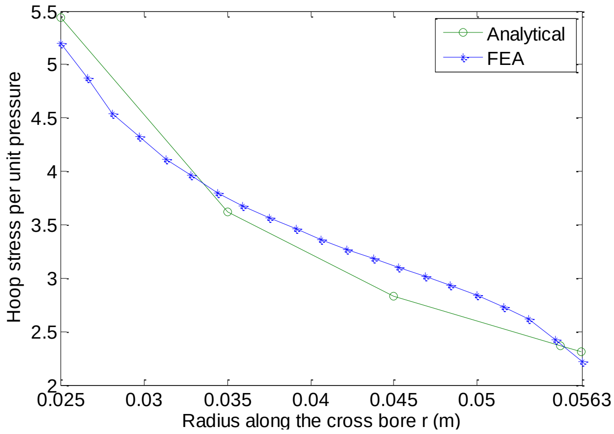

Figure 34: K = 2.25 CB = 0.5

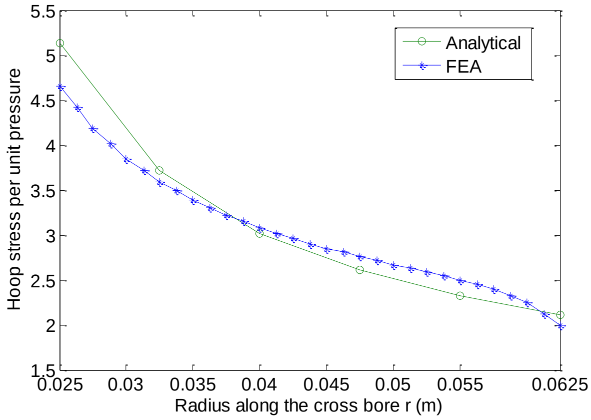

Figure 35: K = 2.5 CB = 0.5

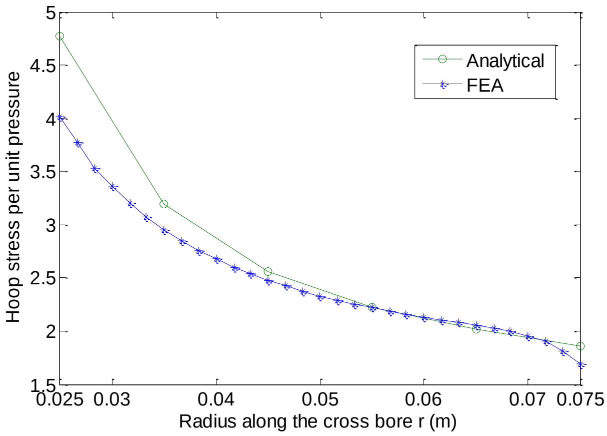

Figure 36: K = 3.0 CB = 0.5

Figures 30 -36: Hoop stress distribution per unit pressure for various thickness ratios along a radial circular cross bore, having cross bore to main bore size ratio of 0.5.

Notable variation in stress distribution between the two methods were seen in K = 1.4 and 1.5, as illustrated in Figures 30 and 31. However, as the thickness ratio increased, a significant reduction in the disparities were noted. The stress distribution predicted by the FEA was higher than that of the analytical method at the cross bore intersection. Nevertheless, FEA predicted lower hoop stresses than the analytical method towards the outer surface of the cylinder.

The hoop stress at the cross bore intersection was a maximum in the cylinder with thickness ratio K = 1.4. In the same thickness ratio, a comparison between cross bore size ratio of 0.3 and that of 0.5 at the cross bore intersection, as shown in figures 23 and 30, indicated a rise in hoop stress by 22.5% for analytical and 35.5% for FEA analyses. This trend signified that the hoop stress increases with increase in the cross bore size. This observation further confirms that the structural stiffness of the cylinder reduces with increase in the cross bore size leading to high magnitude of hoop stresses.

Comparing the results from the two methods presented in this study, acceptable margin of error of 3.3% and 5% were only obtained for the thickness ratios 2.0 and 2.25, respectively. The error margin given by other thickness ratios studied exceeded 11%.

Several studies (Fessler and Lewin (1956); Faupel and Harris (1957) and Gerdeen (1972) have been done on cross bores, with a main bore to cross bore ratio of 0.5 in thick walled pressure vessels using both experimental and analytical methods. The comparison of results at the cross bore intersection from these studies with those of the present study are tabulated in Table 14.

Faupel and Harris (1957) performed both analytical and experimental analyses on pressure vessels with K = 1.5. They reported maximum hoop stresses per unit pressure of 7.54 and 6.11 for analytical and FEA analyses, respectively. Gerdeen (1972) carried out an analytical study on the same cross bore size and reported a hoop stress value of 7.02 at the intersection.

The findings of these two previous studies indicated slightly lower hoop stresses than those presented in this work. The closest prediction was at 7% error when calculated using the analytical results developed in the present study.

Table 14: Hoop stress per unit pressure at the intersection of cross bore size ratio of 0.5

K		1.5	2.0	2.5	3.0
Fessler and Lewin (1956)	Analytical	-	-	-	3.53
Fessler and Lewin (1956)	Experimental	-	-	-	3.5
Faupel and Harris (1957)	Analytical	7.54	4.78	3.94	-
Faupel and Harris (1957)	Experimental	6.11	4.37	3.73	-
Gerdeen (1972)	Analytical	7.02	4.67	-	-
Present study	Analytical	8.11	5.91	5.14	4.77
Present study	FEA	11.95	6.11	4.65	4.02

On cylinders with K = 2, Faupel and Harris (1957) gave hoop stresses per unit pressure at the intersection as 4.784 and 4.367 for analytical and experimental methods, respectively, while the analytical method by Geerden (1972) gave a hoop stress value at the cross bore intersection as 4.667. These two analytical solutions from previous studies compared favourably with those given by the analytical method in this study

In contrast, the results presented by Harris and Faupel for K = 2.5 gave lower hoop stresses of 3.936 and 3.729 for analytical and experimental methods. The minimum error obtained upon comparison with FEA data exceeded 19%.

Fessler and Lewin (1956) predicted hoop stress at the intersection using both analytical and experimental method for K = 3.0. The study gave the hoop stress per unit pressure at the intersection as 3.525 and 3.5 for both analytical and experimental methods, respectively. Interestingly, a similar analytical study by Geerden (1972) predicted the magnitude of hoop stress as 3.5625. However, when these results were compared with those of the present study, errors exceeding 12.8% were noted.

Another study by Ford and Alexander (1977) gave a stress expression for determining hoop stresses in thick walled cylinders with small cross bore as $\frac{4K^2+1}{K^2-1}p_i$, without stating the cross bore size. As defined by Steele *et al*., (1986), a small cross bore has a main bore to cross bore size ratio $\leq$0.5. Therefore, the results given by the preceding expression were compared with those presented in this study for small cross bores.

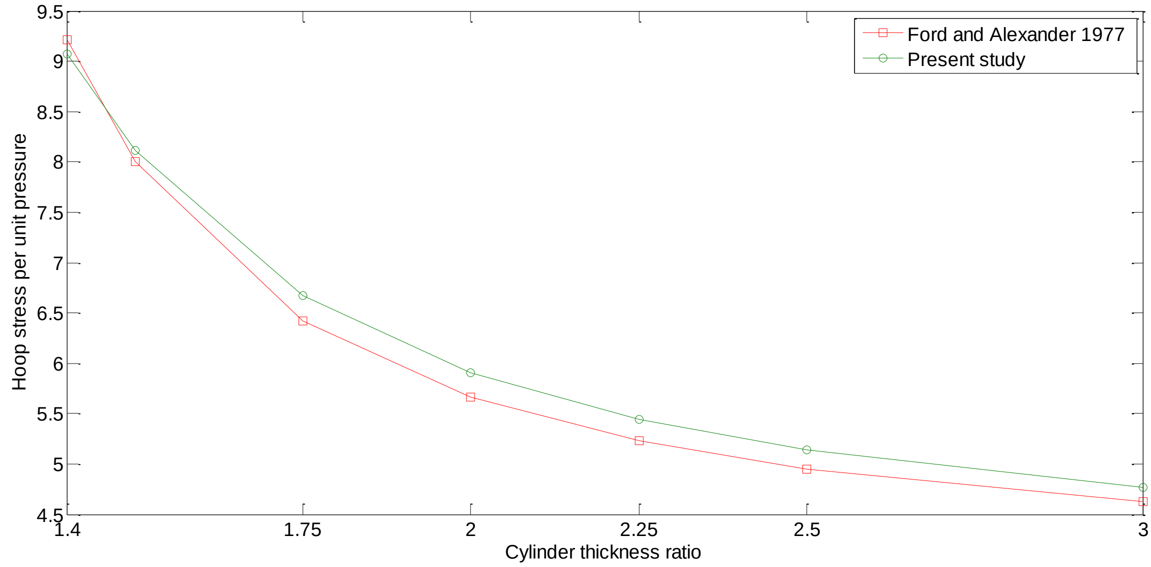

Figure 37: Comparison between hoop stress generated by Ford and Alexander (1977) and that obtained in this study

As illustrated in Figure 37, the analytical results at the intersection presented by this study for cross bore size ratio of 0.5 were found to be in good agreement with those given by Ford and Alexander's (1977) expression. Tabulation of these results is shown in Table 15.

Table 15 : Hoop stress per unit pressure computed using Ford and Alexander's expression and equation 3.28 for a cross bore size ratio of 0.5

K	1.4	1.5	1.75	2.0	2.25	2.5	3.0
Ford and Alexander's (1977) expression	9.21	8	6.42	5.67	5.23	4.95	4.63
Present study (Analytical equation 3.28)	9.07	8.11	6.67	5.91	5.44	5.14	4.77

The percentage errors between these two methods computed based on the present study for K = 1.4, 1.5, 1.75, 2.0, 2.25, 2.5 and 3.0 was 1.5, 1.34, 3.7, 4.04, 3.89, 3.6 and 3.02, percent respectively.

The error was observed to increase slightly with increase in thickness ratio. This occurrence was attributed to different assumptions made during the development of these solutions. For instance, the study by Ford and Alexander (1977) assumed a biaxial stress field in their analysis. Whereas, the present study assumed a triaxial field stress. Nevertheless, it was established that the hoop stress expression by Ford and Alexander (1977) predicts correctly the stresses at the intersection of a cross bore with size ratio of 0.5.

4.2.1.4 Cross bore to main bore ratio of 0.7

Results of high pressure vessels with a main bore to cross bore size ratio of 0.7 are presented in figures 38 - 44 for K = 1.4, 1.5, 1.75, 2.0, 2.25, 2.5 and 3.0.

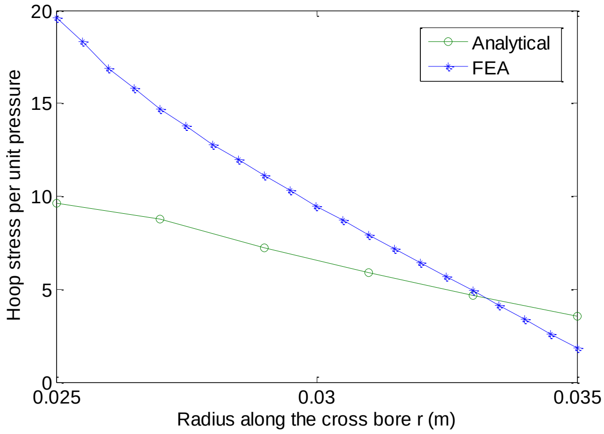

Figure 38 : K = 1.4 CB =0.7

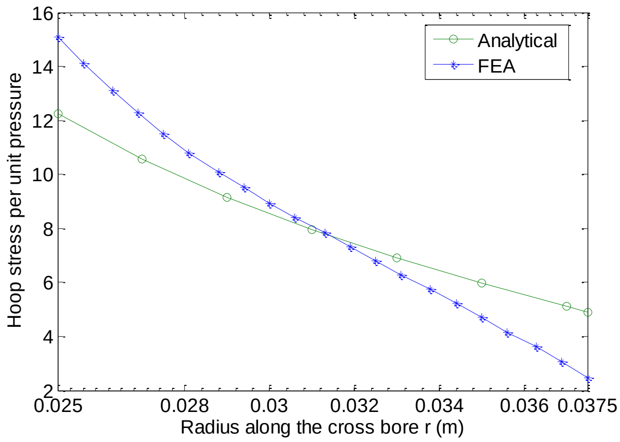

Figure 39: K = 1.5 CB = 0.7

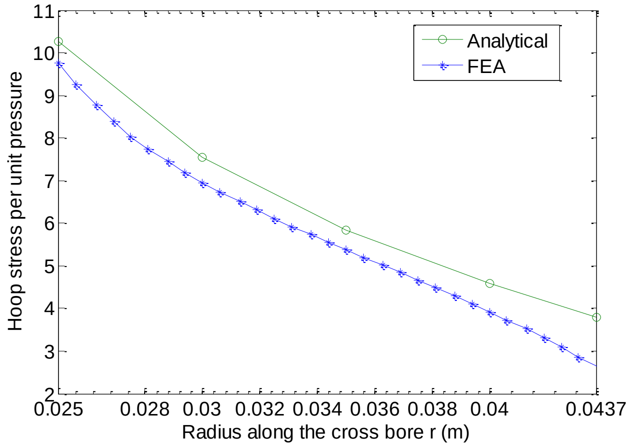

Figure 40: K = 1.75 CB = 0.7

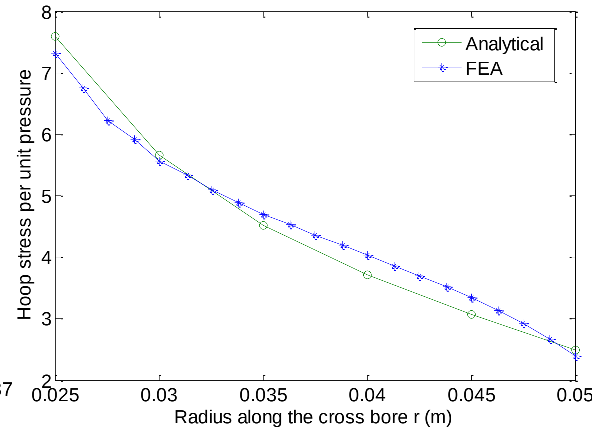

Figure 41: K = 2.0 CB = 0.7

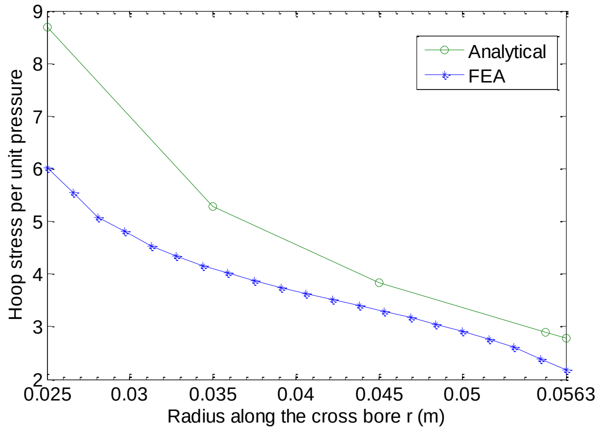

Figure 42: K = 2.25 CB = 0.7

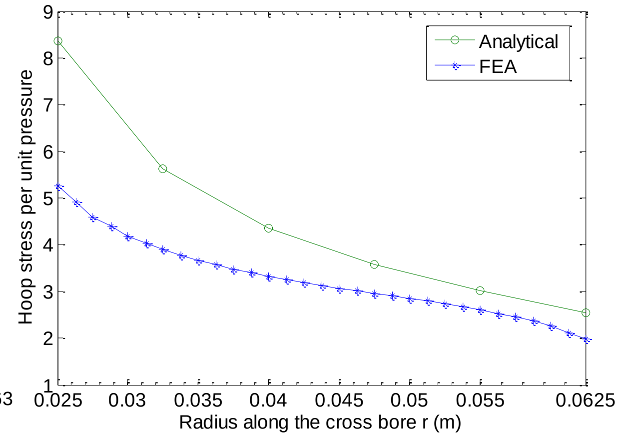

Figure 43: K = 2.5 CB = 0.7

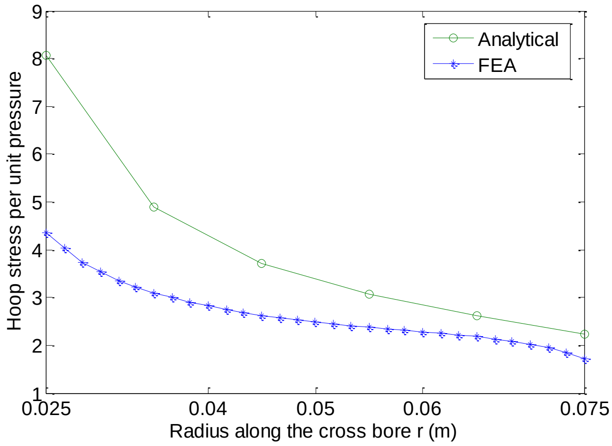

Figure 44: K = 3.0 = 0.7

Figures 38 - 44: Hoop stress distribution per unit pressure for various thickness ratios along a radial circular cross bore, having cross bore to main bore size ratio of 0.7.

Similar stress distribution patterns to those discussed in the preceding section were observed in this section. A comparison between cross bore size ratio of 0.5 and 0.7, as illustrated in figures 30 -36 and 38 -44, revealed that the magnitude of the hoop stress at the intersection, arising from the former cross bore, were higher than the corresponding ones given by the latter cross bore. This signified that the hoop stress at the intersection, increases with the increase of the cross bore size. This observation further confirmed that, the structural stiffness of the cylinder depends on the cross bore size.

The results of hoop stresses given by the two approaches only converged when K = 1.75 and 2.0 as illustrated in Figures 40 and 41, indicating a stress transition point. Other thickness ratios had notably high disparities at the intersection ranging from 19% to 86% for K = 1.5 and 3.0, respectively. Nonetheless, the rate of disparity in hoop stress distribution reduced towards the outer surface of the cylinder. In fact, for cylinders with K = 2.25, 2.5 and 3.0 the inconsistency in stress distribution ceased beyond the radial distance of 0.045 m from the intersection.

Most of the studies reviewed in the literature did not investigate cross bores with a size ratio of 0.7. Geerden (1972) studied cross bores with size ratios ranging from 0.125 to 0.667. However, the author indicated that the solutions give inaccurate results beyond size ratios of 0.667. Therefore, extrapolation of the results could not be done.

4.2.1.5 Cross bore to main bore ratio of 1.0

Results of high pressure vessels with a main bore to cross bore size ratio of 1.0 are presented in figures 45-51 for K = 1.4, 1.5, 1.75, 2.0, 2.25, 2.5 and 3.0.

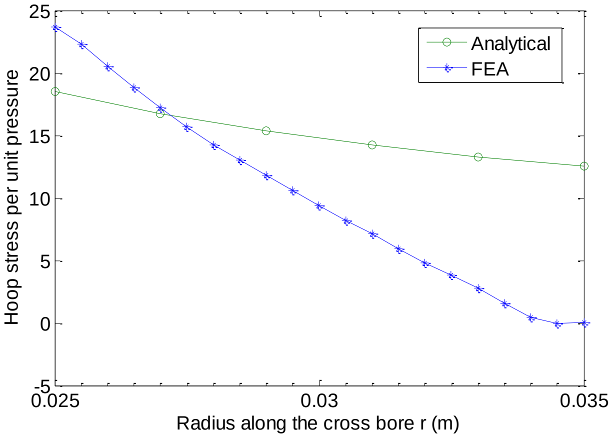

Figure 45: K =1.4 CB = 1.0

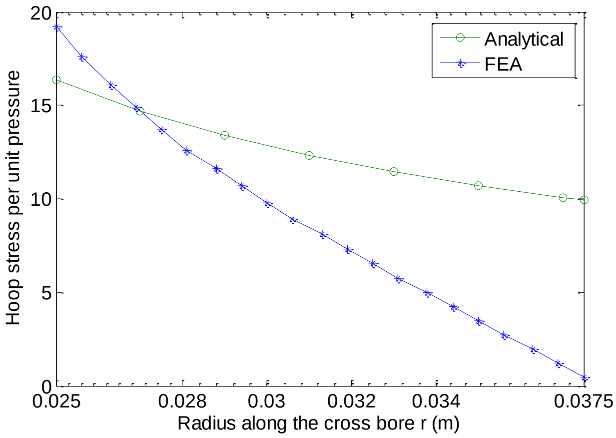

Figure 46: K = 1.5 CB = 1.0

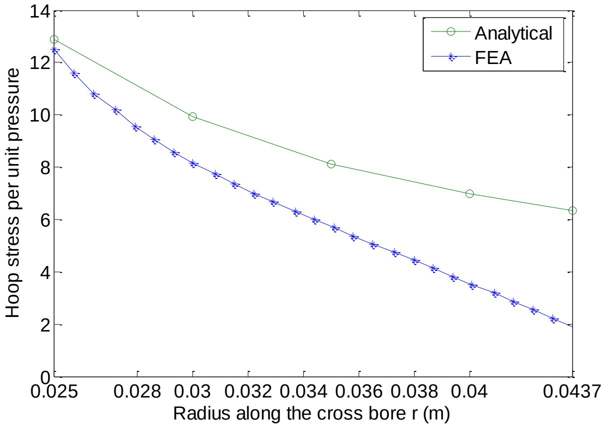

Figure 47 Figure 47 : K = 1.75 CB =1.0

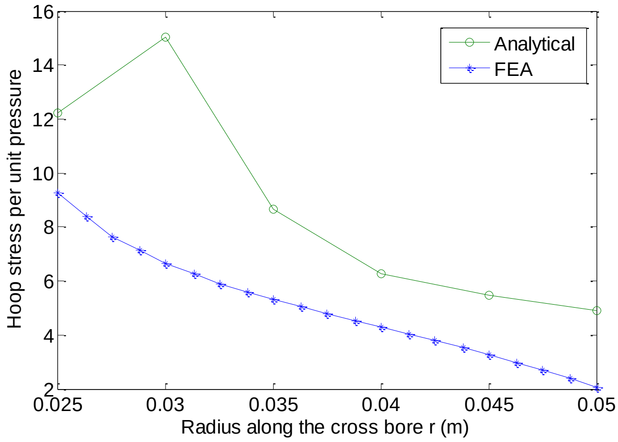

Figure 48: K = 2.0 CB = 1.0

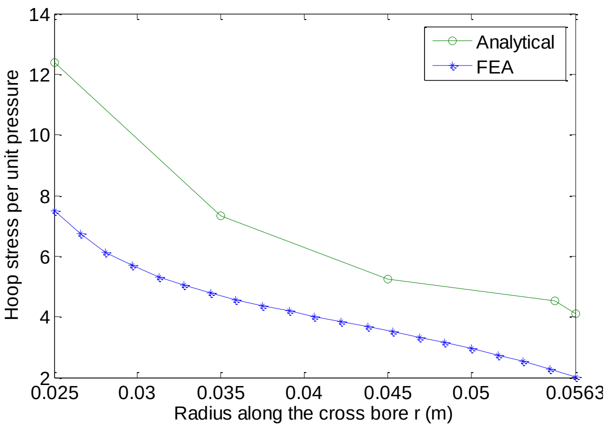

Figure 49: K = 2.25 CB = 1.0

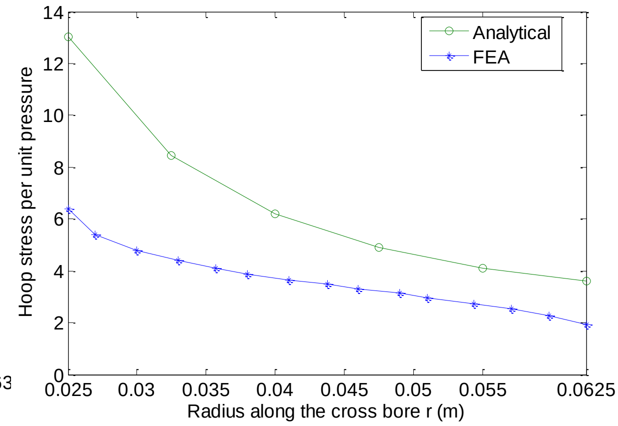

Figure 50: K = 2.5 CB = 1.0

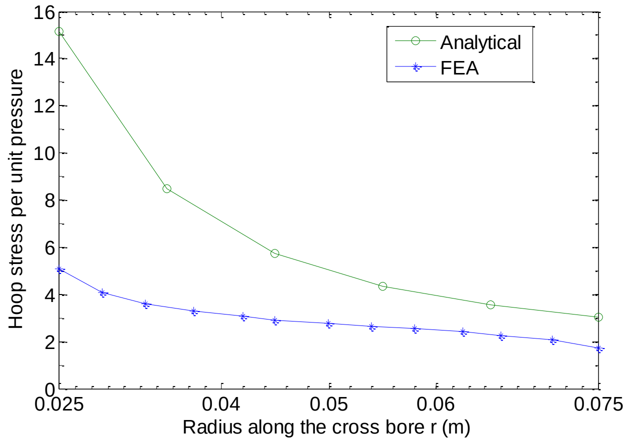

Figure 51: K = 3.0 CB = 1.0

Figures 45-51: Hoop stress distribution per unit pressure for various thickness ratios along a radial circular cross bore, having a cross bore to main bore size ratio of 1.0.

For thickness ratios K = 1.4 and 1.5, the FEA approach gave higher stresses than the developed analytical method in the region near the cross bore intersection. However, at a radius of 0.0275 m, the two methods predicted the same stress. After which, the analytical method predicted higher stresses than the FEA method, as shown in Figures 45 and 46. It was also noted that as the thickness ratio increased, the analytical method predicted slightly higher stress values as illustrated in Figures 49 to 51. Except for K=2.0, the stress distribution along the thickness was seen to reduce gradually from the cross bore intersection towards the outside surface of the cylinder. In K = 2.0, the hoop stress increased sharply after the intersection to a peak value of 15.04 at 0.03 m. After this peak value, the hoop stress began to fall gradually towards the outside surface of the cylinder. Generally, it was observed that the inconsistency in stress distribution reduced towards the outside surface of the cylinder specifically for K = 2.0, 2.25, 2.5 and 3.0.

The magnitudes of hoop stresses given by the cross bore size ratio of 1.0 were higher than those of 0.7 cross bore size presented in the previous section. Only, results of K = 1.75 predicted by the two methods were within the acceptable error margin. Other thickness ratios gave error margins exceeding 15.7%. Fessler and Lewin (1956) studied a similar cross bore for K = 2 using both the analytical and FEA analyses. They reported magnitudes of hoop stress per unit pressure of 3.167 and 5.034 for analytical and experimental approaches, respectively. On the other hand, the presented study gave stress magnitudes of 12.222 and 9.276 per unit pressure for the same cross bore size. These values were found to be lower than those presented in this study. Probably due to the use of different assumptions and associated experimental shortcomings especially during the determination of principal stresses.

In general, it was observed that the total hoop stress in the cylinder increased due to the cross bore introduction. The total hoop stress in the cylinder is the summation of the hoop stress in the cylinder with a bore and the corresponding hoop stress generated by the pressurised cross bore when acting alone, among other factors. Thus, its high magnitude is as a result of the summation of the hoop stresses, because they are acting in the same direction.

4.2.2 Radial stress component in the direction of the main cylinder

Graphs illustrating the radial stress along the cross bore for each thickness ratio are presented as follows in figures 52-58 for K = 1.4, 1.5, 1.75, 2.0, 2.25, 2.5 and 3.0.

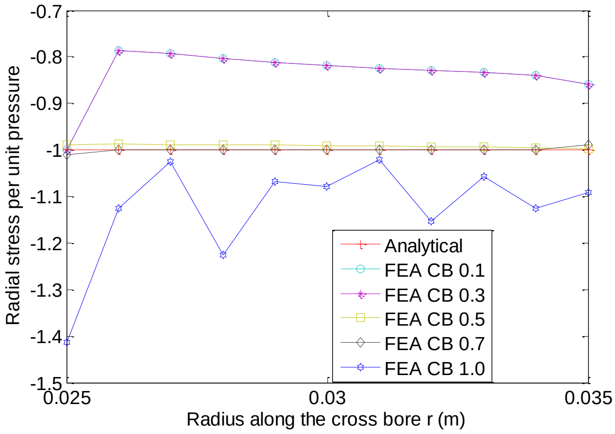

Figure 52 : Radial stress for K=1.4

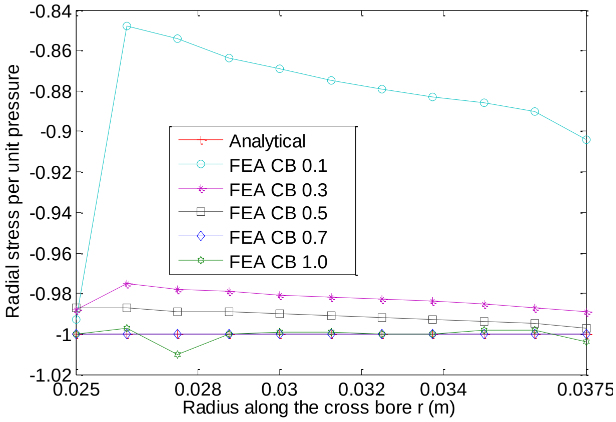

Figure 53: Radial stress for K = 1.5

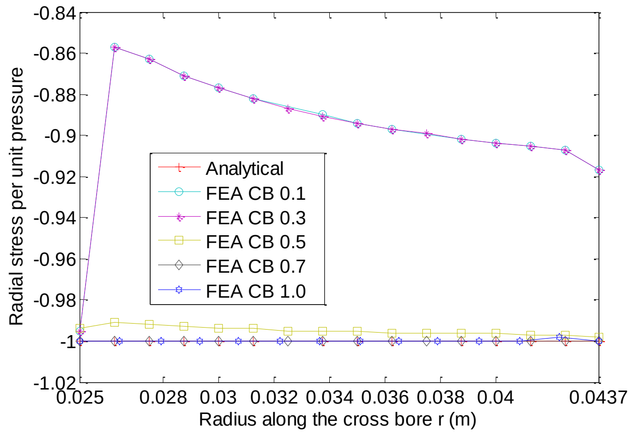

Figure 54: Radial stress for K = 1.75

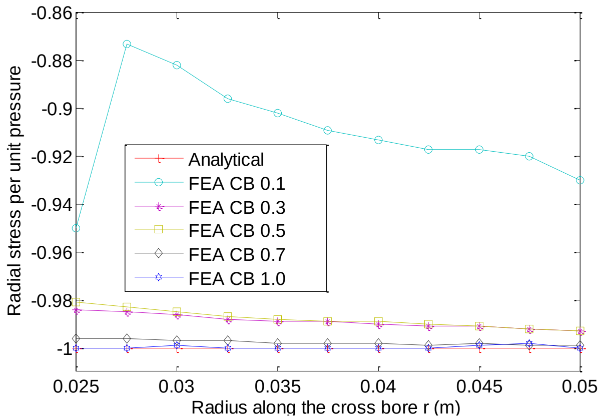

Figure 55: Radial stress for K = 2.0

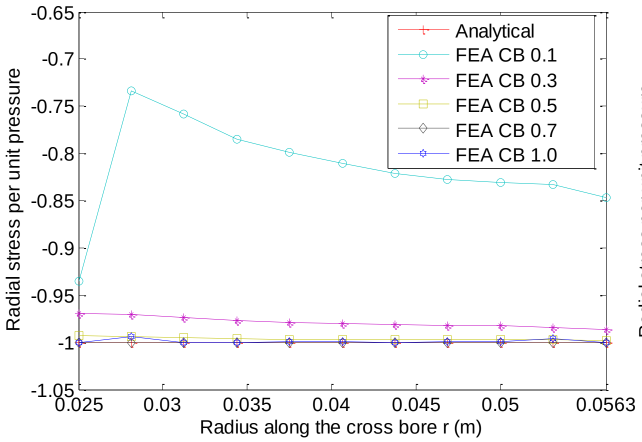

Figure 56 : Radial stress for K = 2.25

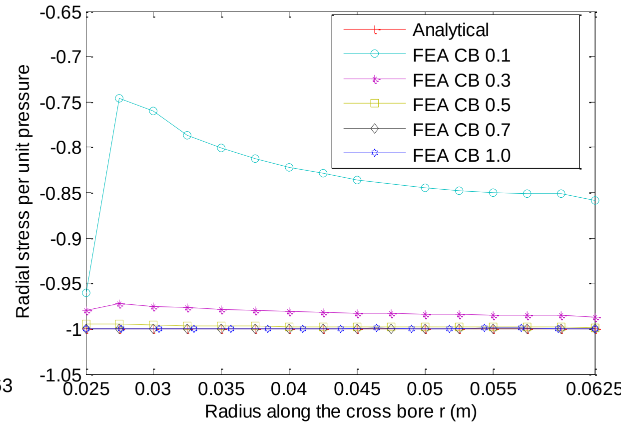

Figure 57: Radial stress for K = 2.5

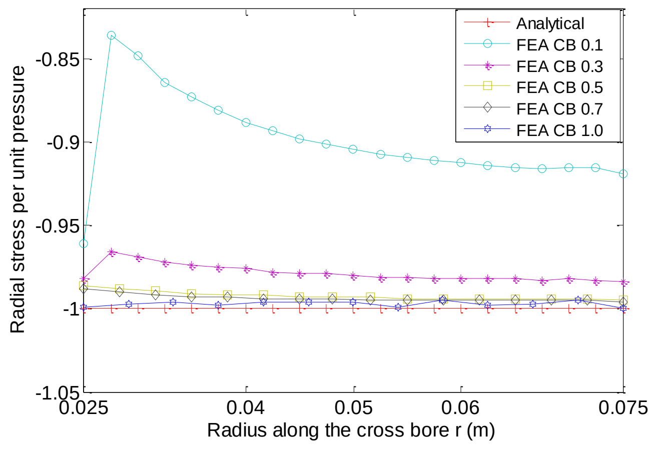

Figure 58 : Radial stress for K = 3.0

Figures 52 -58: Radial stress distribution per unit pressure along a circular cross bore, for various thickness ratios and cross bore sizes.

During the development of the analytical solution, it was assumed that the radial stress along the surface of the cross bore was constant. The magnitude of the constant radial stress per unit pressure was taken as -1 (compressive), which was equal and opposite to the gauge pressure. This assumption was in line with other previous studies by Geerden (1972) and Ford and Alexander (1977).

Interestingly, the FEA data presented in this work, compared favourably with the corresponding analytical ones, when the cross bore size ratios were 0.3, 0.5, 0.7 and 1.0. The radial stress distribution graphs showing the concurrence between the two methods is illustrated in Figures 52-58. However, it was noted that the radial stress distribution curve given by the largest cross bore size on K = 1.4 was considerably different. The appearance of the radial stress curve was close to a sinusoidal wave form but with sharp edges as shown in Figure 52. Moreover, the radial stress per unit pressure at the intersection was slightly lower at -1.414 for the same thickness ratio. Structural stiffness of the cylinder is affected by the cross bore size. Large cross bores causes the structural stiffness of the vessel to reduce leading to higher stresses.

On each thickness ratio, a similar stress distribution pattern as shown in Figures 52 to 58, was observed on the smallest cross bore size ratio of 0.1. At the intersection, the radial stress per unit pressure given by the smallest cross bore size was -1, after which it reduced sharply to a minima, before gradually increasing towards the outside surface of the cylinder. The magnitude of the lowest minima was at 0.734 in K = 2.25. Probably this occurrence might be associated with the stress extrapolation during the job analysis stage in Abaqus software, among other factors. The extrapolation process might lead to the prediction of inaccurate stresses at the surface of the cross bore. Further verification needs to be done to ascertain the accuracy of these results. It is, therefore, recommended that a software package, such as Boundary Integral Element, which is more suitable in analysing stresses at the surface of the elements, should be used. It is worth noting that the total radial stress along the cross bore is the summation of the radial stress in the main cylinder with a bore and the corresponding axial stress produced by the pressurised cross bore. However, since the cross bore is open ended, the corresponding axial stress is zero. Hence the total radial stress is equal to the gauge pressure. This observation agrees with the phenomenon that pressure is equal in all direction.

4.2.3 Axial stress component in the direction of the main cylinder

The axial stress per unit pressure along the transverse edge of the cross bore are presented under the following subheadings:

4.2.3.1 Cross bore to main bore ratio of 0.1

In this section, results of axial stresses in a thick walled cylinder with a main bore to cross bore size ratio of 0.1 are presented in Figures 59-65 for K = 1.4, 1.5, 1.75, 2.0, 2.25, 2.5 and 3.0.

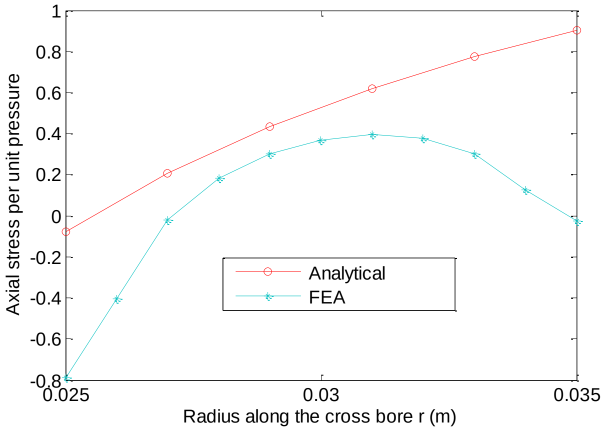

Figure 59: K = 1.4 CB = 0.1

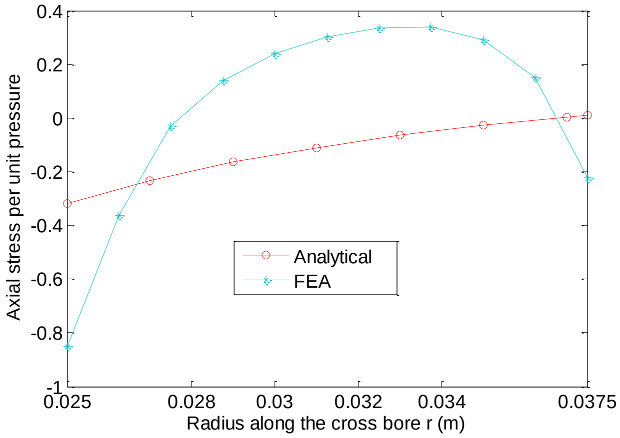

Figure 60: K = 1.5 CB = 0.1

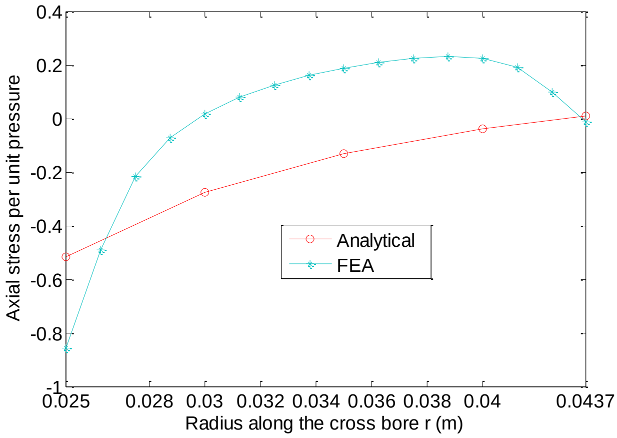

Figure 61: K = 1.75 CB = 0.1

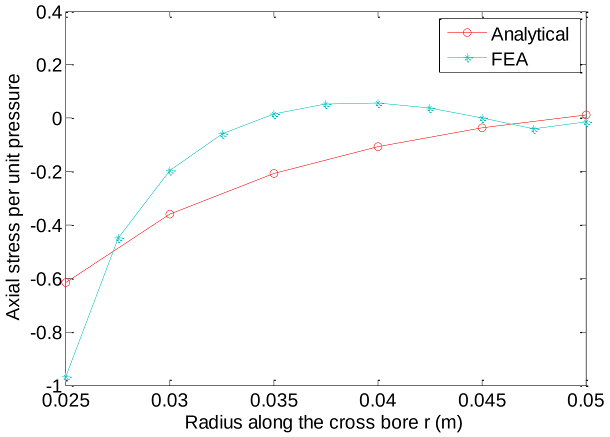

Figure 62: K = 2.0 CB = 0.1

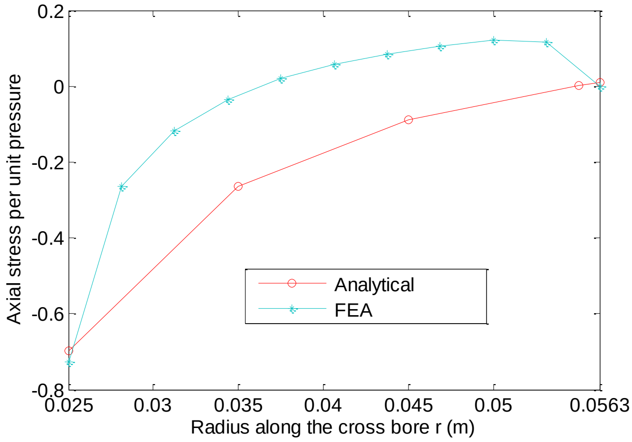

Figure 63: K = 2.25 CB = 0.1

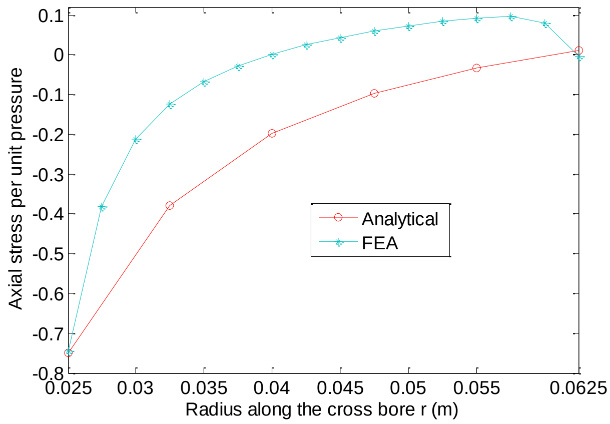

Figure 64: K = 2.5 CB = 0.1

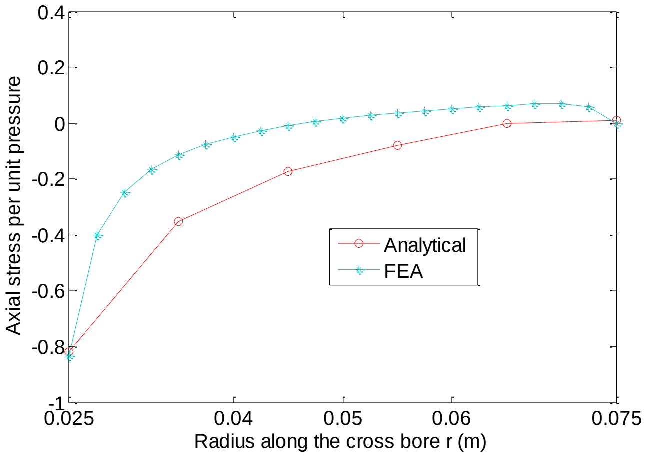

Figure 65: K = 3.0 CB = 0.1

Figures 59-65: Axial stress distribution per unit pressure for various thickness ratios along a radial circular cross bore, with a cross bore to main bore size ratio of 0.1.

Generally, the disparity of stress distribution between the two methods was more pronounced in K = 1.4 as shown in Figure 59, which reduced with an increase in thickness ratio. The axial stresses given by the two approaches along the cross bore were observed to change from a compressive state, at the intersection, to a tensile state along the cylinder thickness as illustrated in Figures 59 to 65. The lowest compressive axial stress per unit pressure at the intersection was given by the FEA approach. It occurred at K = 2.0 with a magnitude of -0.968, while the lowest stress was given by the analytical method at -0.079 for K = 1.4. Only in K = 2.25, 2.5 and 3.0 were the stress predictions at the intersection by the two methods in good agreement as shown in Figures 63, 64 and 65.

On the other hand, the highest tensile axial stress was given by the analytical method at K = 1.4 on the outside surface of the cylinder. Its magnitude was at 0.901. The stress curve given by the FEA data produced a concave curve with a maximum turning point as shown in Figures 59 to 65. The position of this turning point was noted to be skewed towards the outside surface of the cylinder. The maximum turning point occurred on K = 1.4 at 0.395, whereas the minimum was on K = 3.0 at 0.0679 as illustrated by Figures 59 and 65, respectively. Except for K = 1.4 and 1.5, the axial stresses predicted by the FEA data at the outside surface of the cylinder was zero. Contrary to the plain cylinder, where axial stress is constant across the cylinder thickness, it was found to vary along the surface of the cross bore in all the studied cases.

4.2.3.2 Cross bore to main bore ratio of 0.3

Results of axial stresses in pressure vessels with a main bore to cross bore size ratio of 0.3 are presented in Figures 66 to 72 for K = 1.4, 1.5, 1.75, 2.0, 2.25, 2.5 and 3.0.

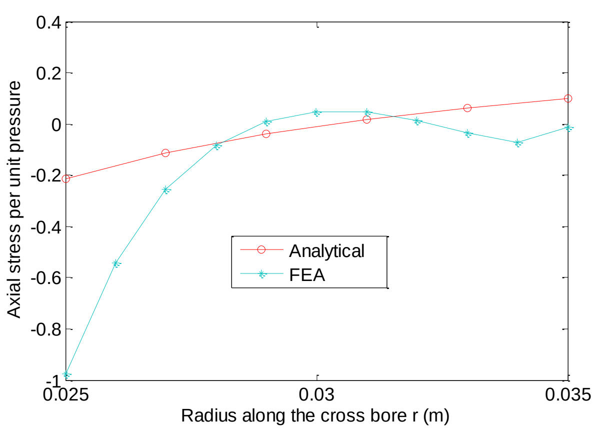

Figure 66: K = 1.4 CB = 0.3

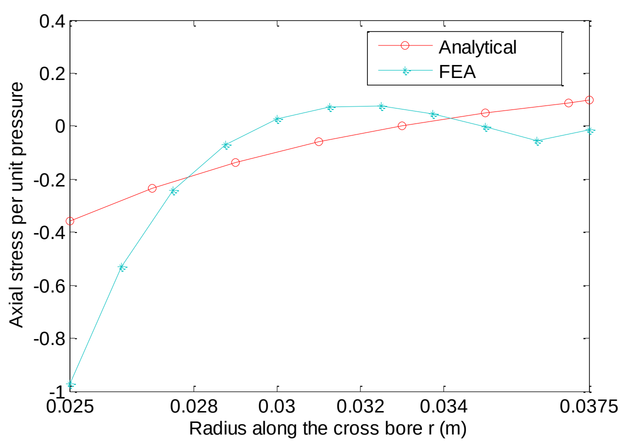

Figure 67: K = 1.5 CB = 0.3

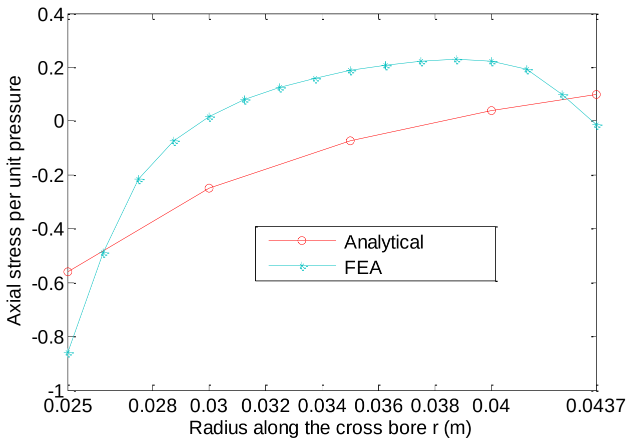

Figure 68: K = 1.75 CB =0.3

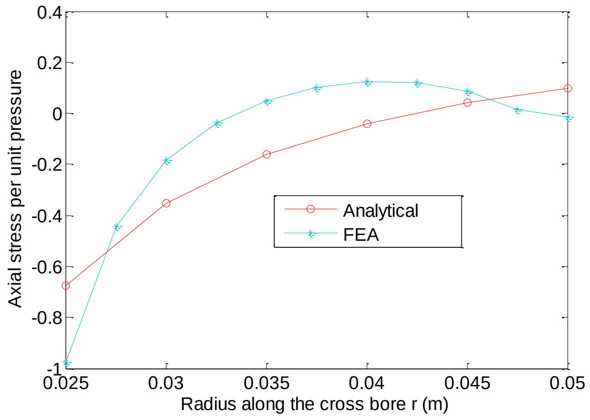

Figure 69: K = 2.0 CB = 0.3

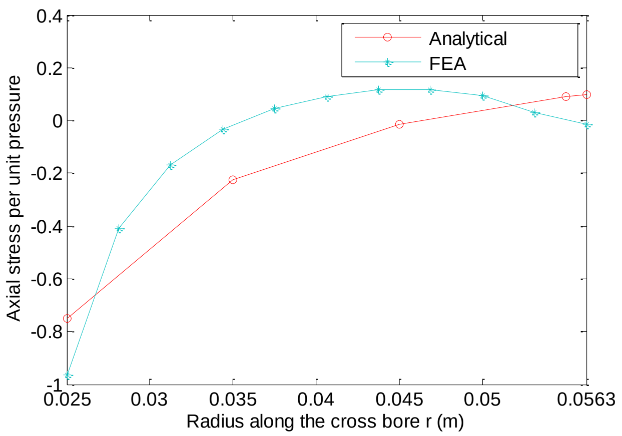

Figure 70: K = 2.25 CB = 0.3

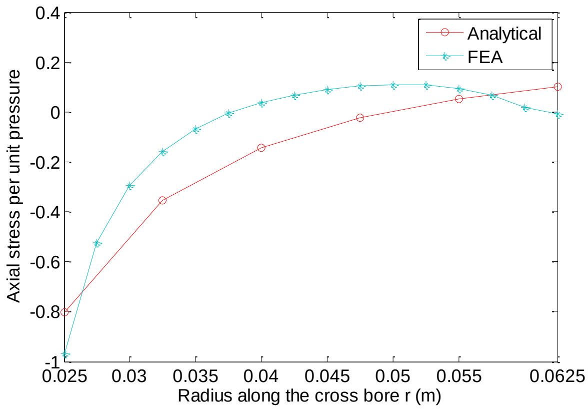

Figure 71: K = 2.5 CB = 0.3

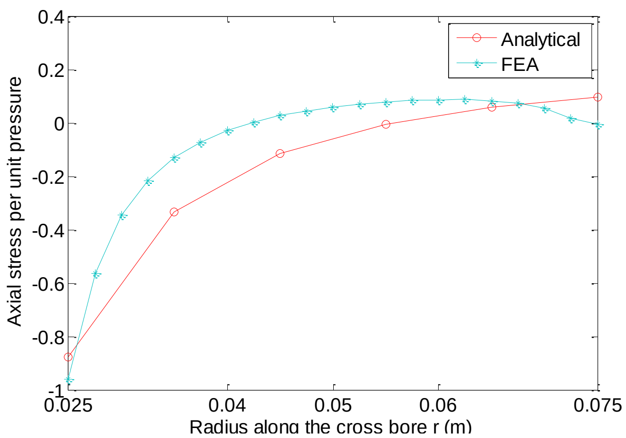

Figure 72: K = 3.0 CB = 0.3

Figures 66 - 72: Axial stress distribution per unit pressure for various thickness ratios along a radial circular cross bore, with a cross bore to main bore size ratio of 0.3.

The axial stress distribution pattern observed in this section was similar to the one discussed in section 4.2.3.1. The disparity in stress distribution given by the two methods at the intersection was higher in K = 1.4 and 1.5 as shown in Figures 66 and 67. However, this disparity in stress distribution reduced as the thickness ratio increased as seen in Figures 71 and 72. The compressive axial stresses at the intersection given by the FEA ranged from -0.85 to -0.976, with the maximum stress occurring on K = 1.4. These stresses determined by FEA were close to those predicted by a similar study by Ford and Alexander (1977). The study by Ford and Alexander had predicted a constant axial stress along the cross bore of magnitude of -1.

The stress distribution given by the two methods along the surface of the cross bore was in close agreement in K = 2.0, 2.5 and 3.0 as illustrated by Figures 70, 71 and 72. The maximum tensile stresses given by the FEA occurred on K = 1.75 at 0.231. Except for K = 1.5, the axial stresses at the outer surface of the cylinder was zero. The analytical approach gave the highest compression stress at the intersection as -0.878 at K = 3.0, whereas, the highest tensile stress occurred at the outside surface of the cylinder reaching a value of 0.1 in all the thickness ratios.

4.2.3.3 Cross bore to main bore ratio of 0.5

Results of axial stresses in a thick walled cylinder with a main bore to cross bore size ratio of 0.5 are presented in figures 73 - 79 for K = 1.4, 1.5, 1.75, 2.0, 2.25, 2.5 and 3.0.

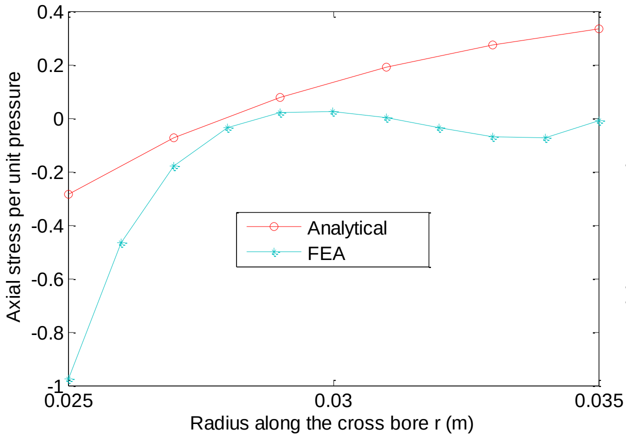

Figure 73: K = 1.4 CB = 0.5

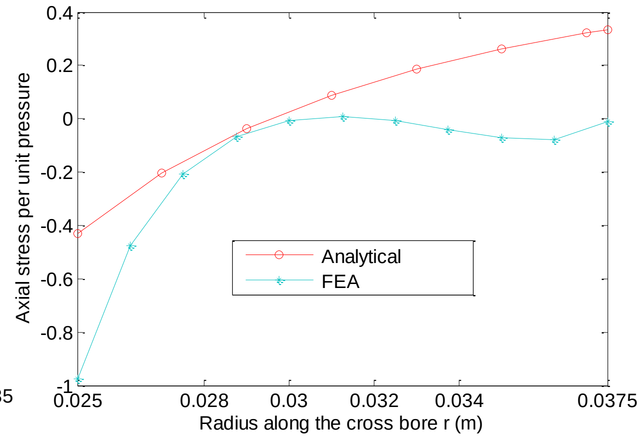

Figure 74: K = 1.5 CB = 0.5

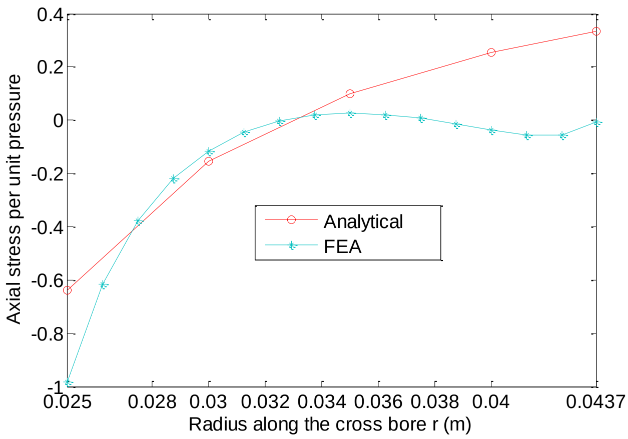

Figure 75: K = 1.75 CB = 0.5

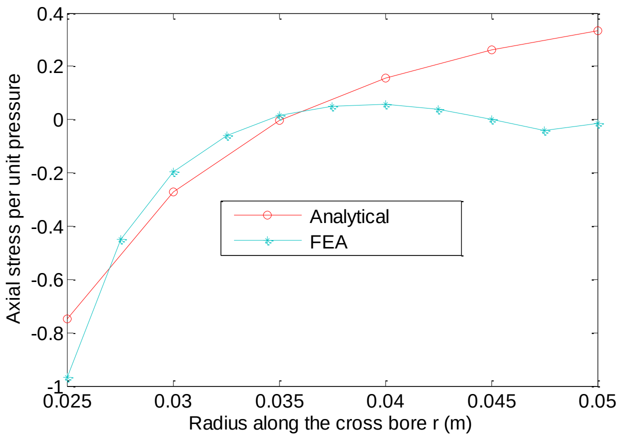

Figure 76: K = 2.0 CB = 0.5

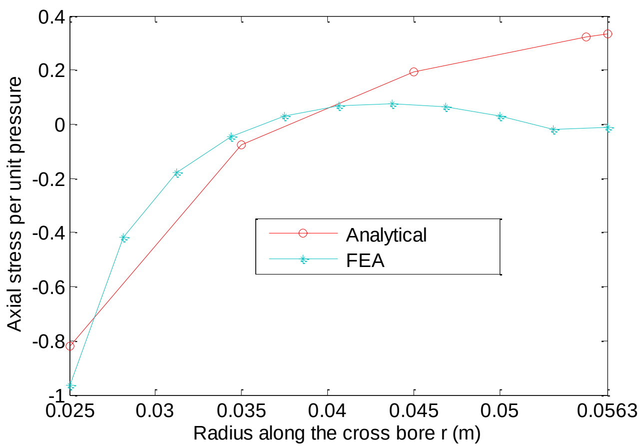

Figure 77: K = 2.25 CB = 0.5

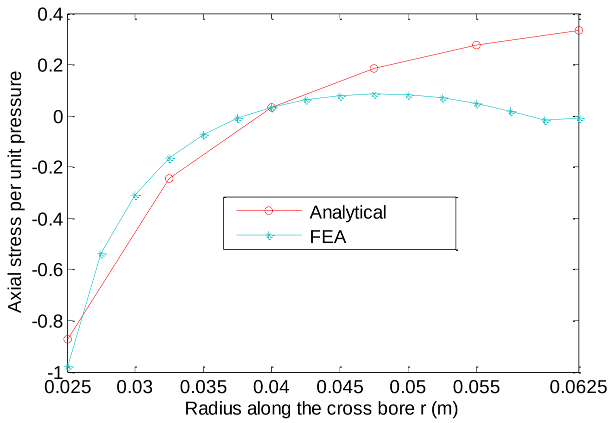

Figure 78 : K = 2.5 CB = 0.5

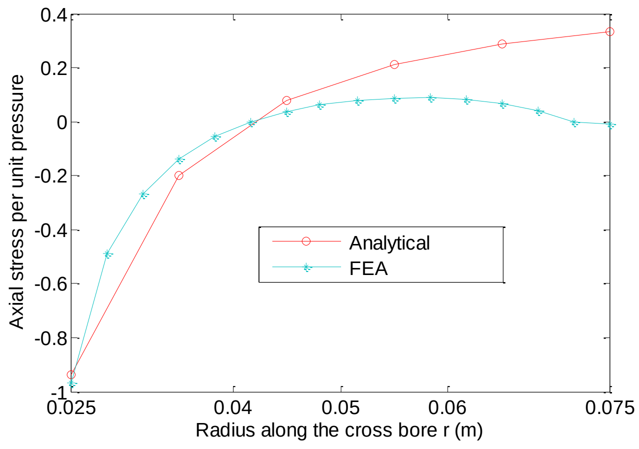

Figure 79: K = 3.0 CB = 0.5

Figures 73-79: Axial stress distribution per unit pressure for various thickness ratios along a radial circular cross bore, with a cross bore to main bore size ratio of 0.5.

As illustrated in Figures 73 to 79, the stress distribution had similar patterns as observed in the preceding sections 4.2.3.1 and 4.2.3.3. The FEA method gave the highest compressive axial stresses at the intersection. The stresses ranged between -0.963 to -0.984, being close to -1. Moreover, for K = 2.25, 2.5 and 3.0 the results from the analytical and FEA at the intersection were in close agreement.

Furthermore, a good agreement in the prediction of stress distribution results by the two methods was seen in thickness ratios of K = 1.75, 2.0, 2.25, 2.5 and 3.0. As shown in Figures 75 to 79, the closest agreement in results between the two methods occurred only at the cross bore intersection, after which, there were large inconsistencies in the stress distributions given by these two methods. This occurrence may be as a result of some of the assumptions made during the derivation of the analytical solution. For instance, large cross bores may introduce varying magnitudes of bending and shearing stresses along curved surface of the cylinder which is contrary to the analytical assumptions during the development of the solution.

With the exception of K = 1.5, the data given by the FEA approach gave small values of tensile axial stresses. The highest stress value was reported at 0.0886 on K=3. From the FEA results, it was noted that there were no axial stresses at the outside surfaces of the cylinders in all the thickness ratios. In contrast, the analytical method predicted high tensile stresses at the cross bore surfaces. The highest analytical stress had a magnitude of 0.0375 occurring at K = 1.5.

4.2.3.4 Cross bore to main bore ratio of 0.7

Results of axial stresses in a thick walled cylinder for cross bore size ratio of 0.7 are presented in Figures 80-86 for K = 1.4, 1.5, 1.75, 2.0, 2.25, 2.5 and 3.0.

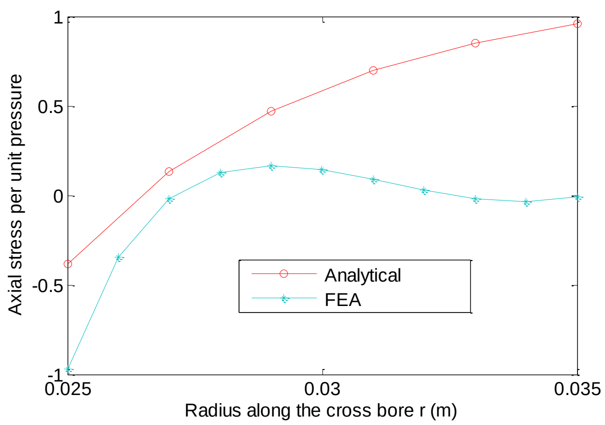

Figure 80: K = 1.4 CB = 0.7

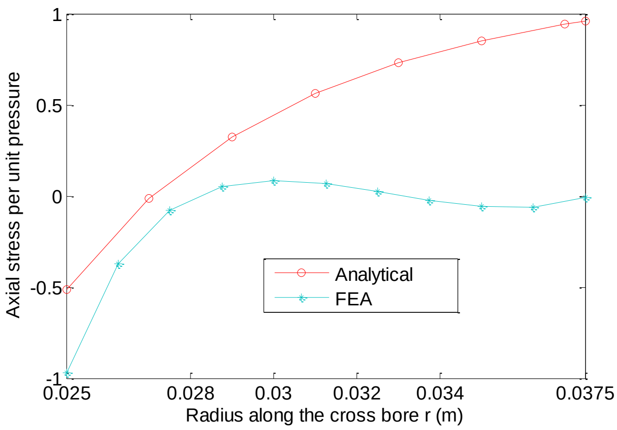

Figure 81: K = 1.5 CB = 0.7

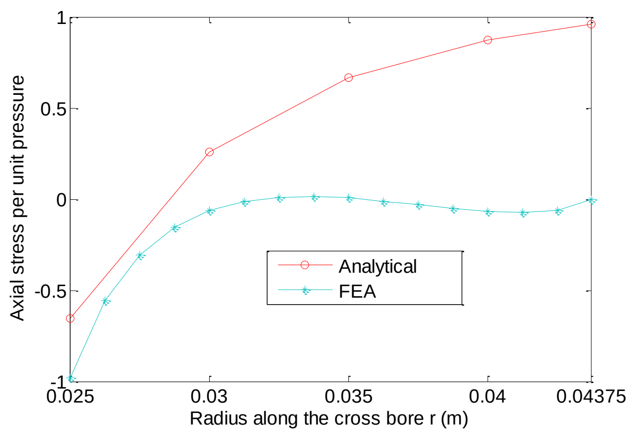

Figure 82: K = 1.75 CB = 0.7

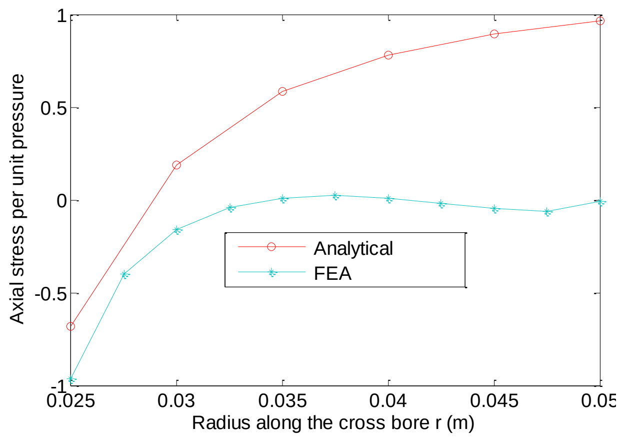

Figure 83 : K = 2.0 CB = 0.7

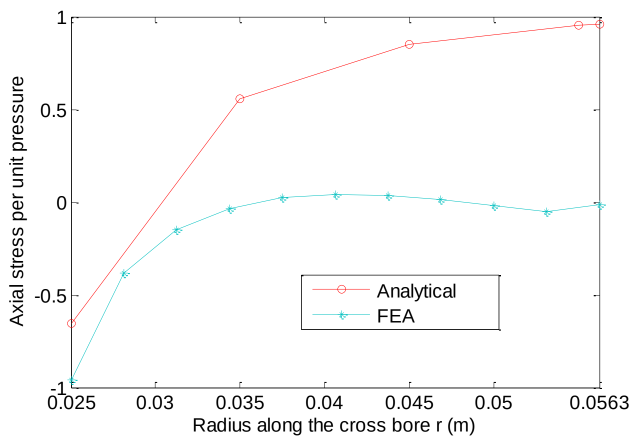

Figure 84: K = 2.25 CB =0.7

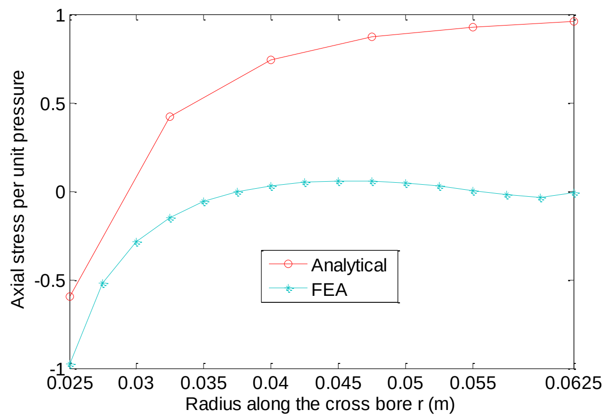

Figure 85 : K = 2.5 CB = 0.7

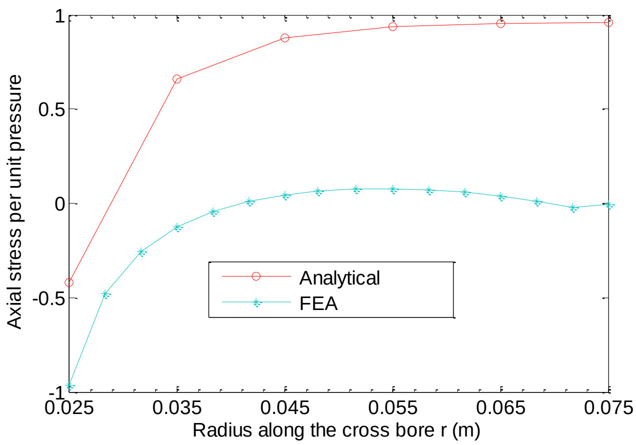

Figure 86: K = 3.0 CB = 0.7

Figures 80 - 86: Axial stress distribution per unit pressure for various thickness ratios along a radial circular cross bore, with a cross bore to main bore size ratio of 0.7.

Inconsistencies in stress distributions predicted by the two methods on this cross bore size were more pronounced in this cross bore ratio than in the preceding three ratios. These stress distribution inconsistencies are shown in Figures 80 to 86. The disparity between the two methods was seen to increase after the centre of the cylinder thickness. From these illustrations, it was evident that there was no meaningful correlation between the results given by the two methods.

The FEA approach predicted compressive axial stresses at the intersection which ranged from -0.957 to -0.983. In contrast, the analytical method gave lower stresses ranging from -0.382 at K = 1.4 to -0.68 at K = 2.0.

At the outside surface of the cylinders, the analytical method gave higher values of tensile axial stress than FEA approach. The stresses given by the analytical method were constant at 0.96 for all the thickness ratios. Conversely, the FEA method predicted zero axial stress at the same point. The highest tensile stress given by the FEA method occurred in K = 1.4 at 0.168, whereas, the lowest was at K = 1.75 at 0.0143.

4.2.3.5 Cross bore to main bore ratio of 1.0

Results of axial stresses in a thick walled cylinder with cross bore size ratio of 1.0 are presented in figures 87 to 93 for K = 1.4, 1.5, 1.75, 2.0, 2.25, 2.5 and 3.0.

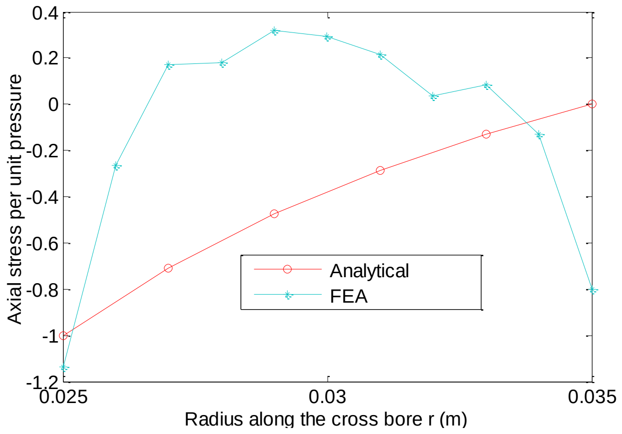

Figure 87: K = 1.4 CB =1.0

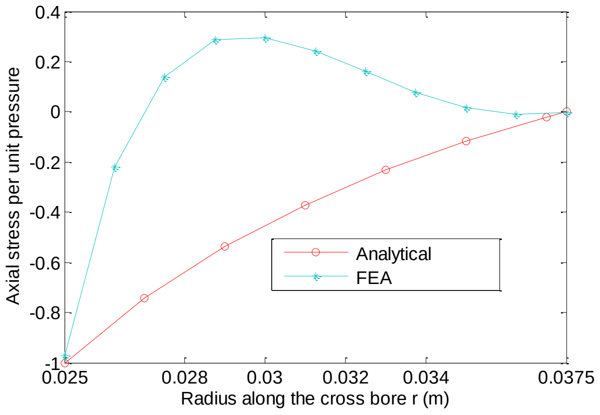

Figure 88: K = 1.5 CB = 1.0

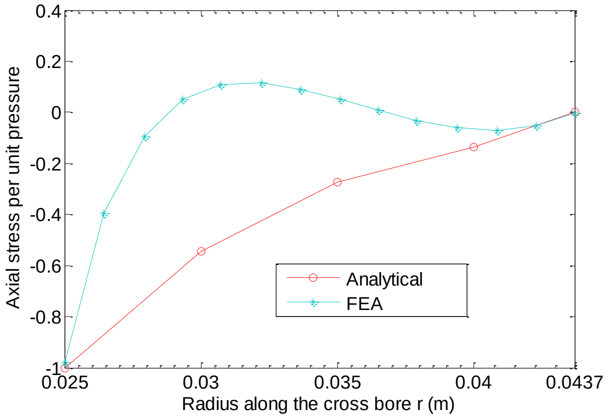

Figure 89: K = 1.75 CB =1.0

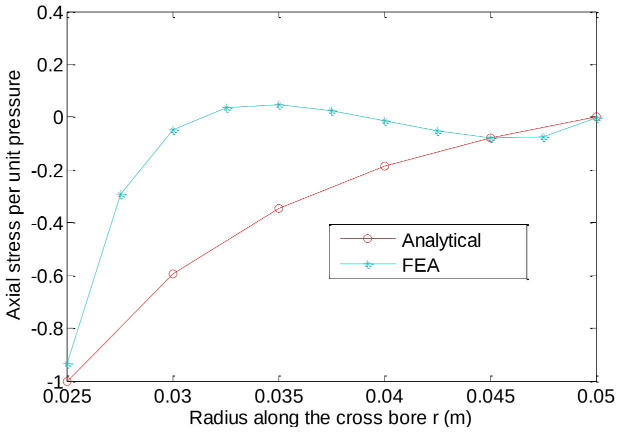

Figure 90: K = 2.0 CB = 1.0

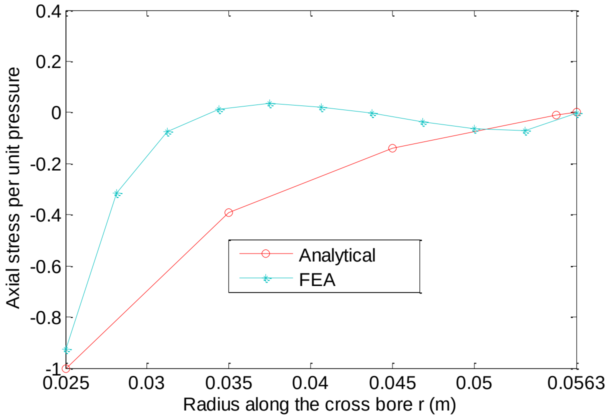

Figure 91: K = 2.25 CB =1.0

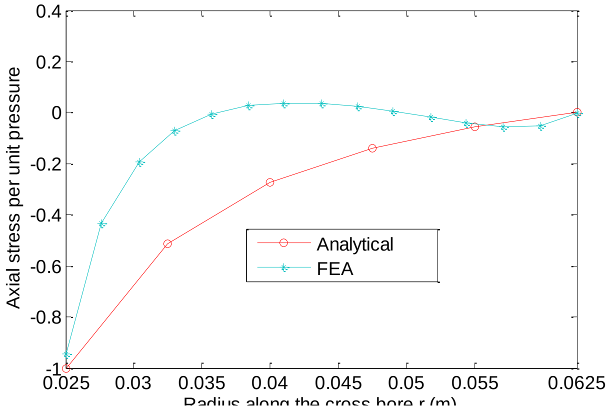

Figure 92: K = 2.25 CB =1.0

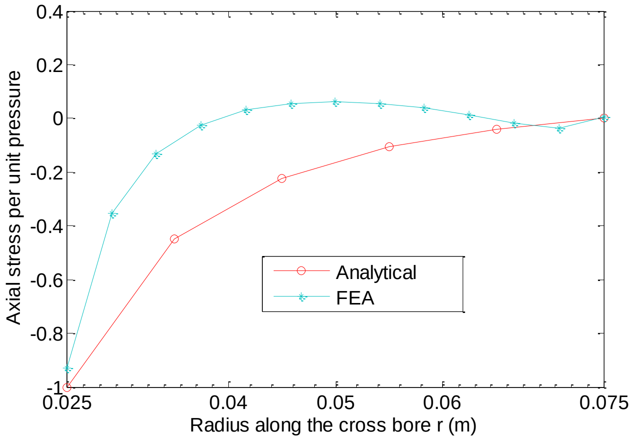

Figure 93: K = 3.0 CB = 1.0

Figures 87 - 93: Axial stress distribution per unit pressure for various thickness ratios along a radial circular cross bore with a cross bore to main bore size ratio of 1.0.

Disparity in axial stress distribution between the two methods was more pronounced in the middle of the cylinder as shown in Figures 87 to 93. However, the disparity in stress distribution was minimal at the cross bore intersection and at the outside surface of the cylinder.

The stresses predicted by the two methods at the cross bore intersection were found to be in good agreement. The analytical stress at the intersection was compressive and constant at -1 for all the thickness ratios, whereas, the FEA stresses ranged between -1.137 at K = 1.4 to -0.924 at K = 2.25. With the exception of K = 1.4 for the FEA method, the axial stresses predicted by the two approaches at the outside surfaces of the cylinders were zero. The FEA approach at K = 1.4 predicted an axial stress per unit pressure of magnitude -0.803 at the same point. Therefore, no tensile axial stresses occurred in this cross bore ratio as predicted by the analytical method.

FEA method predicted a gradual change in stress distribution along the cylinder thickness, except for K = 1.4 where the stress varied sharply as shown in Figure 87. The tensile axial stresses resulting from the FEA method ranged from 0.0346 at K = 2.25 to 0.318 at K = 1.4.

In conclusion, the axial stresses were found to vary along the cross bore depth in all the studied cases. This observation contradicted the earlier studies by Faupel and Harris (1957) and Ford and Alexander (1977) which had indicated that the axial stress is constant along the cross bore. Usually, the total axial stress along the cross bore is the summation of the axial stresses generated by the main cylinder with a bore and the corresponding radial stresses produced by the pressurised cross bore when acting alone. Thus, the sum of these stresses vary along the cross bore. In addition, the presence of varying magnitudes of bending moments and shearing stresses along the depth of the cross bore. This occurrence results to non-uniform stress field around the cross bore.

4.2.4 General discussion on correlation of analytical and numerical solutions

From the results presented in the preceding sections, it was evident that the developed analytical solution predicted correctly some of the principal stresses along the cross bore. In this study, the focus was mainly on the cross bore intersection, where stresses were high. A summary of the cylinder sizes and their corresponding cross bore size ratios, where the analytical hoop stresses' magnitudes were in agreement with FEA at the cross bore intersection, is shown in Table 16. Similarly, Table 17 shows the cylinder sizes and cross bore size ratios where the axial stresses' magnitudes resulting from the two different approaches at the intersection were consistent.

Table 16: Hoop stress at cross bore intersection where the analytical and FEA results were in good agreement.

Cylinder thickness ratio (K)	Cross bore size ratio
2.25 and 2.5	0.1
2.5 and 3.0	0.3
2.0 and 2.25	0.5
1.75 and 2.0	0.7
1.75	1.0

Table 17 : Axial stress at cross bore intersection where the analytical and FEA results were in good agreement.

Cylinder thickness ratio (K)	Cross bore sizes
2.25, 2.5 and 3.0	0.1
2.5 and 3.0	0.3
2.25, 2.5 and 3.0	0.5
None	0.7
All	1.0

Out of 35 models studied, the analytical solution correctly predicted the magnitude of the hoop stresses in 9 models and that of axial stresses in 15 models. Further, the magnitude of the radial stresses along the cross bore compared favourably between the two methods in all the studied cases, except in the largest cross bore with size ratio of 1.0.

In brief, for small cross bores, the total hoop stress along the cross bore in the cylinder is the sum of the hoop stresses in the main cylinder with a bore superimposed to the corresponding one generated by the pressurised cross bore when it is presumed to be acting alone. On the other hand, the total radial stress along the cross bore is the sum of the radial stresses in the main cylinder with a bore and the corresponding axial stresses produced by the pressurised cross bore. Likewise, the total axial stress is the summation of the axial stresses generated by the main cylinder with a bore and the corresponding radial stresses produced by the pressurised cross bore when acting alone.

A preliminary numerical study was done arbitrarily on K = 3.0 having the smallest cross bore size of 0.1 to determine separately the magnitude of the hoop stress generated by the main cylinder and that of the cross bore. For the main cylinder, the internal pressure was applied at the inside surface of the cylinder only. Similarly, for the cross bore, the internal pressure was applied on the cross bore only. The hoop stress per unit pressure due to the separate loading was found to be 3.0 and 0.88 for the main cylinder and cross bore, respectively. Thus, the sum of the hoop stresses per unit pressure in the cylinder was 3.88. Therefore, the hoop stress generated by the main cylinder alone was 77.3%, while that of the cross bore was 22.7%. According to Ford and Alexander (1977) this superimposing phenomenon is true whenever the size of the cross bore size is small, because other factors such as Poisson's ratio have insignificant effects. Further comparison between maximum hoop stresses generated by the cross bored cylinder alone with that of a similar plain cylinder indicated an increase of hoop stress by 140%.

Furthermore, the magnitude of the total radial stress per unit pressure obtained when the inside surfaces were loaded separately were respectively -0.9636 (compressive) and 0.0034 for the main cylinder and the cross bore. Likewise, for axial stress per unit pressure the corresponding values were 0.112 and -0.954 (compressive).

Contrary to the assumption made in the derivation of the analytical solution, it was revealed that despite the magnitude of the axial stress being small it was not necessarily zero. Hence, the disparities in the analytical and numerical results.

Moreover, the disparities in results resulting from the two approaches were attributed to some of the assumptions made during the solution development and the limitations of the Abaqus software, as presented in Chapter 3. For instance, in the development of the analytical solution it was assumed that the cylinder curvature has no effect on stress distribution. In addition, it was assumed that the axial stress was constant along the cross bore. This assumption of constant axial stress was contrary to the axial results presented by this study. Nevertheless, the ability of the Abaqus software in predicting the stresses correctly at the surface was not confirmed. A numerical software suitable for the determination of surface stresses was recommended.

It is worthwhile to mention that, the three principal stresses discussed in the preceding sections are mainly used in stress calculation in elastic failure theories. The commonly used theories in elastic failures are Tresca's and Von Mises's. These theories have many design applications such as in the design of pressure vessel, multi axial yield loading and in fracture mechanics (Comlecki *et al.*, 2007), among others. Thus, their importance can't be over emphasized. However, since this study was based on fatigue failures, as presented earlier in section 3.3, only the hoop stress was more relevant.

The development of an analytical solution in cross bored pressure vessels, whenever the cross bore is neither circular nor at radial position, involves complex mathematical expressions which are cumbersome and time consuming to solve. In this regards, therefore, only the FEA method was used in analysing stresses during the cross bore optimisation process, presented in the following section.

4.3 OPTIMISATION OF THE CROSS BORE

Results generated during the optimisation process for the selected geometric parameters of the cross bore are presented in the following headings:

4.3.1 Optimisation of the radial cross bore size

In this section, the size optimisation for the radial circular cross bore was done on the five selected cross bore sizes. This optimisation process took into consideration the magnitude of maximum hoop stress in the cylinder, which results from the introduction of a circular radial cross bore. Stress concentration factors were then computed based on the maximum hoop stress in the cylinder and its corresponding location in a plain cylinder.

4.3.1.1 Effects of cross bore size and cylinder thickness ratio on maximum hoop stress

Figures 94 and 95 show the variation of hoop stress with cross bore size and thickness ratio, respectively.

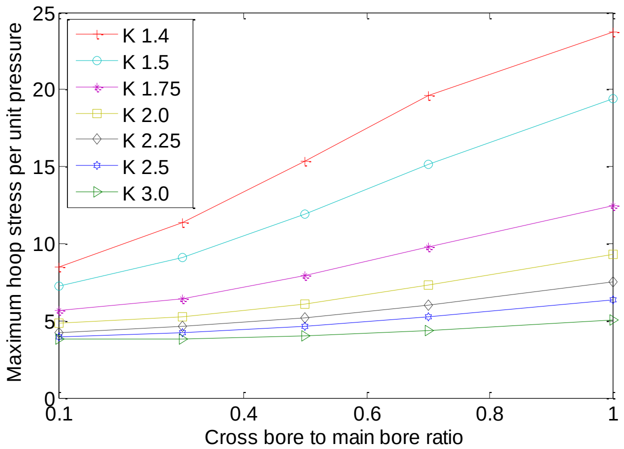

Figure 94: Hoop stress vs cross bore size

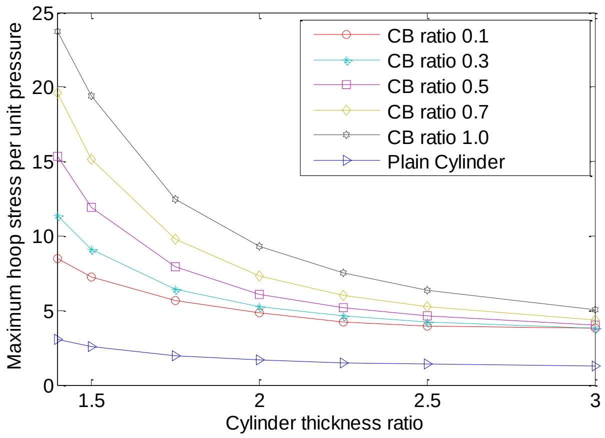

Figure 95: Hoop stress vs thickness ratio

As shown in Figure 94, it was observed that the hoop stress increases with the increase in the cross bore size. This increase in the hoop stress was more pronounced in the cylinders with small thickness ratios, specifically K = 1.4 and 1.5. For instance, the comparison of hoop stress between the cross bore size ratio of 0.1 and that of 1.0 for K = 1.4 and 1.5 gave a hoop stress increase of 180.14% and 167.64%, respectively. The structural stiffness of the cylinder is affected by both the thickness ratio and cross bore size. As the thickness ratio reduce, the structural stiffness reduce leading to high magnitudes of hoop stresses. Further reduction of the structural stiffness is observed whenever there is an increase in the cross bore size leading to much higher magnitudes of the hoop stresses.

For a similar cross bore size ratio, the difference in hoop stresses for K = 2.5 and 3.0, showed a hoop stress increase of 60.94% and 32.95%, respectively. These observations revealed that the rise in hoop stress due to the size of the cross bore, reduces with increase in thickness ratio. Likewise, the structural stiffness of the cylinder increases with increase in thickness ratio leading to lower magnitudes of hoop stresses in comparison to cylinder with smaller thickness ratios.

Figure 95 further confirmed the earlier finding that, the magnitude of hoop stress in a cross bored cylinder reduces as the thickness ratio increases. The increase in hoop stress due to the radial cross bore was highest in K = 1.4. The hoop stress increase in K = 1.4 between the cross bore size ratios of 0.3, 0.5, 0.7 and 1.0 in reference to 0.1 was 27.46%, 72.68%, 120.394% and 166.17%, respectively. In contrast, the rise in hoop stress was observed to reduce gradually with an increase in the thickness ratio. The lowest rise in hoop stress was reported at K=3 since at this value, the rise in hoop stress between cross bore size ratio of 0.1 in comparison to that of cross bore size ratios of 0.3, 0.5 and 0.7 was below 14.34%. Only, a rise of 32.96% in hoop stress between similar cross bore sizes as indicated in preceding paragraph was noted.

The magnitude of hoop stress in a cylinder with radial cross bore was higher in comparison to a similar plain cylinder without a cross bore as indicated in Figure 95. This observation was in line with other previous studies done by Masu (1997), Comlecki *et al*. (2007) and Makulsawatudom *et al*. (2004).

Noticeably, the cross bore size ratio of 0.1 gave the lowest rise in hoop stress when compared to the other four cross bore sizes. Further comparison was done between the hoop stresses generated by the cross bore size ratio of 0.1 and that of the plain cylinder without the cross bore. This comparison established the behaviour of stress variation in reference to the plain cylinder. The rise in hoop stress for thickness ratios 1.4, 1.5, 1.75, 2.0, 2.25, 2.5 and 3.0 was found to be 174.67%, 178.5%, 186.34%, 192.2%, 183.58%,186.97 and 204.4%, respectively, with the lowest and highest rise, occurring at K = 1.4, and 3.0 respectively. A significant drop in the hoop stresses between K = 2.0 and 2.25 was also observed. This stress drop implied an existence of stress transition point between the two thickness ratios. This is probably an indication of change of state of stress from plane stress to plane strain. Usually at the transition point there is stress redistribution around the cross bore that may lead to the stress drops and peaks.

In general, the cross bore size ratios of 0.1 gave the lowest hoop stress, while the highest stress occurred in 1.0. Similar occurrence had been reported by other previous studies by Hearn (1999) and Nihous *et al.* (2008). Usually large cross bores entail excessive removal of materials in the cylinder, and as a result, only little material is left to bear the applied load. This excessive removal of material leads to an increase in hoop stress which might cause failure of the cylinder.

4.3.1.2 Location of maximum principal stress in the cylinder

The location of the maximum hoop stress on the cylinder generally occurred along the radial cross bore. The exact position for all the studied cases are tabulated in Table 18. This data is given in the

Table 18 : Location of maximum hoop stress in the cylinder

Thickness	Cross bore size ratio	Radius R (m)	Horizontal distance measured from the transverse axis of the main cylinder (m)
1.4	0.1	0.026	0
	0.3	0.025	0
	0.5	0.025	0
	0.7	0.025	0
	1.0	0.025	0.001
1.5	0.1	0.02625	0
	0.3	0.025	0
	0.5	0.025	0
	0.7	0.025	0
	1.0	0.025	0
1.75	0.1	0.02625	0
	0.3	0.025	0
	0.5	0.025	0
	0.7	0.025	0
	1.0	0.025	0

Thickness	Cross bore size ratio	Radius R (m)	Horizontal distance measured from the transverse axis of the main cylinder (m)
2.0	0.1	0.025	0
	0.3	0.025	0
	0.5	0.025	0
	0.7	0.025	0
	1.0	0.025	0.001
2.25	0.1	0.025	0
	0.3	0.025	0
	0.5	0.025	0
	0.7	0.025	0
	1.0	0.025	0.001
2.5	0.1	0.025	0
	0.3	0.025	0
	0.5	0.025	0
	0.7	0.025	0
	1.0	0.025	0.001

Thickness	Cross bore size ratio	Radius R (m)	Horizontal distance measured from the transverse axis of the main cylinder (m)
3.0	0.1	0.026	0
	0.3	0.025	0
	0.5	0.025	0
	0.7	0.025	0
	1.0	0.025	0.001

form of the main cylinder radius and the horizontal distance from the transverse edge of the cross bore. From this tabulation, the maximum hoop stress for most of the studied cases occurred in the transverse plane, at the intersection between the main bore and the cross bore except for the values of K = 1.4, 1.5 and 1.75. The location of the maximum hoop stress for K = 1.4, 1.5 and 1.75 due to the cross bore size ratio of 0.1 occurred approximately 1.25 mm away from the intersection along the transverse plane. This occurrence was attributed to the change in state of stress from plane stress to plane strain usually resulting from geometry change. The change of state of stress results to stress redistribution around the cross bore causing stress peaks. Similar observations had earlier been reported by Masu (1997).

Generally the maximum hoop stress occurred along the cross bore transverse plane for all the cross bore sizes ratios between 0.1 and 0.7. This occurrence signified an existence of uniform stress field distribution around the cross bore indicating plane stress conditions.

With the exception of K = 1.5 and 1.75 it was also noted that the location of maximum principal stress due to the largest cross bore size, 1.0, shifted slightly away from the cross bore transverse plane. Upon loading, large cross bores experience varying bending and shearing stresses along cross bore. This occurrence causes non uniform stress fields around the cross bore leading to the location shift of maximum principal stresses.

4.3.1.3 Effects of cross bore size and thickness ratio on hoop stress concentration factor

Stress Concentration Factor (SCF) is a dimensionless quantity that enables effective comparison of stresses between different parameters regardless of their size, shape, thickness or the applied load. In this work the stress concentration factor was defined as the ratio of localised critical stresses in a cross bore cylinder to the corresponding one in a similar cylinder without a bore. The SCFs for cylinders with different cross bore sizes and thickness ratios were calculated based on locations with the highest magnitudes of hoop stress in the cylinder. Figures 96 and 97 show the variation of stress concentration factor with cross bore size and thickness ratio.

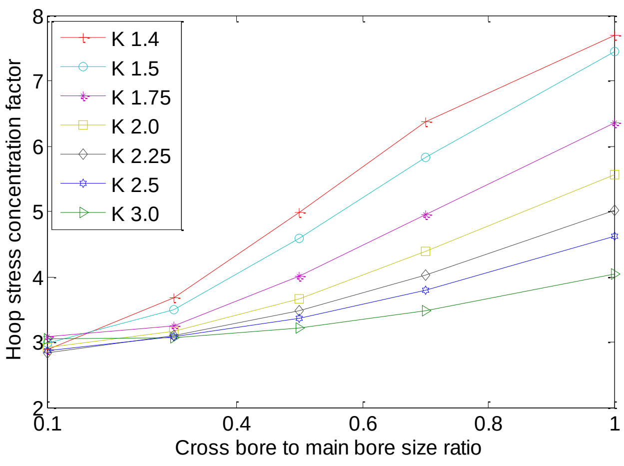

Figure 96: Hoop SCF vs cross bore size

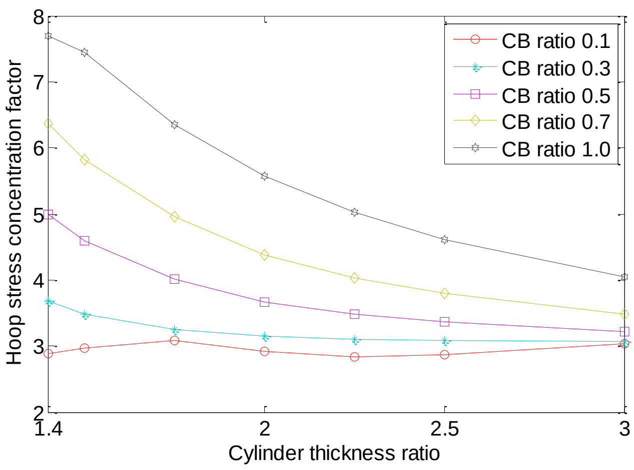

Figure 97: Hoop SCF vs thickness ratio

As illustrated in Figure 96, the hoop stress concentration factor was lowest at smallest cross bore with size ratio of 0.1. Moreover, the lowest SCF given by this cross bore size occurred in K = 2.25 with a magnitude of 2.836, while the highest stress concentration factor predicted by the same cross bore size occurred at K = 3.0 with a magnitude of 3.044, being an increase of 7.33%. In contrast, the highest SCF in the cylinder was reported in the largest cross bore size of 1.0. In this cross bore size of 1.0, the highest SCF occurred at K = 1.4 with magnitude of 7.687, whereas, the lowest SCF was noted at K=3.0 with a magnitude of 4.047. Generally, it was observed that, the magnitude of SCF increased with increase in the cross bore size. As the cross bore size increase, the structural stiffness of the cylinder reduce. This leads to generation of high hoop stresses and consequently high SCFs.

With the exception of the smallest cross bore size, the SCF was observed to reduce with increase in the thickness ratio as illustrated in Figure 97. The rise in magnitude of SCF given by the smallest cross bore of 0.1, in comparison to similar ones of the plain cylinder for K= 1.4, 1.5, 1.75, 2.0, 2.25, 2.5 and 3.0 which were found to be 188.8%, 197.7%, 207.8%, 192.2%, 183.6%,186.9% and 204.4%, respectively. This rise in SCF profile was slightly higher than that of hoop stresses presented earlier in Section 4.3.1.1. The rise in stress value was attributed to the consideration of location of the maximum principal stress during the computation of the SCF. It is worthwhile noting that the hoop stress does not take into consideration the location effects.

A summary of some of the results from the present work in comparison to the existing published data is indicated in Table 19.

Table 19 : Comparison of stress concentration factors for radial cross bores

	Comlekci *et al*. (2007) study	Present study	Makulsawatudom *et al*. (2004) study	Comlecki *et al*. (2007) study	Present study
K	CB = 0.1	CB = 0.1	CB = 0.1	CB = 0.25	CB =0.25
1.4	2.76	2.888	-	3.01	3.482
1.5	2.81	2.977	-	2.95	3.361
1.75	2.93	3.078	-	2.91	3.208
2.0	3.03	2.922	2.89	2.92	3.090
2.25	3.11	2.869	-	2.95	3.036
2.5	3.18	3.044	-	2.98	3.03

Unlike in the other previous studies, the comparison of SCF took into consideration both the cross bore size and the thickness ratio. The results of the hoop SCF presented in this study were compatible with those published by Comlecki *et al*. (2007) and Makulsawatudom *et al*. (2004) for the cross bore size ratio of 0.1. Comlecki *et al*. (2007) published other additional data having different cross bore size ratios. The closest cross bore size ratio to the present study being 0.25. This occurrence necessitated the results of the presented study to be interpolated between the cross bore ratios of 0.1 and 0.3 to give SCF values for 0.25. The values were read from Figure 96. Upon comparison, the two results were also found to be in close agreement.

Contrary to the solution of the circular hole in a plate, where the stress concentration factor reduces with increasing hole size (Nagpal *et al.*, 2011), and a maximum SCF of 3.0, regardless of the hole size was found, the hoop stress as well as stress concentration factor resulting from the introduction of circular radial cross bores in thick cylinders was found to increase with an increase in the cross bore size. For instance, in the development of the solution of the circular hole in a plate, it was assumed that the width of the plate is large in comparison to the cross bore. Further, it was also assumed that the applied load was in the axial position. In addition, the plane stress theory ignores the effects of the shearing stress as well as the bending moment around the cross bore. Thus, it assumes a uniform stress distribution field around the cross bore. These assumptions might not be applicable in thick walled cylinders due to their curvature nature.

Another analytical study published by Faupel and Harris (1957) gave the SCF for a circular hole in a closed thick cylinder as being constant at 2.5 without taking into consideration the size of the cross bore. This analytical solution by Faupel and Harris (1957) was also in contradiction with the findings of this study. In conclusion, the size of a cross bore as well as the thickness ratio plays a significant role in determining the hoop stress as well as the stress concentration factor. These finding are also extended to the fatigue behaviour of the component.

4.3.1.4 Shearing stresses

4.3.1.4.1 Effects of cross bore size and thickness ratio on maximum shearing stress

The magnitude of maximum shear stress depends on the difference between the hoop and radial stresses. Since the hoop stress depends on the thickness ratio, a direct comparison among the thickness ratios is not possible. The maximum shearing stress was found to be affected by both the cross bore size and thickness ratio as illustrated in Figures 98 and 99.

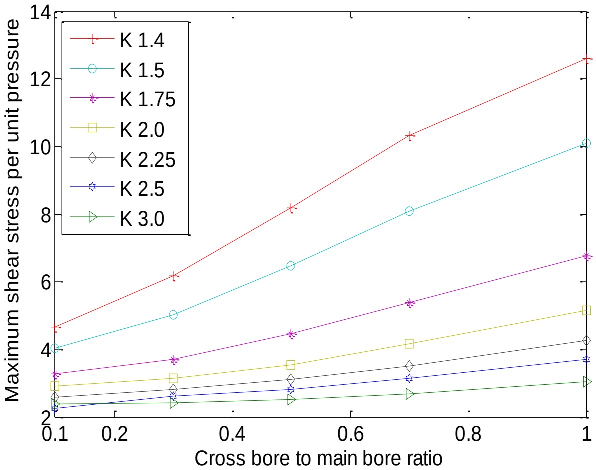

Figure 98: Maximum shear stress vs cross bore size

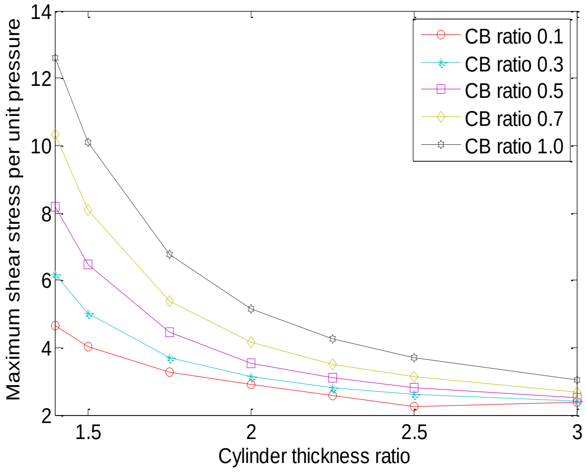

Figure 99: Maximum shear stress vs thickness ratio

The maximum shear stress increased with an increase in cross bore size. Moreover, it was also observed to reduce with increase in the thickness ratio. Remarkably, a similar stress pattern exhibited previously in graphs of hoop stress versus the cross bore size ratio, was also observed in shear stress curves. This occurrence was attributed to the varying magnitude of the hoop stress along the cross bore. Since the corresponding radial stress along the cross bore is constant.

Generally, the highest magnitude of shear stress was observed to occur in RZ plane of the cylinder in the radial circular cross bores.

4.3.1.5 Elastic failure theories

In this section the working stresses together with their corresponding stress concentration factors were computed using elastic failure theories applicable to ductile materials, namely the Tresca's and the Von Mises's Theories. The results obtained were then evaluated to establish their effects on cross bore size in addition to the thickness ratio.

4.3.1.5.1 Effects of the cross bore size and cylinder thickness ratio on elastic working stress

A similar stress distribution pattern exhibited in the previous section was also displayed in this section as shown in Figures 100 to 103.

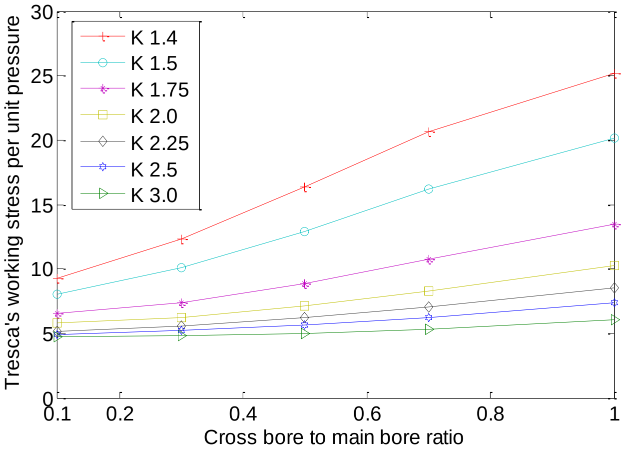

Figure 100: Tresca's stress vs cross bore size

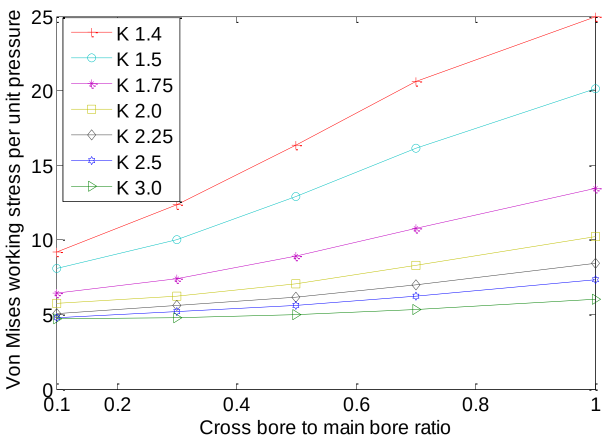

Figure 101: Von Mises's stress vs cross bore size

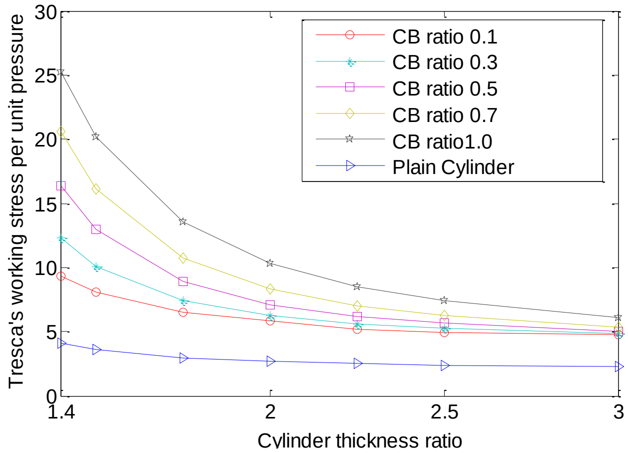

Figure 102: Tresca’s stress vs thickness ratio

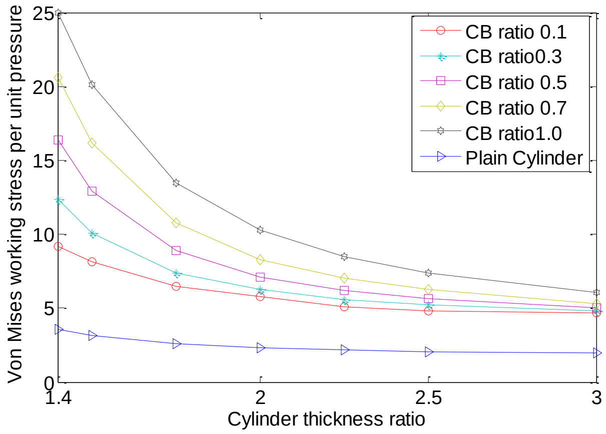

Figure 103: Von Mises’s stress vs thickness ratio

Usually, the difference between the working stress of the Tresca’s and the Von Mises’s Theories in plain cylinders without cross bore is approximately 15.5%. However, after the introduction of the cross bore, it was seen that the difference in the magnitude resulting from the two theories reduced tremendously. For instance, for K=1.4, the differences in working stress magnitude between the two failure theories due to the introduction of cross bore size ratios of 0.1, 0.3, 0.5, 0.7 and 1.0 were 1.13%, 0.08%, 0.06%, 0.1% and 0.92%, respectively. A similar trend was also replicated in K=3 where the working stress differences for the same cross bore ratio sizes discussed previously were 1.32%, 0.2%, 0.16%, 0.21% and 0.43%, respectively. This occurrence was attributed to small magnitudes of axial stresses along the cross bore surface. In fact, the analytical solution derived earlier in Chapter 3, assumed a zero magnitude of axial stress along the cross bore. This finding was contrary to that of plain cylinders where the axial stress is constant across the thickness and its magnitude is relatively high.

Further comparison between cross bored cylinders and plain cylinders revealed higher working stresses in the latter as illustrated in Figures 102 and 103.

4.3.1.5.2 Effects of cross bore size and cylinder thickness ratio on elastic working stress concentration factor

The variation of elastic working stress concentration factor with cross bore size and thickness ratio are illustrated in Figures 104 to 107.

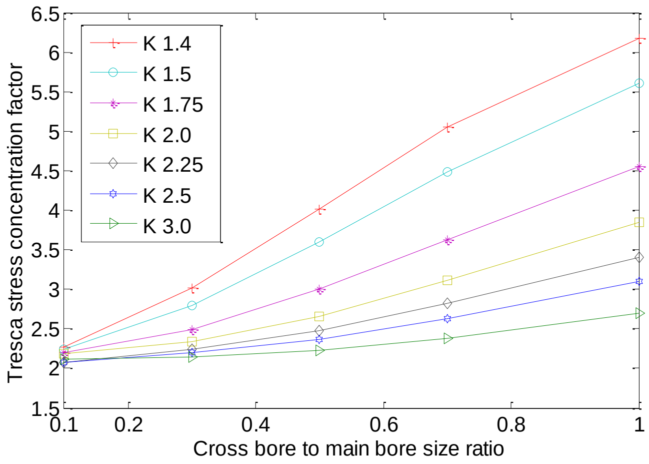

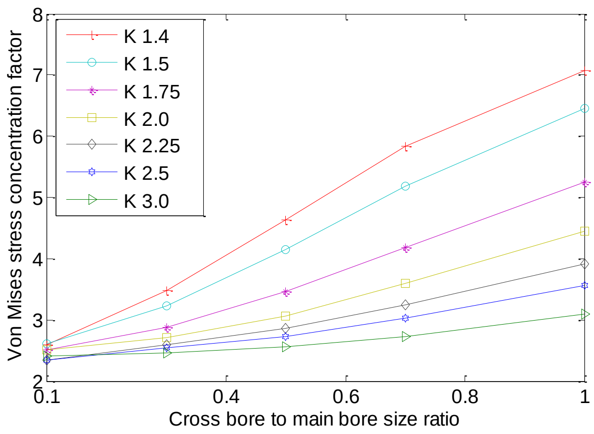

Figure 104: Tresca's SCF vs cross bore size

Figure 105: Von Mises's SCF vs cross bore size

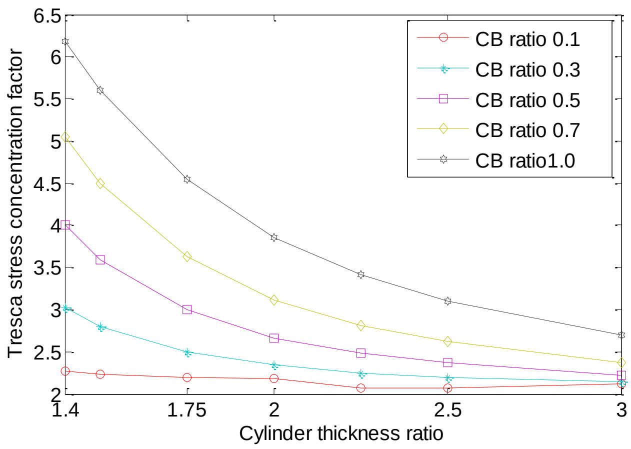

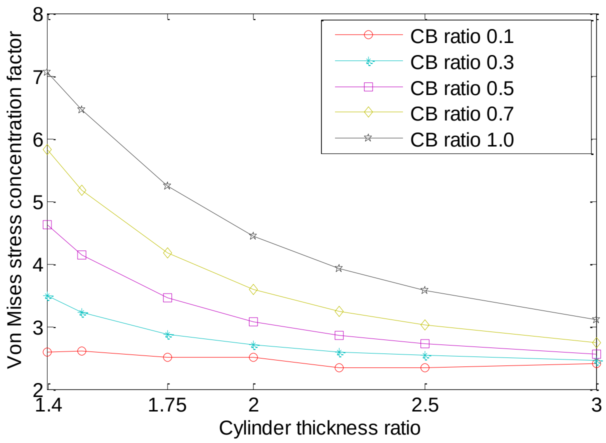

Figure 106: Tresca's SCF vs thickness ratio

Figure 107: Von Mises's SCF vs thickness ratio

It was observed that as the cross bore size ratio increased from 0.1 to 1.0, the maximum working stresses predicted by the two theories increased by a factor of approximately 2.5 to 7.07, in K = 1.4. Likewise, within a similar range, the minimum increase in working stresses was recorded in K = 3 where the working stress factor predicted by the two theories increased from 2.1 to 3.1. Therefore, for a pressure vessel to operate under elastic stress conditions, the internal pressure would be reduced by a similar corresponding factor with regard to the choice of thickness ratio and the cross bore size.

From the preceding sections, it is evident that the stress variation emanating from the elastic working stress and the maximum shear stress exhibited a close resemblance to those of hoop stress and stress concentration factor. This occurrence was attributed to the fact that these stress theories are dependent on the three principal stresses, namely hoop, radial and axial. From section 4.2, it was established that only the maximum principal stress (hoop) had a major effect on the overall stress along the cross bore depth due to its high magnitude. This is because the magnitude of the radial stress was found to be constant along the cross bore, while that of the axial stress was small. With this information, therefore, from now henceforth, the subsequent sections were more based on the hoop stress and the hoop stress concentration factors.

Figures 108 and 109 show the optimal SCF curves at each cross bore size ratio and thickness ratio obtained from the studied radial circular cross bores.

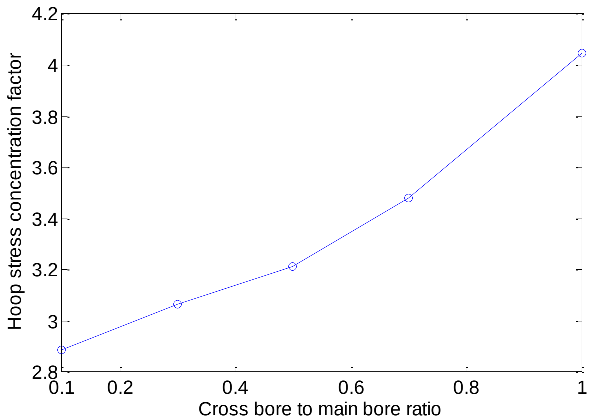

Figure 108: Optimal SCF vs cross bore size

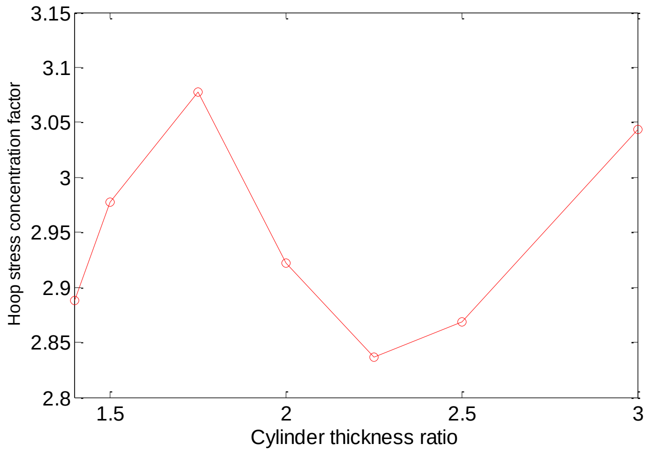

Figure 109: Optimal SCF vs thickness ratio

Amongst the five cross bore sizes studied, the smallest cross bore size ratio of 0.1 gave the lowest magnitude of SCF of 2.836 at K=2.25. This SCF magnitude indicated a reduction of pressure carrying capacity by 64.7% in comparison to a similar plain cylinder without a cross bore. This pressure carrying capacity was slightly higher than 60% cited earlier by Masu's (1989) study. In this regard, therefore, this cross bore size ratio was selected as the optimal size for a radial circular cross bore.

In the succeeding sections, further cross bore optimisation is done based on this optimum cross bore size ratio of 0.1, to establish the corresponding optimal location and shape of this cross bore.

4.3.2 Optimisation of cross bore shape and location

4.3.2.1 Introduction

In this section, the results obtained by offsetting a circular and elliptical optimised cross bore at five different location along the X axis plane, as shown in Figure 110 are presented. The actual offset positions $\bar{x}$ in the cylinders were 0, 6, 12, 17.125 and 22.5 mm. However, for the results to be compared directly with the existing literature, these offset position were converted to either offset location ratio or an included angle. As illustrated in Figure 110, the actual offset distance $\bar{x}$, was divided by the main bore radius R_i, i.e., ${}^{\bar{x}}/_{R_i}$, to give the offset location ratio. Whilst, the included angle θ was calculated using the trigonometric relationship between $\bar{x}$ and R_i.

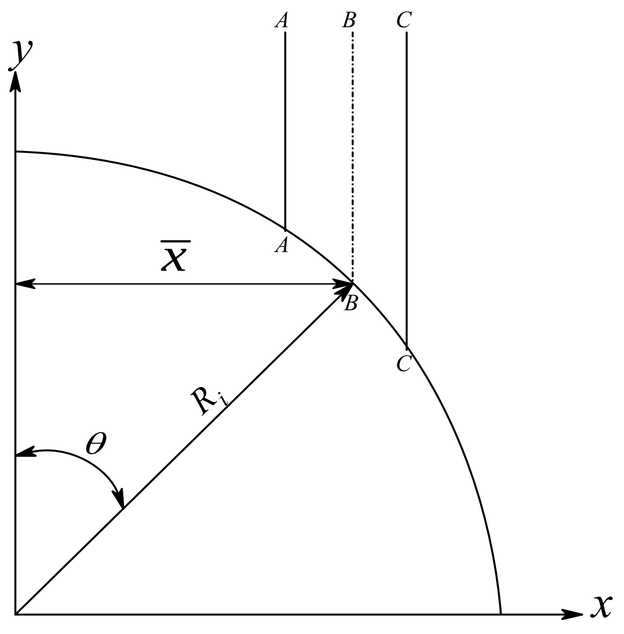

Figure 110 : Configuration of an offset cross bore

The data showing the conversion of these offset positions is tabulated in table 20.

Table 20: Conversion of offset positions

S/No.	Actual Offset distance $\bar{x}$ mm in the cylinder	Actual Offset distance $\bar{x}$ m in the cylinder	Offset ratio	Offset angle θ^0
1	0	0	0	0
2	6	0.006	0.24	13.8
3	12	0.012	0.48	25.64
4	17.125	0.017125	0.685	43.24
5	22.5	0.0225	0.9	64.16

4.3.2.2 Offsetting of Circularly shaped Cross bore

4.3.2.2.1 Location of maximum principal stress in the cylinder

The location of maximum principal stress on the cylinder due to the introduction of an offset circular cross bore is tabulated in Table 21. The data is presented in the form of the main cylinder radius and the corresponding horizontal distance measured from the transverse plane of the main cylinder.

The radial location of the maximum hoop stress in the cylinder as shown in Table 21 occurred mostly at the intersection between the cross bore and the main bore. However, with exception of radial cross bore, the location of maximum principal stress was observed to occur slightly away from the cross bore transverse position in the cylinder. In most of the offset cross bores, the location of maximum principal stress occurred close to plane axis AA (see Figure 110). This observation was contrary to the notion that maximum principal stress occurs along the cross bore transverse position, plane BB. Thus, this occurrence implied that any reduction in offset location ratio results to an increase of hoop stress. This trend confirms that the stress field distribution in the vicinity of cross bore is not uniform whenever the cross bore is at an offset position. Hence the plane stress conditions cease to apply.

Table 21 : Location of the maximum hoop stress in the cylinder due to an offset circular cross bore

K	Offset Ratio	Actual offset distance $\bar{x}$ m	Distance of the Cross bore Configuration measured from the transverse axis of the main cylinder			Position of Maximum Principle Stress in the Cylinder (m)	
			Plane AA	Plane BB	Plane CC	Radius R (m)	Horizontal distance $\bar{x}$, measured from the transverse axis of the main cylinder
1.4	0	0		0	0.0025	0.026	0
	0.24	0.006	0.0035	0.006	0.0085	0.025	0.006
	0.48	0.012	0.0095	0.012	0.0145	0.025	0.0111
	0.685	0.017125	0.014625	0.017125	0.019625	0.025	0.0163
	0.9	0.0225	0.02	0.0225	0.025	0.025	0.0206
1.5	0	0		0	0.0025	0.02625	0
	0.24	0.006	0.0035	0.006	0.0085	0.025	0.006
	0.48	0.012	0.0095	0.012	0.0145	0.025	0.0114
	0.685	0.017125	0.014625	0.017125	0.019625	0.025	0.0166
	0.9	0.0225	0.02	0.0225	0.025	0.025	0.02061

K	Offset Ratio	Actual offset distance $\bar{x}$ m	Distance of the Cross bore Configuration measured from the transverse axis of the main cylinder			Position of Maximum Principle Stress in the Cylinder	
			Plane AA	Plane BB	Plane CC	Radius R (m)	Horizontal distance $\bar{x}$, measured from the transverse axis of the main cylinder
1.75	0	0		0	0.0025	0.02625	0
	0.24	0.006	0.0035	0.006	0.0085	0.0258	0.006
	0.48	0.012	0.0095	0.012	0.0145	0.025	0.0111
	0.685	0.017125	0.014625	0.017125	0.019625	0.025	0.01631
	0.9	0.0225	0.02	0.0225	0.025	0.025	0.0206
2.0	0	0		0	0.0025	0.025	0
	0.24	0.006	0.0035	0.006	0.0085	0.025	0.006
	0.48	0.012	0.0095	0.012	0.0145	0.025	0.0111
	0.685	0.017125	0.014625	0.017125	0.019625	0.025	0.0163
	0.9	0.0225	0.02	0.0225	0.025	0.0253	0.021

K	Offset Ratio	Actual offset distance $\bar{x}$ m	Distance of the Cross bore Configuration measured from the transverse axis of the main cylinder			Position of Maximum Principle Stress in the Cylinder	
			Plane AA	Plane BB	Plane CC	Radius R (m)	Horizontal distance $\bar{x}$, measured from the transverse axis of the main cylinder
2.25	0	0		0	0.0025	0.025	0
	0.24	0.006	0.0035	0.006	0.0085	0.025	0.006
	0.48	0.012	0.0095	0.012	0.0145	0.0265	0.012
	0.685	0.017125	0.014625	0.017125	0.019625	0.025	0.0163
	0.9	0.0225	0.02	0.0225	0.025	0.025	0.0206
2.5	0	0		0	0.0025	0.0025	0
	0.24	0.006	0.0035	0.006	0.0085	0.025	0.006
	0.48	0.012	0.0095	0.012	0.0145	0.0264	0.012
	0.685	0.017125	0.014625	0.017125	0.019625	0.025	0.0163
	0.9	0.0225	0.02	0.0225	0.025	0.025	0.02108

K	Offset Ratio	Actual offset distance $\bar{x}$ m	Distance of the Cross bore Configuration measured from the transverse axis of the main cylinder			Position of Maximum Principle Stress in the Cylinder	
			Plane AA	Plane BB	Plane CC	Radius R (m)	Horizontal distance $\bar{x}$, measured from the transverse axis of the main cylinder
3.0	0	0		0	0.0025	0.025	0
	0.24	0.006	0.0035	0.006	0.0085	0.0287	0.006
	0.48	0.012	0.0095	0.012	0.0145	0.025	0.0111
	0.685	0.017125	0.014625	0.017125	0.019625	0.025	0.0163
	0.9	0.0225	0.02	0.0225	0.025	0.025	0.0211

Stress peaks occurring slightly away from the cross bore intersection were observed at various thickness ratios in all the offset positions. As noted previously, the location shift of the stress peak was also attributed to the change of state of stress from plane stress to plane strain. Existence of varying magnitudes of bending moments and shearing stress at each offset position due to the curvature of the cylinder also affect the location of the stress peak.

The stress peaks occurring away from the intersection of the cross bore and main bore lead to high stress concentration factors. The magnitude of SCF is obtained by the ratio of maximum hoop stress in a cross bored cylinder and the corresponding one in a similar plain cylinder. It is worth noting that the hoop stresses in plain thick cylinders are at a maximum at the inner surface of the bore and reduce gradually towards the outside surface of the cylinder. Thus, the magnitude of dividing ratio reduces towards the outside surface of the cylinder. Remarkably, only in K = 2.0 the stress peak occurred at the intersection of the cross bore and the main bore in all the offset positions.

4.3.2.2.2 Effects of cross bore location on hoop stress concentration factor

The curves showing the variation of hoop stress concentration factor with offset location and cylinder thickness ratios are shown in Figures 111 and 112, respectively.

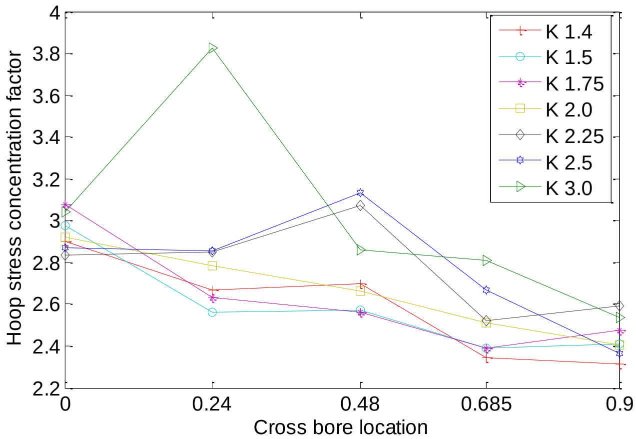

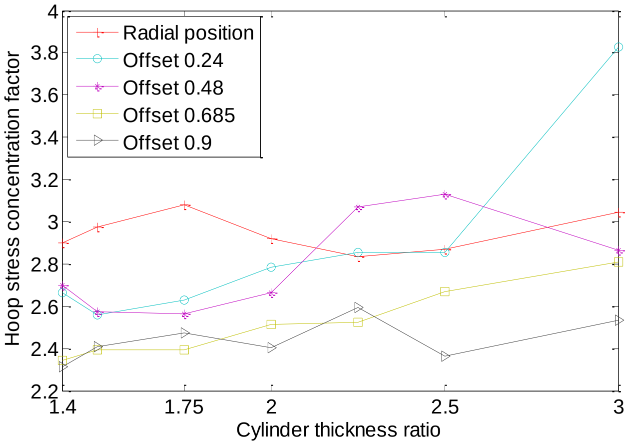

Figure 111: Hoop SCF vs cross bore location

Figure 112: Hoop SCF vs thickness ratio

The magnitude of hoop stress concentration factor at the radial position (zero offset) ranged from 2.836 to 3.078, occurring at K= 2.25 and 1.75. However, these SCF values recorded at radial position were generally higher than those at the 0.24 offset position except for K=3.0. The SCF at K=3.0 had the highest peak magnitude of 3.825. This stress peak was attributed to the position of the maximum hoop stress in the cylinder which occurred slightly away from the intersection at a radius of 0.0287 m.

The hoop stress concentration magnitude at 0.48 offset position was slightly higher than that of 0.24, for cylinders with K=1.4, 1.5, 2.25 and 2.5. However, for the other thickness ratios, the SCF magnitude was seen to reduce gradually.

For all the cylinders studied, the lowest magnitudes of SCF occurred either at 0.689 or 0.9 offset positions. For K= 1.5, 1.75 and 2.25, the minimum SCF were recorded at 0.689 with optimal magnitudes of 2.392, 2.391, 2.521, respectively, whereas for K= 1.4, 2.0, 2.5 and 3.0 the minimum SCF occurred at the 0.9 offset position. Respectively, the optimal SCF magnitudes were 2.312, 2.404, 2.365 and 2.535. A graph showing optimal SCF magnitudes at each thickness ratio for an offset circular cross bore is shown in Figure 113.

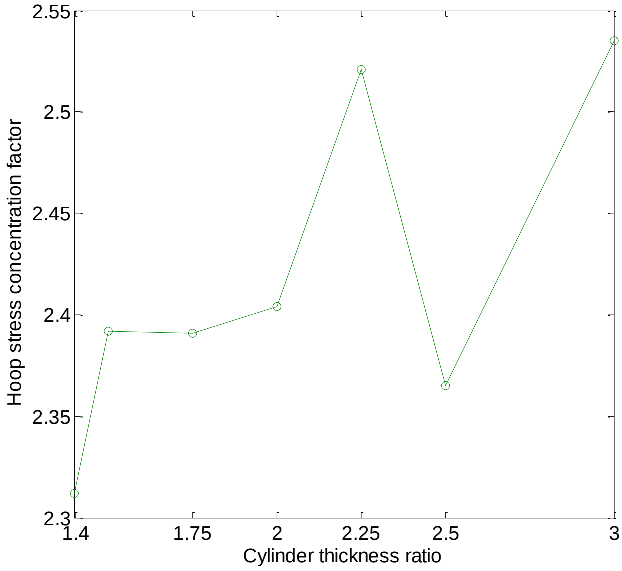

Figure 113: Optimal hoop SCF vs thickness ratio

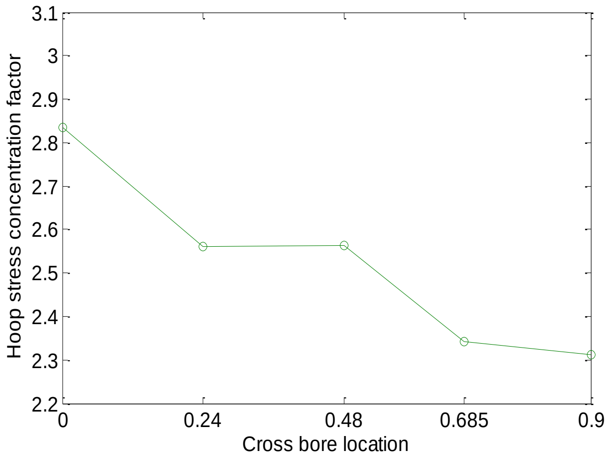

Figure 114: Optimal hoop SCF vs cross bore location

Likewise, the lowest SCF magnitude at offset position 0, 0.24, 0.48, 0.685 and 0.9 considering all the studied thickness ratios were found to be 2.836, 2.561, 2.563, 2.343 and 2.312, respectively. In the same order as described in the preceding sentence, the optimal cylinder thickness ratios were

K=2.25, 1.5, 1.75, 1.4 and 1.4. A graph showing optimal SCF magnitudes at each offset position for an offset circular cross bore is exemplified in Figure 114.

Interestingly, only the SCF for K=2.0 reduced gradually for the 0 to 0.9 offset positions. This observation was in agreement with other previous studies by Masu (1998) and Cheng (1978). Masu (1997) studied slightly smaller circular cross bore sizes, having a size ratio of only 0.064 for K=2.0. Even though the cross bore sizes were smaller, the data presented were generally consistent with the finding of this study. The SCFs presented by Masu (1997), considering the offset positions 0, 0.24 and 0.9, were 2.30, 1.9 and 1.33 respectively. This being a reduction of 17.3% and 42.17% from the values at the radial position. However, low SCF reductions of 8.86 % and 17.72% were reported by this study at the same offset position as Masu (1998). These two studies indicated a downward trend in SCFs as a result of circular cross bore offsetting. Nevertheless, the variation in percentage reduction of the SCFs between the two studies was attributed to the dissimilar sizes of the cross bore sizes studied. Another study conducted by Cheng (1978) experimentally investigated three different circular cross bore sizes, with size ratios of 0.05, 0.1 and 0.2 at varying offset locations for K=1.84. The SCFs given by the cross bore size ratio of 0.05 at offset position of 0.317 and 0.633 were 2.81 and 2.35, respectively. Likewise, the SCFs given by a cross bore size ratio of 0.1 at offset positions 0.3 and 0.6 2.58 and 2.23, respectively. Lastly, the SCFs reported for cross bore size ratio of 0.2 at offset positions of 0.267 and 0.533 were 2.5 and 2.08. This data by Cheng (1978) confirmed a significant reduction in SCFs due to the offsetting of the cross bore.

Another study by Makulsawatudom *et al.* (2004) erroneously cited the optimal offset location as being 0.112b, where b was termed as the outer radius of the cylinder. Unfortunately, this study by Makulsawatudom *et al.* (2004) had only been done on a single offset position. Therefore, this discussion did not take into consideration the results published by this author on offsetting of circular cross bores.

Further computation was done to establish the highest possible reduction of SCF that can be achieved by offsetting of the cross bore. The computation was based on the maximum and minimum SCF magnitudes obtained at each thickness ratio. Similar approaches were also done at each offset position. For K=1.4, 1.5 1.75, 2.0, 2.25, 2.5 and 3.0, the possible SCF reductions given by this optimisation process were 20.28%, 13. 973%, 16.73%, 17.72%, 11.61%, 17.57% and 33.73%, respectively. Likewise, for the offset locations 0, 0.24, 0.48, 0.685 and 0.9 the corresponding reductions were at 6.32%, 33.05%, 18.17%, 16.61% and 10.87%, respectively.

In general, whenever a circular cross bore is drilled in an offset position, the axis of the circular cross bore cylinder does not intersect with that of the main bore. Thus, the resulting configuration, when viewed at the intersection between the cross bore and main bore, resembles a slender elliptical hole with major and minor diameters. The major diameter, denoted as ‘a’ which is parallel to the direction of hoop stress tends to increase when the offset position is moved further away from the transverse plane of the cylinder. Whereas, the corresponding minor diameter, denoted as ‘b’, which is parallel to the axial direction of the cylinder reduces. This diameter configuration where $a > b$ leads to reduction in hoop stress as cited by Harvey (1985). Moreover, in section 3.3.3.2, the diameter ratio of 2 was proved as the optimal ratio in elliptical cross bores.

In conclusion, the optimal location for K= 1.5, 1.75 and 2.25, was at 0.689 offset ratio, while for K= 1.4, 2.0, 2.5 and 3.0 was realized at 0.9 offset position. Coincidently, the overall minimum SCF due to the introduction of a circular offset cross bore, with size ratio 0.1, satisfied both the thickness ratio and the offset position conditions. This optimum location was found to be at 0.9 offset position for K=1.4, with a SCF magnitude of 2.312. This SCF magnitude indicated a reduction of pressure carrying capacity by 56.7% in comparison to a similar plain cylinder without a cross bore. This pressure carrying capacity was slightly lower than 60% cited earlier by Masu’s (1989) study.

4.3.2.3 Elliptically shaped cross bores

4.3.2.3.1 Location of maximum principal stress in the cylinder

The location of maximum principal stresses on the cylinder due to the introduction of an offset elliptical cross bore is tabulated in Table 22. The data are presented in the form of the main cylinder radius and the corresponding horizontal distance measured from the transverse plane of the cylinder.

With the exception of K= 2.25 and 3.0, the radial location of the maximum stress peaks in the cylinder occurred away from the cross bore intersection, signifying stress transition points. Probably from the plane stress to plane strain. Similar to the circular offset cross bores, the location of maximum principal stress in the cylinder occurred away from the cross bore transverse axis plane BB. In fact, the position of the maximum principal stress in the cylinder occurred close to plane CC (see Figure 110). This observation was in contrast to that discussed earlier in section 4.3.2.2.1 for circular offset cross bores. This trend implied that any increase in offset location ratio results to an increase of the hoop stress.

Moreover, the location of the maximum principal stress in the cylinder, defined in terms of radial and transverse positions, also signified the presence of a high stress concentration factor in the cylinder. Usually, in pressure vessels design, the use of reinforcement pads are recommended whenever the maximum hoop stress is anticipated to occur close to the outside surface of the cylinder in order to prevent any failure

Table 22 : Location of the maximum hoop stress in the cylinder due to an offset elliptical cross bore

K	Offset Ratio	Actual offset distance $\bar{x}$ m	Distance of the Cross bore Configuration measured from the transverse axis of the main cylinder			Position of Maximum Principle Stress in the Cylinder	
			Plane AA	Plane BB	Plane CC	Radius R (m)	Horizontal distance $\bar{x}$, measured from the transverse axis of the main cylinder
1.4	0	0		0	0.0025	0.0336	0.0025
	0.24	0.006	0.0035	0.006	0.0085	0.035	0.0085
	0.48	0.012	0.0095	0.012	0.0145	0.035	0.0145
	0.685	0.017125	0.014625	0.017125	0.019625	0.035	0.019625
	0.9	0.0225	0.02	0.0225	0.025	0.035	0.025
1.5	0	0		0	0.0025	0.0359	0.0025
	0.24	0.006	0.0035	0.006	0.0085	0.0375	0.0085
	0.48	0.012	0.0095	0.012	0.0145	0.0375	0.0145
	0.685	0.017125	0.014625	0.017125	0.019625	0.025	0.019625
	0.9	0.0225	0.02	0.0225	0.025	0.025	0.025

K	Offset Ratio	Actual offset distance $\bar{x}$ m	Distance of the Cross bore Configuration measured from the transverse axis of the main cylinder			Position of Maximum Principle Stress in the Cylinder	
			Plane AA	Plane BB	Plane CC	Radius R (m)	Horizontal distance $\bar{x}$, measured from the transverse axis of the main cylinder
1.75	0	0		0	0.0025	0.0422	0.0025
	0.24	0.006	0.0035	0.006	0.0085	0.04375	0.0085
	0.48	0.012	0.0095	0.012	0.0145	0.04375	0.0145
	0.685	0.017125	0.014625	0.017125	0.019625	0.025	0.014625
	0.9	0.0225	0.02	0.0225	0.025	0.025	0.020158
2.0	0	0		0	0.0025	0.0265	0.0024567
	0.24	0.006	0.0035	0.006	0.0085	0.0475	0.008392
	0.48	0.012	0.0095	0.012	0.0145	0.05	0.01439
	0.685	0.017125	0.014625	0.017125	0.019625	0.05	0.019625
	0.9	0.0225	0.02	0.0225	0.025	0.05	0.025

K	Offset Ratio	Actual offset distance $\bar{x}$ m	Distance of the Cross bore Configuration measured from the transverse axis of the main cylinder			Position of Maximum Principle Stress in the Cylinder	
			Plane AA	Plane BB	Plane CC	Radius R (m)	Horizontal distance $\bar{x}$, measured from the transverse axis of the main cylinder
2.25	0	0		0	0.0025	0.025	0.000491
	0.24	0.006	0.0035	0.006	0.0085	0.025	0.007933
	0.48	0.012	0.0095	0.012	0.0145	0.025	0.00969
	0.685	0.017125	0.014625	0.017125	0.019625	0.025	0.014625
	0.9	0.0225	0.02	0.0225	0.025	0.025	0.02
2.5	0	0		0	0.0025	0.025	0.000491
	0.24	0.006	0.0035	0.006	0.0085	0.052	0.0085
	0.48	0.012	0.0095	0.012	0.0145	0.0625	0.0145
	0.685	0.017125	0.014625	0.017125	0.019625	0.025	0.014625
	0.9	0.0225	0.02	0.0225	0.025	0.025	0.02

K	Offset Ratio	Actual offset distance $\bar{x}$ m	Distance of the Cross bore Configuration measured from the transverse axis of the main cylinder			Position of Maximum Principle Stress in the Cylinder	
			Plane AA	Plane BB	Plane CC	Radius R (m)	Horizontal distance $\bar{x}$, measured from the transverse axis of the main cylinder
3.0	0	0		0	0.0025	0.025	0.0017648
	0.24	0.006	0.0035	0.006	0.0085	0.025	0.00793
	0.48	0.012	0.0095	0.012	0.0145	0.025	0.00969
	0.685	0.017125	0.014625	0.017125	0.019625	0.025	0.01463
	0.9	0.0225	0.02	0.0225	0.025	0.025	0.02

4.3.2.3.2 Effects of elliptical cross bore location on hoop stress concentration factor

The graphs showing the variation of hoop stress concentration factors with offset locations and thickness ratios are shown in Figures 115 and 116, respectively.

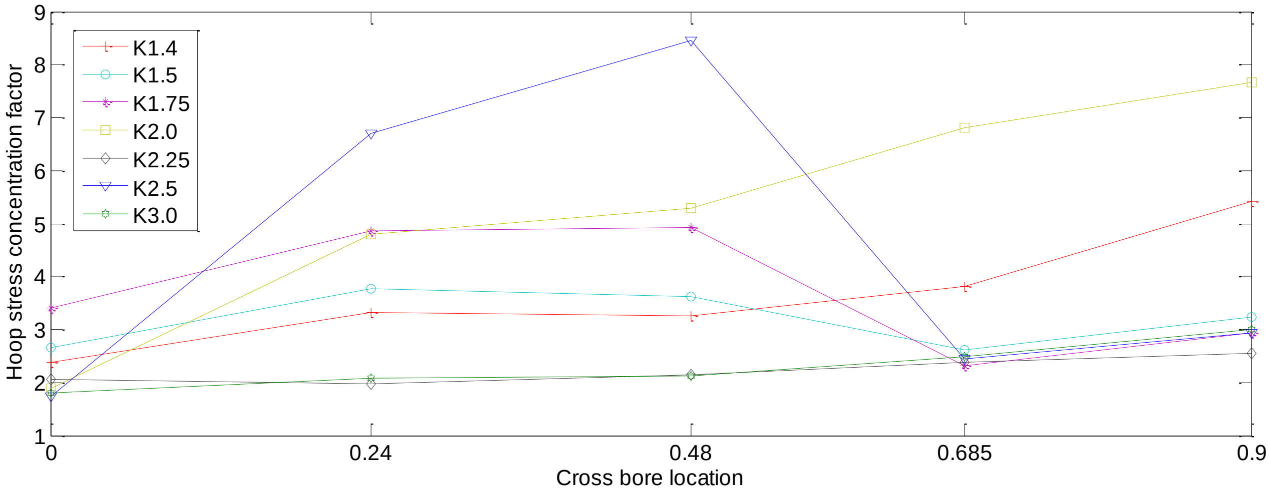

Figure 115: Hoop SCF vs cross bore location due to an elliptical cross bore

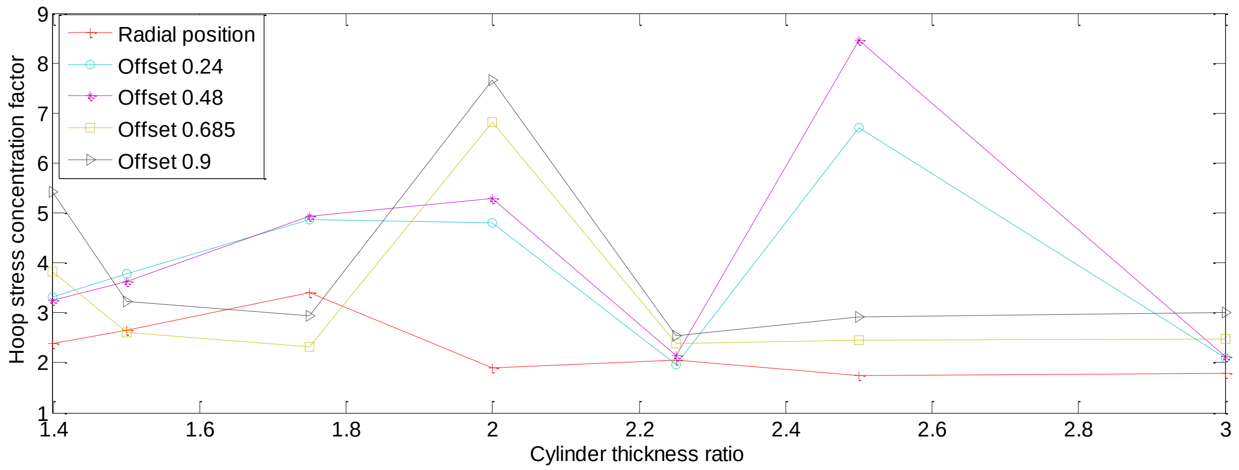

Figure 116: Hoop SCF vs cylinder thickness ratio due to an elliptical cross bore

With the exception of K=1.5 and 1.75, the lowest magnitudes of hoop stress concentration factor in a thick cylinder with elliptical cross bore occurred at the radial position, ranging from 1.733 to 2.375. As illustrated in Figures 115 and 116, it was generally observed that the stress concentration factors due to the elliptical cross bore tend to increase with increasing offset location ratio. The highest SCF peaks were observed at the 0.48 and 0.9 offset positions for K=2.5 and 2.0, with respective magnitudes of 8.457 and 7.661. These high peaks were attributed to the location of maximum hoop stress being close to the outside surface of the cylinder. Conversely, the thickness ratio of 2.25 gave the lowest SCF magnitudes for all offset positions except at 0.48. At 0.48 offset position, the minimum SCF occurred at K=1.75. As tabulated in Table 22, the location of these lowest SCFs in the cylinder were found to occur at the intersection between the cross bore and the main bore. Remarkably, the overall best results occurred in K=2.25 as illustrated in Figure 116. Nevertheless, the overall lowest SCF occurred at K=2.5 with a magnitude of 1.733. This lowest SCF magnitude indicated a reduction of pressure carrying capacity by 42.3% in comparison to a similar plain cylinder without a cross bore. An improvement from the 60% reduction cited earlier by the Masu (1989) study.

Several studies (Timoshenko (1940), Faupel and Harris (1957), Adenya and Kihiu (1995) Makulsawatudom *et al.* (2004), Harvey (1985) and Nihous *et al*. (2008)) on elliptically shaped holes, have been carried out previously. In these reviewed studies, the optimal cross bore diameter size ratio was 2. In addition, the minor diameter of the cross bore was placed parallel to the axial direction for cylinders. These two configurations had earlier been shown in Chapter 3 to give minimum SCF magnitudes.

Using the expression cited by Timoshenko (1940) and Nihous *et al*. (2008), the minimum SCFs that can be obtained from an optimally sized elliptically shaped hole in a plate under uniaxial or biaxial loading is 2.0 and 2.5, respectively. Whereas, the corresponding maximum SCFs values are 5.0 and 4.5. Further, another study by Harvey (1985) gave a minimum SCF of 1.5 for a thin cylinder having an optimum sized and correctly configured elliptical cross bore.

Faupel and Harris's (1957) study gave a SCF of 1.5 for a radial elliptical cross bore in a closed thick walled cylinder, regardless of the cross bore size. While in a similar elliptical cross bore, Adenya and Kihiu (2010) gave a maximum SCF of 2.0 after investigating three cylinders with thickness ratios 2.0, 2.25 and 2.5. These results by Adenya and Kihiu's (2010) study compared favourably with those presented in this study. For instance, in this study, the SCFs for radial elliptical cross bores for K=2.0, 2.25 and 2.5 were found to be 1.898, 2.05 and 1.733, respectively. Another study by Makulsawatudom *et al.* (2004) gave the SCF by a radial elliptical cross bore for K=2.0 as 2.01 comparing well with 1.898 obtained in this study. In general, optimum configured elliptical holes in plates were noted to give fairly similar SCF magnitudes to those of radial elliptical cross bores in thick cylinder.

The study by Makulsawatudom *et al.* (2004) had investigated the effects of offsetting of elliptical cross bores in a single offset position. However, the offset results presented by this author were ignored due to the error noted during the selection of the optimal offset position.

Generally, it was observed that the SCF increased as the cross bore location moved further away from the radial axis of the main cylinder. This occurrence was attributed to the cross bore shape which resembled an ellipse when viewed at the intersection between the cross bore and the main bore. In an ellipse, the major diameter denoted as ‘a’, is parallel to the axial direction of the cylinder. Whereas, the minor diameter denoted as ‘b’, is parallel to the direction of the hoop stress. The minor diameter increases with increase in offset position ratio. This cross bore configuration where $a < b$ results in high magnitudes of hoop stress in the cylinder as cited by Harvey (1985). The configuration is opposite to that observed in offsetting of the circular cross bore.

Graphs showing optimal SCF magnitudes at each thickness ratio and offset position for an offset elliptical cross bore is exemplified in Figures 117 and 118.

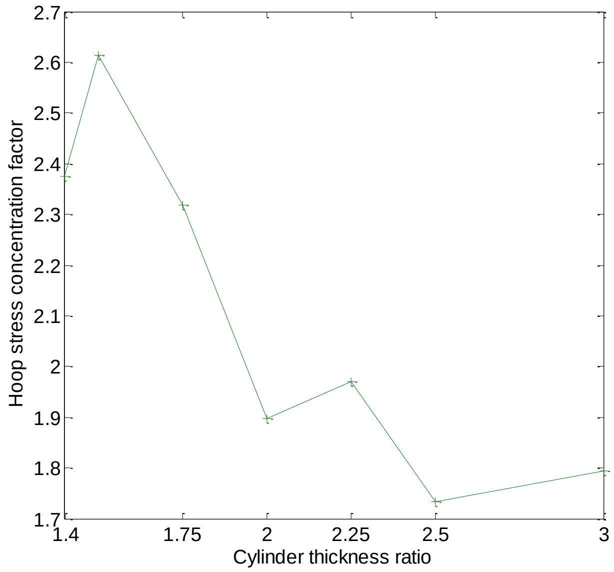

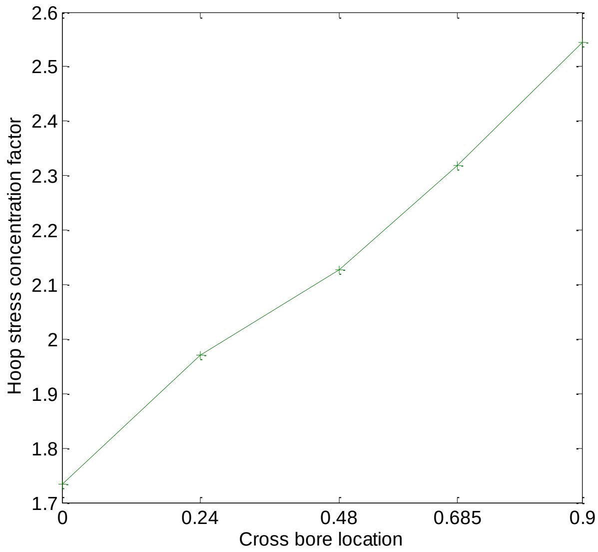

Figure 117: Optimal hoop SCF vs thickness ratio

Figure 118: Optimal hoop SCF vs cross bore location

4.3.2.4 Comparison of Stress profiles between circular and elliptically shaped offset cross bores

In this section, the comparison between stress profiles given by optimum circular and elliptically shaped cross bores at each offset position are discussed under the following sub headings;

4.3.2.4.1 Maximum principal stress

Figures 119 to 125 show the comparison of maximum principal stresses predicted by circular and elliptical cross bores together with a plain cylinder at each offset position for thickness ratios K=1.4, 1.5, 1.75, 2.0, 2.25, 2.5 and 3.0.

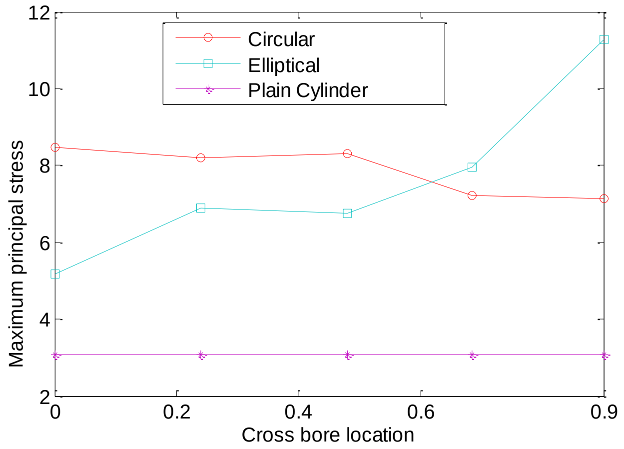

Figure 119 : Offset cross bore for K=1.4

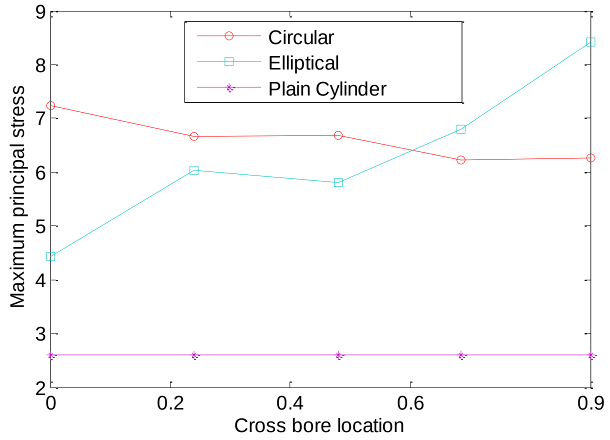

Figure 120: Offset cross bore for K=1.5

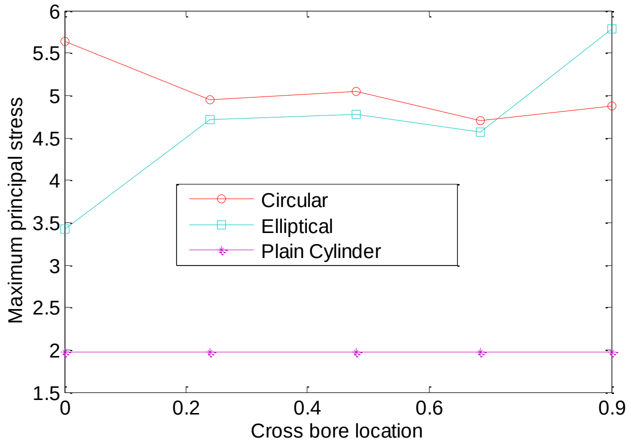

Figure 121: Offset cross bore for K=1.75

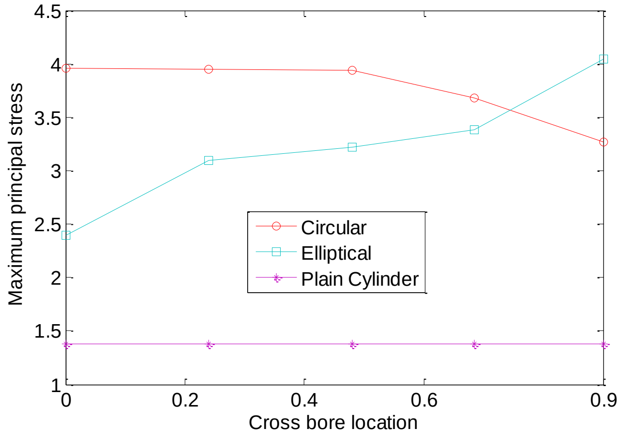

Figure 122: Offset cross bore for 2.0

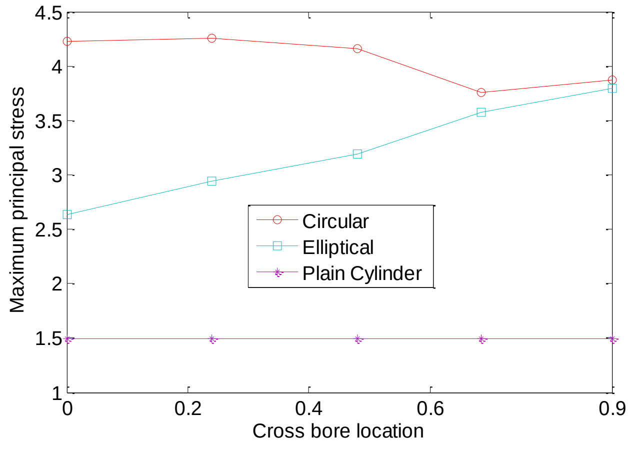

Figure 123: Offset cross bore for K=2.25

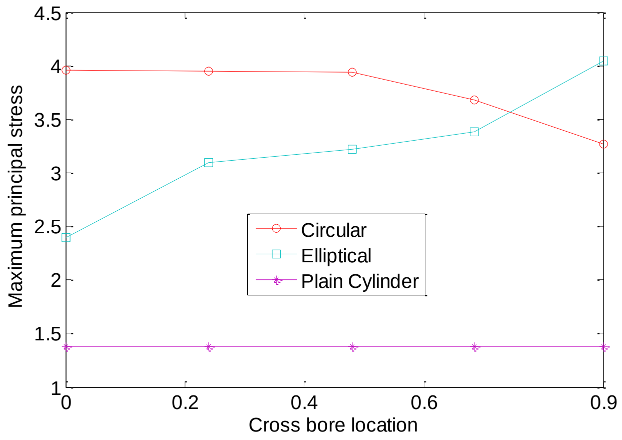

Figure 124: Offset cross bore for K =2.5

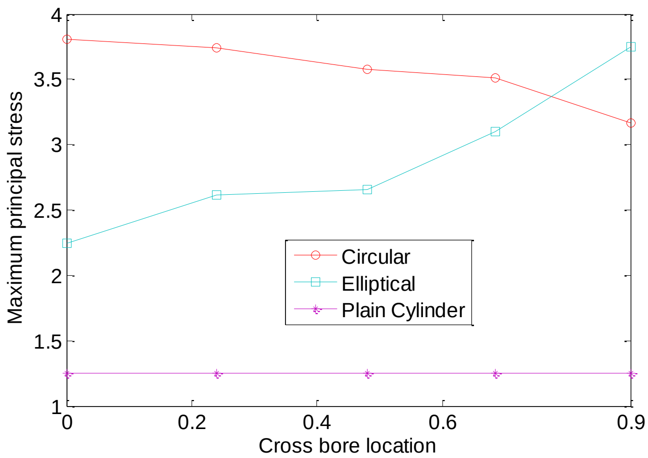

Figure 125 : Offset cross bore for K =3.0

With the exception of K = 2.25, it was observed that elliptical cross bores gave lower principal stresses than those of circularly shaped ones ranging from offset position 0 to approximately 0.6 for all the studied thickness ratios. Only, in K = 2.25 where the maximum principal stresses predicted by the elliptical cross bores were lower than that of circular cross bores in all the offset positions. For the other thickness ratios, the prediction of equal stress magnitudes between the circular and elliptical shapes occurred between 0.6 and 0.8 offset positions. Thereafter, the circular cross bores gave lower stresses.

Generally, the variation in stress between the two shape profiles was more pronounced at the radial position. Table 23 shows a summary of stress variation between the two shapes at radial position, taking elliptical shape as the reference.

Table 23: Comparison between hoop stresses due to radial circular and elliptical shaped cross bores

Thickness	Circular shape	Elliptical shape	Percentage difference %
1.4	8.212	5.162	59.1
1.5	6.658	4.438	50.02
1.75	4.944	3.419	44.6
2.0	4.64	2.885	60.8
2.25	4.255	2.634	61.5
2.5	3.944	2.393	64.8
3.0	3.743	2.242	66.9

Overall, the stress variation at radial position ranged from 44.6% to 66.9% depending on the thickness ratio. The highest stress reduction was noted at K = 1.75. Nevertheless, the stress variation between the two shapes tended to reduce as the cross bore offset ratio increased.

As illustrated in Figures 119 to 125, the circularly shaped cross bore gave low stresses at the 0.9 offset position except in K = 2.25. However, only a mere 2% reduction in hoop stress would be gained by use of an elliptically shaped cross bore instead of a circular one at 0.9 offset position in K = 2.25, despite the manufacturing difficulties.

4.3.2.4.2 Hoop stress concentration factor

Figures 126 to 132 show the comparison of stress concentration factors predicted by circular and elliptical cross bores together with a plain cylinder at each offset position for thickness ratios, K = 1.4, 1.5, 1.75, 2.0, 2.25, 2.5 and 3.0.

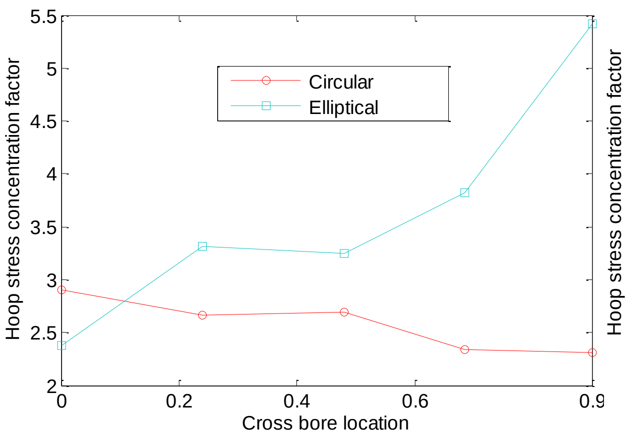

Figure 126: Offset cross bore for K=1.4

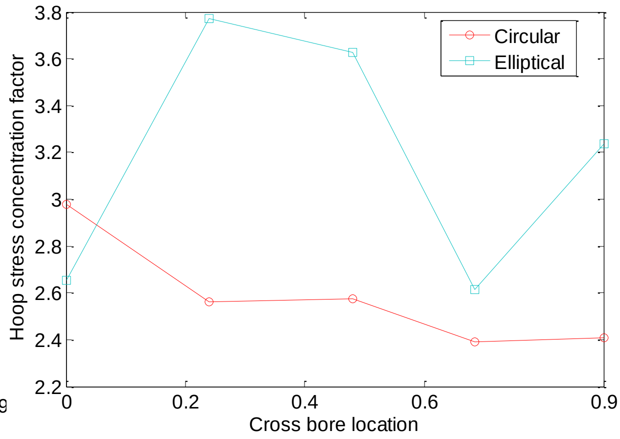

Figure 127: Offset cross bore for K=1.5

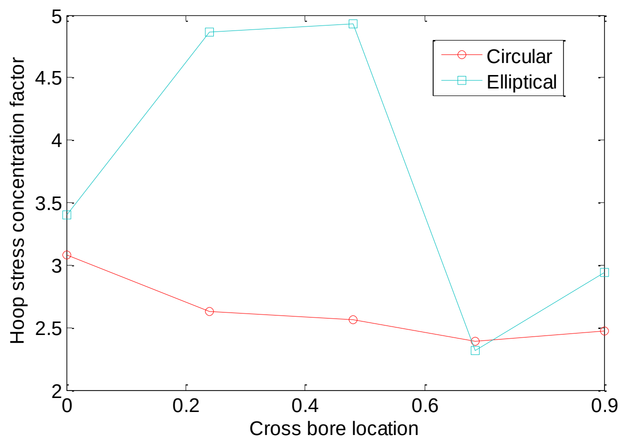

Figure 128: Offset cross bore for K=1.75

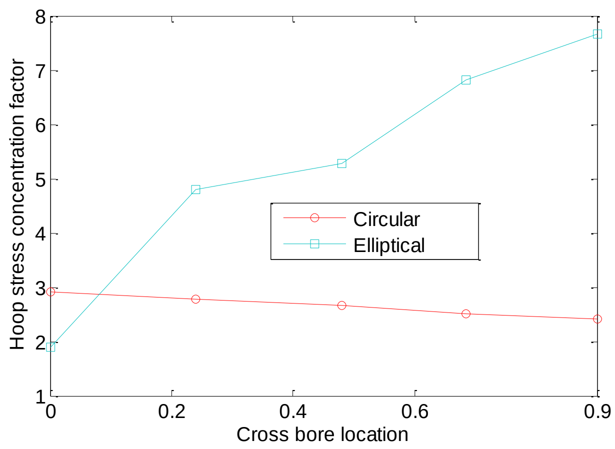

Figure 129: Offset cross bore for K=2.0

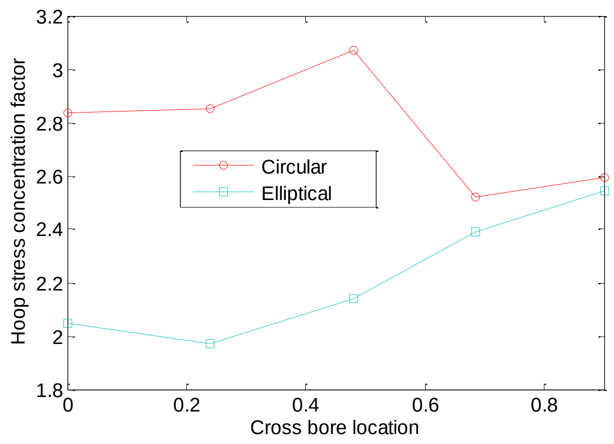

Figure 130: Offset cross bore for K=2.25

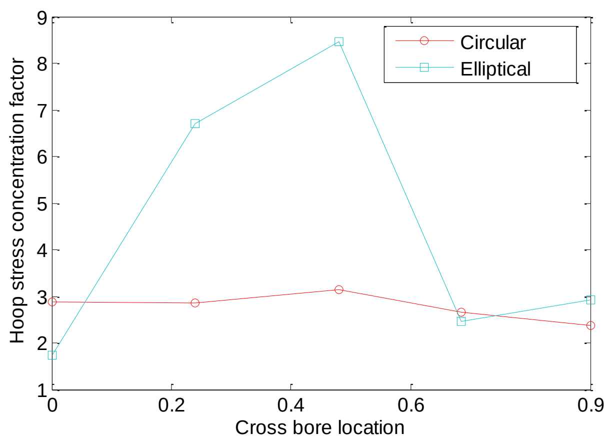

Figure 131: Offset cross bore for K=2.5

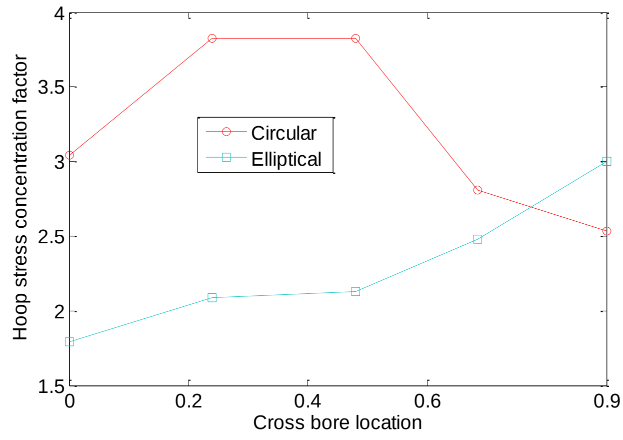

Figure 132 : Offset cross bore for K=3.0

With the exclusion of K = 1.75, the SCFs at the radial position due to the elliptically shaped cross bores were lower than that due to circularly shaped ones. This occurrence signified an existence of stress transition point at K = 1.75. The lowest SCF magnitude recorded at this radial position was 1.733 at K = 2.5. Noticeably, this magnitude also doubled as the overall lowest magnitude due to elliptically shaped cross bores. Similar to the preceding sections, offsetting of elliptically shaped cross bores led to the increase of SCF magnitudes. The highest SCF due to elliptically shaped cross bores was recorded at 0.48 offset ratio with a magnitude of 8.457.

On the other hand, the minimum overall SCF magnitude due a circularly shaped cross bore occurred at 0.9 offset position in K=1.4, with a magnitude 2.312. On the other hand, the highest magnitude occurred at 0.24 at K=3.0 with a magnitude of 3.825.

In this regard, therefore, the optimal location of elliptical cross bores reduce SCF magnitudes by 33% in comparison to a similar circular cross bore. However, an incorrect positioning of the same cross bore may lead to a rise of SCF magnitude by 121%.

4.3.3 Optimization of cylinder thickness ratio

In the design of pressure vessels, various types of cylinders with varying geometric parameters are considered for different applications. Therefore, the need for identifying an optimal cross bore location for each thickness ratio, taking into account the shape, is important. The graphs showing the comparison between optimal SCF magnitudes predicted by circular and elliptical cross bores at each thickness ratio and offset positions are illustrated in Figures 133 and 134, respectively.

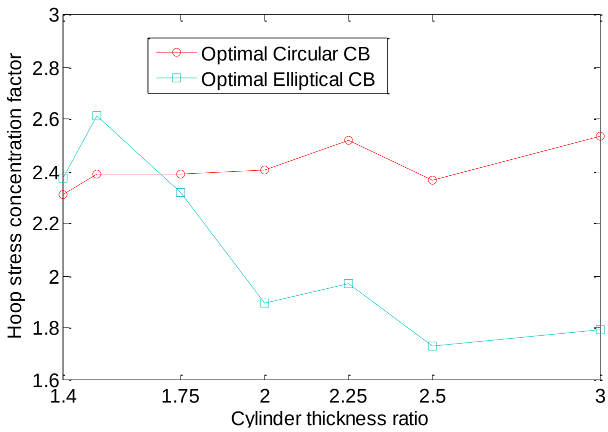

Figure 133: Optimal SCF vs thickness ratio

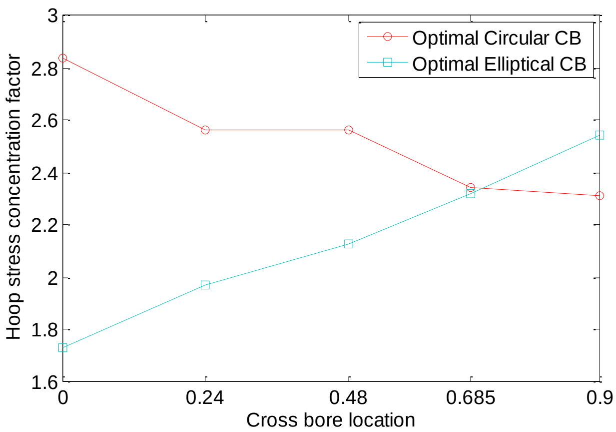

Figure 134: Optimal SCF vs cross bore location

Subsequently, the optimal shape and location were selected from these two graphs using the lowest SCFs. The optimum thickness ratio and location are summarised in Tables 24 and 25.

Table 24: Optimum thickness ratio

K	1.4	1.5	1.75	2.0	2.25	2.5	3.0
SCF	2.312	2.392	2.319	1.898	2.05	1.733	1.794
Location	0.9	0.685	0.685	0	0	0	0
Shape	Circular	Circular	Elliptical	Elliptical	Elliptical	Elliptical	Elliptical

Table 25: Optimal offset locations

Location	0	0.24	0.48	0.685	0.9
SCF	1.733	1.971	2.128	2.319	2.312
K	2.5	2.25	3.0	1.75	1.4
Shape	Elliptical	Elliptical	Elliptical	Elliptical	Circular

This optimisation process revealed that three of the cylinder sizes, namely K=1.4, 1.75 and 2.5 had the same optimal SCF magnitude. Thus, the same cylinder satisfied optimal design requirements for both the cross bore location and shape.

For a circular cross bore, coincidence in SCF between the optimum thickness and location occurred in K=1.4 at the 0.9 offset position which also gave the best circular shape. Whereas for an elliptical shape, similar coincidence in SCF occurred respectively in K=1.75 and 2.5 at 0.685 and 0 offset positions. It is worthwhile noting that elliptical cross bore predicted the overall minimum stress concentration factor, despite being associated with high manufacturing cost or difficulties.

Lastly, the geometric parameter of the cross bore to be optimised in this study was the angle of obliquity. Due to limitations of the software, the investigation was only conducted on the circularly shaped cross bore. The cross bore inclination was done at 0.9 offset position. Since this location had been in the preceding paragraphs as the optimum location of the circular cross bore.

4.3.3 Optimisation of circular cross bores obliquity

4.3.3.1 Introduction

In this section, optimisation of the cross bore was done at seven different oblique angles α with orientation of 15^0, 30^0, 45^0, 60^0, 75^0 and 90^0 as shown in Figure 135 for the studied thickness ratios at the 0.9 offset position. Oblique angles below 15^0 were found to cause severe mesh element distortion. Usually, distortion of elements occur when the software tolerances are exceeded leading to premature termination of the job analysis. It is worthwhile to note that, only sizeable oblique angles, which allow the considerable penetration of the cross bore to the main bore, are applicable.

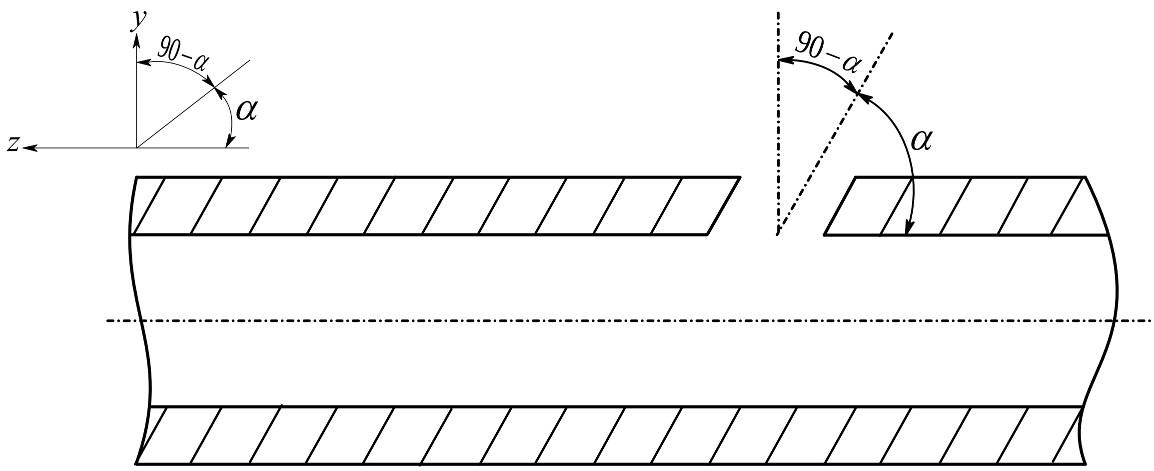

Figure 135: Configuration of offset oblique cross bore

4.3.3.2 Effects of cross bore obliquity and thickness ratio on the stress concentration factor

The effects of cross bore obliquity and thickness ratio on hoop stress concentration factor are shown in Figures 137 and 138.

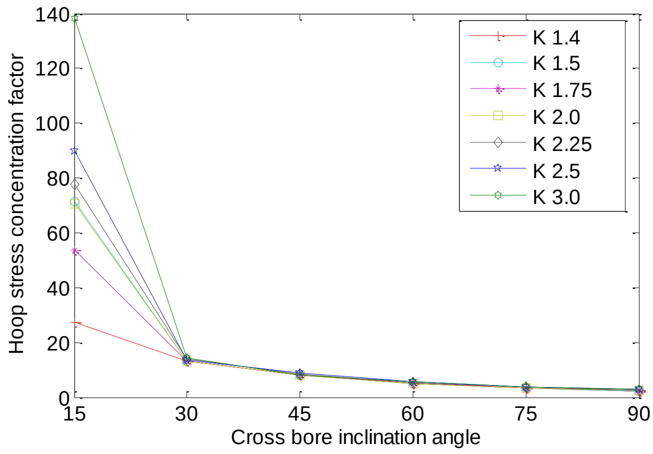

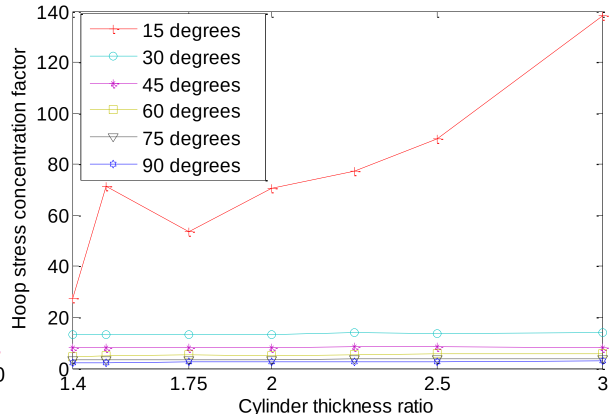

Figure 136: Hoop SCF vs oblique cross bores

Figure 137: Hoop SCF vs thickness ratio

It was observed in Figures 136 and 137 that as the oblique angle was reduced from 90^0 to 30^0, the SCF increased progressively for all the seven thickness ratios studied. For instance, for the mentioned oblique range, the rise in SCF was approximately four times. Furthermore, as the oblique angle reduced from 30^0 to 15^0 the SCF magnitude increased significantly. The highest SCF magnitude ranging from 27.404 to 138.16 was noted at 15^0 for all the thickness ratios. These findings were in line with earlier studies done by Nihous *et al.* (2008) and Cheng (1978). Nihous *et al.* (2008) had studied various radial oblique cross bores oriented at five different angles. Fortunately, one of the studied cross bores had a size ratio of 0.1, similar to the current study thus, enabling effective comparison. Further, the study by Nihous *et al.* (2008) had defined its oblique angles in the plane of $(90 - \alpha)^0$ as shown in Figure 135. Thus for compatibility with the present study, the angles in Nihous *et al.* (2008) were converted to the orientation adopted in this work. The oblique angles compared were 30^0, 45^0, 60^0, 75^0 and 90^0. Similar to the findings of the current study, Nihous *et al.* (2008) had also cited increased mesh element distortion whenever the obliquity angle was below 30^0.

Although, the work by Nihous *et al*. (2008) was done at the radial position, the data published was compared with a similar one given in this study to ascertain the effects of offsetting in an oblique cross bore. Figure 138 shows the comparison of results between oblique holes at radial position and corresponding ones at 0.9 offset position, for K=2.25 having cross bore size ratio of 0.1.

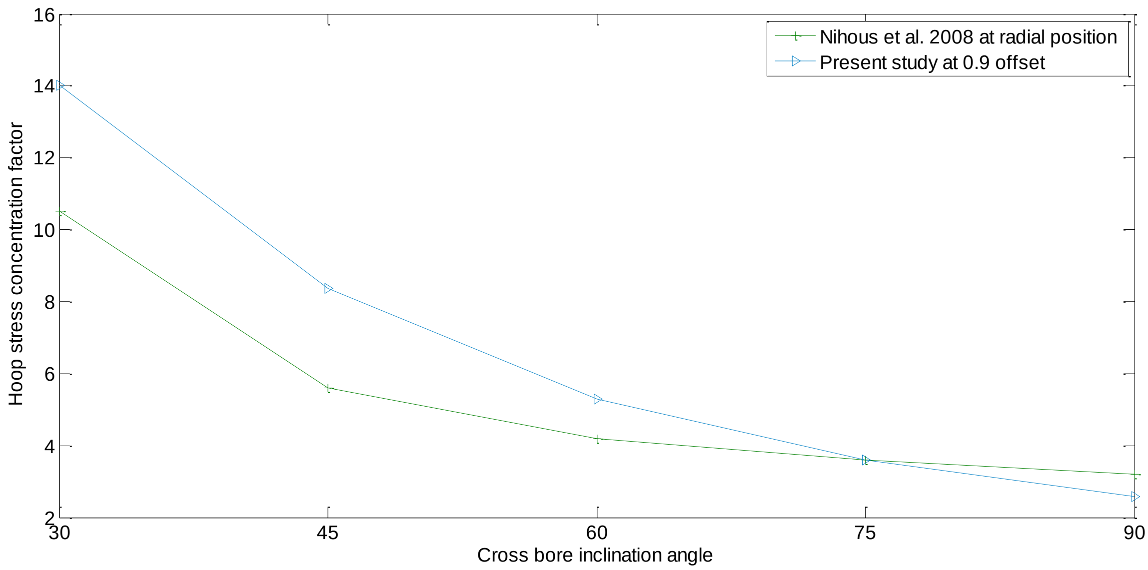

Figure 138: Comparison of hoop SCF between oblique holes at radial and optimum offset location.

As in preceding sections, the offsetting of radial cross bore was seen to predict lower SCFs up to 24.03%. However, with reduction of the oblique angle, the offset cross bores gave higher SCFs than those located at the radial position. The highest increase of 49.6% in SCF was observed at 45^0. Only at an oblique angle of 75^0 , the variation in SCFs between the two locations were insignificant. Additionally, Cheng (1978) had investigated experimentally a cross bore size ratio of 0.1 for K=1.84 at oblique angles α of 30^0 and 50^0. The study also reported an increase in SCFs as the oblique angle α reduced.

With the exception of oblique angle 15^0, the effect of thickness ratio was minimal across the studied thickness ratios as indicated in Figure 137. In general, whenever the cross bore is viewed at the intersection between the inclined cross bore and main bore, its shape resembles that of an ellipse with major diameter parallel to the axial direction of the cylinder. This increase in the minor diameter is more pronounced whenever the obliquity angle reaches 15^0. The resulting configuration leads to high stress profiles as discussed previously in section 4.3.2.3.2. In these cases, therefore, any cross bore obliquity in pressure vessel design that is located in the RZ plane should be avoided.

After taking into consideration all the major geometric parameters of a cross bore namely the size, location, shape and its obliquity, only the results presented previously in tables 24 and 25 had the minimum stress concentration factors. Therefore, only these geometrically optimised cross bores were studied further to establish the effects of SCF due to combined thermo-mechanical loading.

4.4 COMBINED THERMO-MECHANICAL STRESS ANALYSIS

4.4.1 Introduction

The combined thermo-mechanical stress analysis was performed only on the geometrically optimised cross bore sizes tabulated in Tables 24 and 25. The modelling was done under transient conditions to simulate the start up conditions of pressure vessels until steady state conditions were reached. Throughout the analyses, the fluid pressure was assumed to be constant at 1 $\mathrm{MN/m^2}$. The resulting stresses were recorded at 17 different temperature distribution intervals, ranging from 20 ^{o}C to 300 ^{o}C according to the thickness ratio.

4.4.2 Effects of the combined thermo-mechanical loading on hoop stress

Figures 139 – 145, show the variation of hoop stresses with temperature distribution for thickness ratios, K =1.4, 1.5, 1.75, 2.0, 2.25, 2.5 and 3.0:

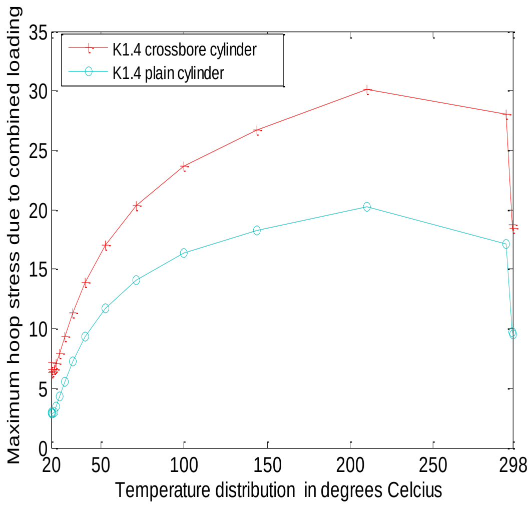

Figure 139: Optimum cross bore for K=1.4

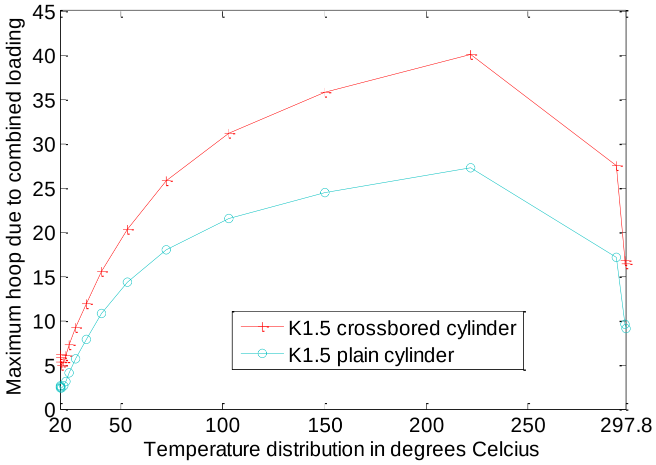

Figure 140: Optimum cross bore for K=1.5

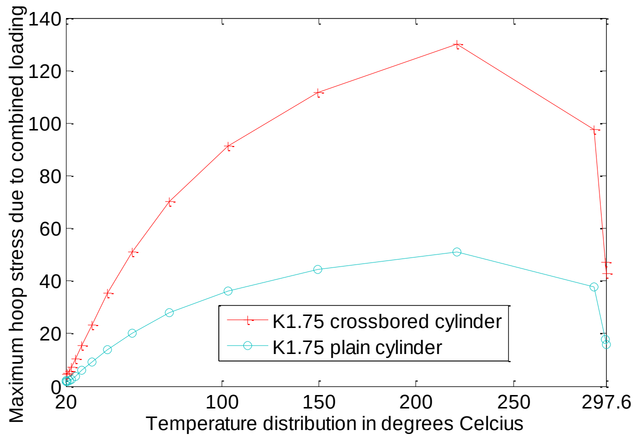

Figure 141: Optimum cross bore for K=1.75

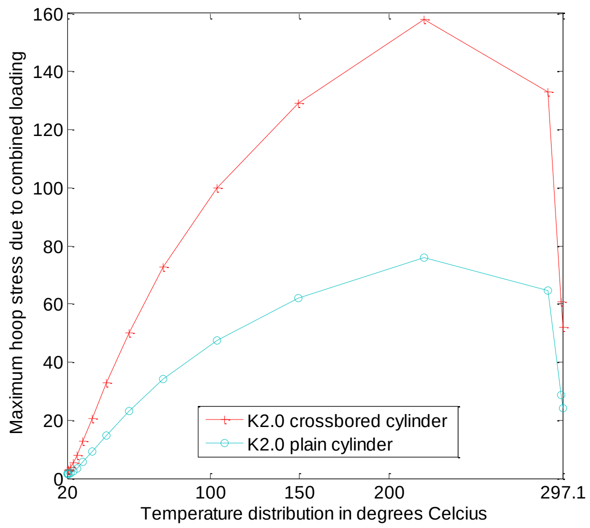

Figure 142: Optimum cross bore for K=2.0

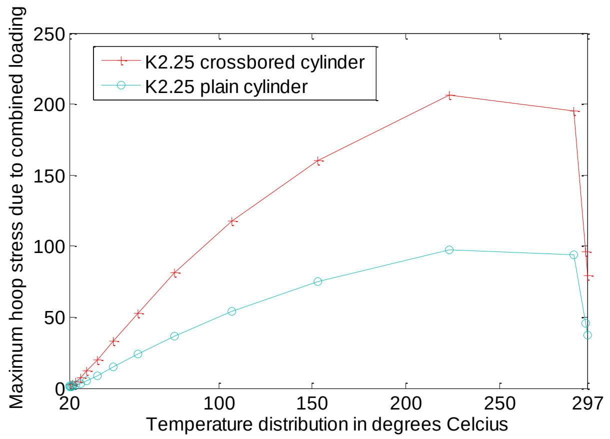

Figure 143: Optimum cross bore for K=2.25

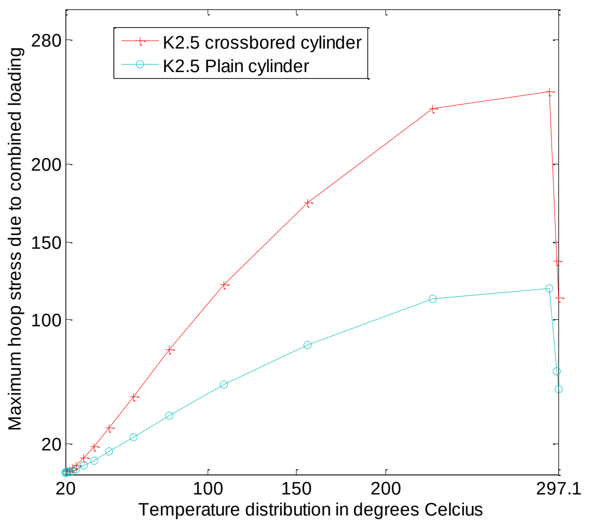

Figure 144: Optimum cross bore for K=2.5

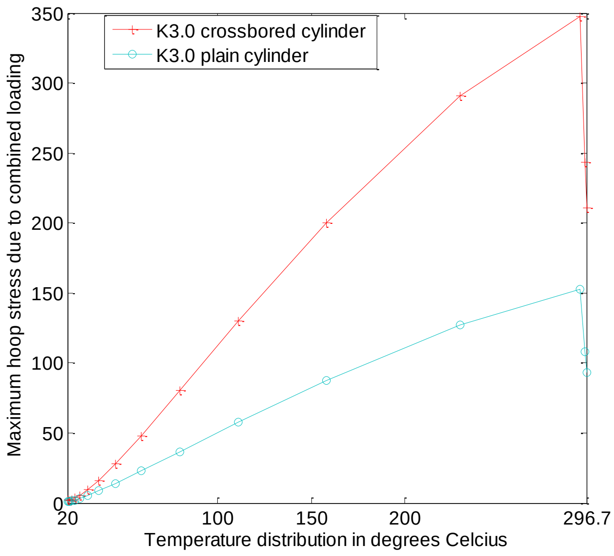

Figure 145: Optimum cross bore for K=2.5

A similar stress distribution pattern was exhibited between the cross bored cylinder and the plain cylinder as illustrated in Figures 139 – 145. However, the hoop stresses present in the cross bored cylinder was higher than those in the plain cylinder. Generally, the hoop stresses increased gradually with an increase in temperature until they reached a maxima after which they began to fall sharply. The temperatures in the cylinder which corresponded to the stress maxima for K =1.4, 1.5, 1.75, 2.0, 2.25, 2.5 and 3.0 were 210.3, 221.8, 220.9, 219.7 223.3, 292.0 and 293.4 ^{o}C, respectively. At these mentioned temperatures, the increase in hoop stress magnitudes between the cross bored cylinders and those of plain cylinders were 48.57%, 47.23%, 153.96%, 74.78%, 111.67%, 105.79% and 127.33 %, respectively.

From the preceding paragraph, it was noted that the lowest maximum temperature point occurred at K = 1.5. Similarly, the minimum increase in stress magnitude between the cross bored and plain cylinder occurred at K = 1.5. In contrast, the highest magnitudes of these discussed parameters were recorded at K=3.0.

Usually, thermal stress in cylinders is mainly dependent on the temperature variation between the inner and outer surfaces, among other factors. During the starting up of the pressure vessel, the inner surface is at a higher temperature, causing the inner fibres to undergo compression. On the other hand, at the outer surface, the temperature is low leading to stretching of the outer fibres of the cylinder. As the operating time increases, the difference in the temperature gradient across the cylinder wall reduces and this reduction in the temperature gradient between inner and outer surfaces results to a reduction of the hoop stress. Probably, at this maximum stress point, the operating conditions of the cylinder begin to change from transient to steady state conditions. As reported in the study by Kandil *et al* (1994), the magnitude of the maximum stress in the cylinder can be reduced by upto 60 % when the cylinder walls are warm up to operating temperature before start-up.

4.4.3 Effects of combined thermo-mechanical loading on stress concentration factors

The stress concentration factor due to thermo-mechanical loading was computed based on the ratio of localised maximum principal stresses in a cross bore cylinder to the corresponding ones present in a similar plain cylinder. Figures 146 and 147 show the variation of stress concentration factors with temperature due to thermo-mechanical loading at the selected optimal thickness ratios and offset positions, respectively.

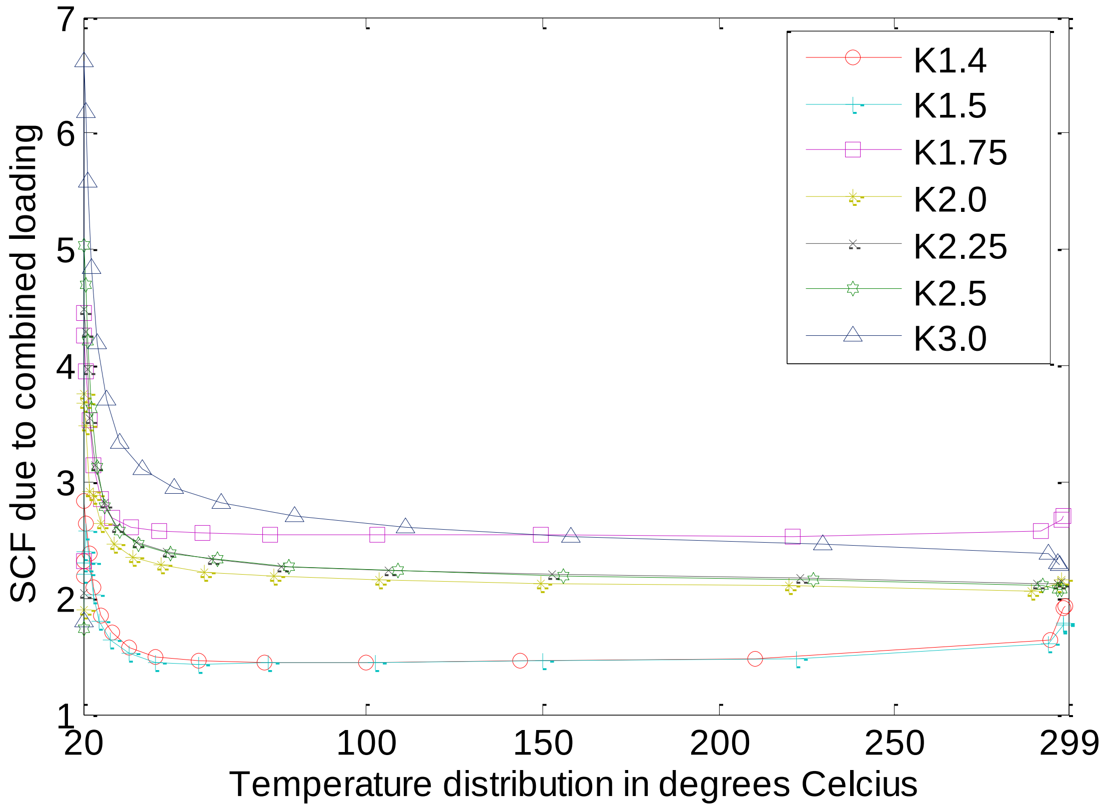

Figure 146: variation of stress concentration factors with temperature on optimal thickness ratios.

As illustrated in Figure 146, as the temperature increased, the corresponding stress concentration factor reduced gradually until it reached a uniform steady state. After which, any further increase in temperature caused an insignificant change in the stress conentration factor. A similar observation had been cited by Kandil *et al* (1994).

The lowest stress concentration factors occurred at the thickness ratios of 1.4 and 1.5, reaching a minimum magnitude of 1.433. This SCF magnitude indicated a reduction of pressure carrying capacity by 30.2% in comparison to a similar plain cylinder without a cross bore.

On the other hand, the highest stress concentration factors occurred at thickness ratios of 1.75 and 3.0 having a SCF magnitude of approximately 2.50. These stress concentration magnitudes due to combined thermo-mechanical loading were lower than those presented in Table 24 arising from mechanical loading only. This occurrence was attributed to the compressive nature of thermal stresses during the starting-up of the vessel which acts as a relief to tensile mechanical stresses.

As cited by Harvey (1985), it is worthwhile to note that thermal stresses do not cause failures or ruptures on a ductile material upon their first application irrespective of the magnitude. Failures or ruptures of ductile material occur due to repeated cycling loading over a period of time.

Variation in stress concentration factors with temperature as exhibited in Figure 146 were also replicated in Figure 147.

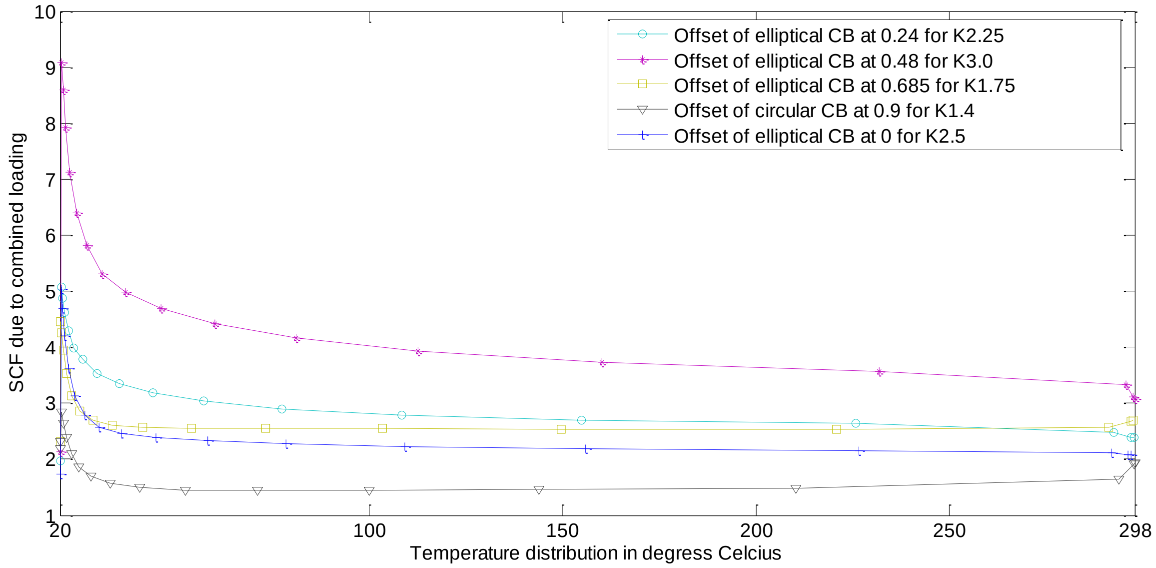

Figure 147: Variation of stress concentration factors with temperature at offset position

As illustrated in Figure 147, the minimum stress concentration factor occurred at the offset position ratio of 0.9 at a thickness ratio of 1.4 of a circular cross bore. However, the highest corresponding stress concentration factor was recorded at an offset ratio of 0.24 in K=2.25 cylinder.

In conclusion, therefore, the optimal cylinder size due to combined thermo-mechanical loading was K=1.4 having a circularly shaped cross bore at 0.9 offset position ratio. The corresponding optimal magnitude of SCF generated at these conditions was 1.433.

In a nutshell, this study provides a large broad database of the cross bore effects in high pressure vessels. The data are presented in the form of analytical solutions, principal stresses and stress concentration factors taking into account the cross bore geometry and the operating conditions.

CHAPTER FIVE: CONCLUSIONS AND RECOMMENDATIONS

5.1: CONCLUSIONS

The following conclusions were drawn from the present study,

i. The analytical solution developed correctly predicted all the radial stresses at the intersection of the cross bore and main bore. However, out of 35 models studied, the analytical solution correctly predicted the magnitude of hoop stress in 9 of these models and that of axial stresses in 15 models.
ii. The maximum hoop stress increases with the increase in the cross bore size. Amongst the five different circular radial cross bore size ratios studied in seven cylinders, the smallest cross bore size ratio of 0.1, gave the lowest hoop stress while the highest stress occurred with a cross bore size of 1.0.
iii. The difference in the working stress between the Von Mises' and Tresca's theories along a radial circular cross bore was insignificant. Unlike that of a plain cylinder without a cross bore which is constant at 15.5%.
iv. Introduction of a radial circular cross bore increases the magnitude of the working stress. The maximum working stress predicted by Von Mises' and Tresca's theories in a cylinder with a radial circular cross bore increased by a stress factor ranging from 2.5 to 7.07.
v. Amongst the five different circular radial cross bore ratios studied in seven cylinders, the lowest SCF occurred in the smallest cross bore size ratio of 0.1 when K=2.25 with a SCF magnitude of 2.836. This SCF magnitude indicated a reduction of pressure carrying capacity of 64.7% in comparison to a similar plain cylinder without a cross bore.
vi. Offsetting of circularly shaped cross bores reduced the magnitude of SCFs. Among the five offset position studied in seven cylinders, the minimum SCF magnitudes occurred at either offset location ratios of 0.685 or 0.9. However, the optimum location was found to be at 0.9

offset position for K=1.4, with a SCF magnitude of 2.312. This SCF magnitude indicated a reduction of pressure carrying capacity of 56.7% in comparison to a similar plain cylinder without a cross bore.

vii. Offsetting of elliptically shaped cross bores increased the magnitude of SCFs. Overall, lowest SCF occurred at radial position when K=2.5 with a magnitude of 1.733. This lowest SCF magnitude indicated a reduction of pressure carrying capacity of 42.3% in comparison to a similar plain cylinder without cross bores.

viii. Oblique circular offset cross bores along the Z axis of the cylinder increase SCFs. The SCF increased as the oblique angle reduced from 90^0 to 15^0. However, as the oblique angle reduced from 30^0 to 15^0 the SCF magnitude increased significantly. The highest SCF magnitudes ranging from 27.404 to 138.16 occurred at 15^0 for all the thickness ratios studied.

ix. The hoop stresses due to combined thermo-mechanical loading increased gradually with an increase in temperature until it reached a maximum after which it began to fall sharply.

x. The stress concentration factor due to the combined thermo-mechanical loading reduced gradually with an increase in temperature until it reached a uniform steady state. After which, any further increase in temperature had insignificant change in the stress conentration factor.

xi. The optimal cylinder size due to combined thermo-mechanical loading was K=1.4 having a circularly shaped cross bore at 0.9 offset position ratio. The corresponding magnitude of SCF generated was 1.433. This SCF magnitude indicated a reduction of pressure carrying capacity of 30.2% in comparison to a similar plain cylinder without a cross bore.

5.2 RECOMMENDATIONS

The following recommendations for further work are suggested,

i. Development of analytical solutions to predict three dimensional stresses in elliptically shaped cross bores in high pressure vessels using a similar analogy adopted in this study.
ii. Use of Boundary Integral Element (BIE) software to determine the stresses at the cross bore surface. BIE method is highly preferred when calculating surface stresses since it gives results of the surface nodes only.
iii. Use of Linear Programming (LP) methods to carry out optimisation process of the geometric configuration of the cross bore. Since, the major factors that affect cross bore configuration can be considered concurrently in LP method, contrary to one factor at a time method adopted in this study.
iv. Perform three dimensional experimental work using either photo-elasticity or strain gauge methods to further ascertain the results present in this study which were obtained using numerical and analytical methods.
v. Determination of optimal geometric configuration of a cross bore in high pressure vessels under autofrettage conditions and fully plastic deformation.

REFERENCES

Abdul-Mihsein, M. J. and Fenner, R. T. (1983), "Some boundary integral equation solutions for three dimensional stress concentration problems", *Journal of strain analysis,* Vol.18, No.4. pp.207

Adam, V. and Askenazi, A. (1999), "Building better products with finite element analysis", Onward press, USA, ISBN 1-56690-160X

Adenya, C.A. and Kihiu, J. M. (2010), "Stress concentration factors in thick walled cylinders with elliptical cross bore", *Master's thesis, Jomo Kenyatta University of Science and Technology.*

Babu, N. R., Ramana, K. V. and Rao, K. M. (2010), "Prediction of stress concentration effect under thermal and dynamic loads on a high pressure turbine rotor", *International journal of engineering science and technology*, Vol. 2, No. 8, pp. 3456-3467.

Carvalho, de. E. A. (2005), "Stress concentration factors for an internally pressurized circular vessel containing a radial U-notch", *International journal of pressure vessels and piping,* No. 82, pp. 517-521.

Chaaban, A. and Burns, D. J. (1986), “Design of high pressure vessels with radial crossbores”, Physica B and C, No. 139-140, pp. 766-772.

Chaudhry, V., Kumar, A., Ingole, S. M., Balasubramanian, A. K. and Muktibodh, U. C. (2014), “Thermo-mechanical transient analysis of reactor pressure vessel”, *Procedia engineering,* No. 86, pp. 809-817.

Choudhury, A., Mondol, S. C. and Sarkar, S. (2014),”Finite element analysis of thermos mechanical stresses of two layered composite cylindrical pressure vessel*”, International journal of research in applied science & engineering technology,* Vol. 21. No. XI, pp. 341-349.

Cheng, Y. F. (1978), “Stress concentration around inclined holes in pressurized thick-walled cylinders” *Technical Report -Arlcb-TR-78019.*

Choi, W., Fujiyama, K., Kim, B. and Song, G. (2012), “Development of thermal stress concentration factors for life assessment of turbine casing”, *International journal of pressure vessels and piping,* Vol. 98, pp. 1-7.

Cole, B. N., Craggs, G., and Ficenec, I. (1976), “Strength of cylinders containing radial or offset cross-bores”, *Journal mechanical engineering science,* Vol. 18, No. 6.

Comlekci, T., Mackenzie, D., Hamilton, R. and Wood, J. (2007),"Elastic stress concentration at radial crossholes in pressurized thick cylinders, *Journal of strain analysis*, Vol. 42, pp.

Decock, J. (1975), "Reinforcement method of openings in cylindrical pressure vessels subjected to internal pressure", Centre de Recherches Scientifiques et Techniques de L'Industriedes Fabrications Metalligues, Report No. MT 104.

Dharmin, P., Khushbu, P. and Chetan, J. (2012), "A review on stress analysis of an infinite plate with cut-outs", *International journal of scientific and research publications*, Vol. 2, issue 11.

Diamantoudis, A. Th. and Kermanidis, Th. (2005), "Design by analysis versus design by formula of high strength steel pressure vessels: a comparative study*", International journal of pressure vessels and piping*, No. 82, pp. 43-50.

Erickson, P. E. and Riley, W. F. (1978), "Minimizing stress concentration around circular holes in uniaxially loaded plates", *experimental mechanics*, Vol 18, No.3, pp. 97 -100.

Fagan, M. J. (1992), "Finite element analysis theory and practice", Longman, UK, ISBN 0-470-21817-7

Faupel, J. H. and Fisher, F. E. (1981), ”Engineering design- A synthesis of stress analysis and materials engineering”, John Wiley and sons, Canada, ISBN 0-471-03381-2.

Faupel, J. H. and Harris, D. B. (1957),” Stress concentration in heavy-walled cylindrical pressure vessels”, *Industrial and engineering chemistry,* Vol. 49, pp. 1979-1986.

Fessler, H. and Lewin, B. H. (1956), “Stress distribution in a tee-junction of thick pipes”, *British journal of applied physics*, Vol. 7, pp. 76-79.

Ford, H. and Alexander, J. (1977), “Advanced mechanics of materials”, John wiley and sons inc., Canada, second edition.

Gerdeen J. C. (1972), “Analysis of stress concentration in thick cylinders with sideholes and crossholes”, Trans. ASME, *Journal Engineering Industry*, No. 94, pp. 815-823.

Gurumurthy K., Jain R and Salpekar, V. Y. (2001), Simplified formula for stress concentration factor in radial nozzle shell junctions under internal pressure loading, *ASME PVP*- 430, 3-6.

Harvey, J. F. (1985), “Theory and design of pressure vessels”, Van Nostrand Reinhold Company Inc., ISB No. 0-442-23248-9.

Hearn, E. J. (1999), “Mechanics of materials 2”, Butterworth-Heinemann, Great Britain, ISBN 0-7506 3266-6, Third edition.

Heywood, R. B. (1952), “Designing by photoelasticity, *Chapman & Hall Ltd.*, London, 296-298.

Hyder, J. M. and Asif, M. (2008), “Optimization of location and size of opening in a pressure vessel cylinder using ANSYS”, *Engineering failure analysis*, Vol.15, pp. 1-19.

Jeyakumar, M. and Christopher, T. (2013), “Influence of residual stresses on failure pressure of cylindrical pressure vessels”, *Chinese journal of aeronautics*, Vol. 26, No. 6. pp. 1415-1421.

Kandil, A., El-kady, A. A. and El-kafrawy, A. (1994), “Transient thermal stress analysis of thick-walled cylinders”, *International journal of mechanical science*, Vol. 37, pp. 721-732.

Kharat, A. and Kulkarni, V. (2013), “Stress concentration at openings in pressure vessels- A review”, *International journal of innovative in science, engineering and technology,* Vol. 2, Issue 3.

Kihiu, J. M. (2002), “Numerical stress characterization in cross bored thick walled cylinders under internal pressure”, *The University of Nairobi*, PhD thesis.

Kihiu, J. M. and Masu, L. M. (1995), “The effect of chamfer and size on the stress distributions in thick-walled cylinder with a cross bore under internal pressure*”, R & D,* pp. 73-78.

Kihiu, J. M. (2007), “Universal SCF and optimal chamfering in cross-bored cylinders”, *International journal of pressure vessels and piping*, Vol. 84, pp.396-404.

Kihiu, J. M., Rading, G. O. and Mutuli, S. M. (2003), “Geometric constants in plain cross bore cylinders*”, International journal of pressure vessels and piping*, Vol. 125, pp.446-453.

.

Kihiu, J. M., Rading, G. O. and Mutuli, S. M. (2004), “Overstraining of flush plain cross-bored cylinders*”, Proc. Instn Mech. Engrs*, Vol. 218, Part C.

Li, H., Johnston, R. and Mackenzie, D. (2010), “Effect of autofrettage in thick-walled cylinder with a radial cross-bore”, *Journal of pressure vessel technology*, No. 132 (1). 011205.

Lind, N. C. (1967), Approximate stress concentration analysis for pressurize branch pipe connections*, ASME,PVP* -7.

Little, R. E. and Bagci, C. (1965), "Stress analyses of pressurized cylinders", Engineering research bulletin, publication No. 145, Oklahoma state university.

Mackerle, J. (1996), "Finite elements in the analysis of pressure vessels and piping - a bibliography (1976 -1996)", *International journal of pressure vessels and piping*, No. 69, pp. 279 – 339.

Mackerle, J. (1999), "Finite elements in the analysis of pressure vessels and piping, an addendum (1996 - 1998)", *International journal of pressure vessels and piping*, No. 76, pp. 461- 485.

Mackerle, J. (2002), "Finite elements in the analysis of pressure vessels and piping, an addendum: A bibliography (1998 -2001)", *International journal of pressure vessels and piping*, No. 79, pp. 1-26.

Mackerle, J. (2005), "Finite elements in the analysis of pressure vessels and piping, an addendum: A bibliography (2001 -2004)", *International journal of pressure vessels and piping*, No. 79, pp. 1-26.

Makulsawatudom, P., Mackenzie, D., and Hamilton, R. (2004), "Stress concentration at crossholes in thick cylindrical vessels", *The journal of strain analysis of engineering design*, Vol. 39, pp. 471-481.

Marie, S. (2004), “Analytical expression of thermal stresses in a vessel or pipe with cladding submitted to any thermal transient”, *International journal of pressure vessels and piping,* No. 81, pp. 303-312.

Masu, L. M. (1989), “The effect of cross bore geometry on the strength of pressure vessels”, *PhD thesis, University of leeds*.

Masu, L.M. (1991), "Cross bore geometry effects on the strength of pressure vessels", Proceedings of the international conference on mechanics of solids and structures, Nayang Technological University, Singapore, 11-13th, September, pp. 261-272.

Masu, L. M. (1994), “Stress and fatigue behavior model for a pressure vessel containing a cross bore”, *East African journal of engineering*, Vol. 1, No. 2.

Masu, L. M. (1997), “Cross bore configuration and size effects on the stress distribution in thick-walled cylinders”, *International journal of pressure vessels and piping*, No. 72, pp. 171-176.

Masu, L. M. (1998), “Numerical analysis of cylinders containing circular offset cross bores”, *International journal of pressure vessels and piping,* No. 75, pp. 191-196.

Masu, L. M. and Craggs, G. (1992), "Fatigue strength of thick-walled cylinders containing cross bores with blending features", *Proc. Instn Mech Engrs*, Vol. 206, pp. 299-309.

Moffat, D. G., Mistry, J. and Moore, S. E. (1999). Effective stress factor correlation equations for piping branch junctions under internal pressure loading, *Journal of pressure vessel technology*, No. 121, pp. 121 -6.

Moffat, D. G., Mwenifumbo J. A. M, Xu, S. H., Mistry J. (1991). Effective stress factors for piping branch junctions due to internal pressure and external moments loads, *journal of strain analysis*, No. 26, pp. 84-101.

Money, H. A. (1968). Designing flush cylinder to cylinder intersections to withstand pressure, *ASME PVP* – 17.

Nabhani, F., Ladokun, T. and Askari, V. (2012), "Reduction of stresses in cylindrical pressure vessels using Finite Element Analysis", Finite Element Analysis - Biomedical Applications to Industrial Developments, Dr. David Moratal (Ed.), ISBN: 978-953-51-0474-2.

Nagpal, S., Jain, N. and Sanyal, S. (2012), "Stress concentration and its mitigation techniques in flat plate with singularities- A critical review", *Engineering journal*, Vol. 16, issue 1.

Nayebi, A. and Sadrabadi, S. A. (2013), "FGM elastoplastic analysis under thermomechanical loading", *International journal of pressure vessels and piping*, No. 111-112, pp. 12-20.

Nihous, G. C., Kinoshita, C. K. and Masutani, S. M. (2008),"Stress concentration factors for oblique holes in pressurized thick walled cylinders", *Journal of pressure vessel technology*, Vol.130/021202-1. DOI: 10.1115/1.2891915.

O'hara, G. P. (1968), "Experimental investigation of stress concentration factors of holes in thick walled cylinders", watervliet arsenal technical report WVT-6807.

Okrajni, J. and Twardawa M. (2014), "Description of the thermo-mechanical fatigue of thick-walled pressure vessels", *Procedia materials science,* No. 3, pp. 918-923.

Peters, D. T. (2003), "Effect of blend radius on stress concentration factor of crossbored holes in thick walled pressure vessels", *Conference proceeding on high pressure technology for the future,* Cleveland, Ohio, USA, July 20-24, pp. 53-57.

Peterson, R. E. (1953),"Stress concentration design factors", Wiley, New York.

Radu, V., Taylor, N. and Paffumi, E (2008), "Development of new analytical solutions for elastic thermal stress components in a hollow cylinder under sinusoidal transient thermal loading" *International journal of pressure vessels and piping*, No. 85, pp. 885-893.

Qadir, M. and Redekop, D. (2009), "SCF analysis of a pressurised vessel-nozzle intersection with wall thinning damage", *International journal of pressure vessels and piping*, Vol. 86, pp. 541-549.

Sanyal, S and Yadav, P. (2005), "Relief holes for stress mitigation in infinite thin plate with single circular hole loaded axially*", ASME international mechanical engineering congress and exposition*.

Segall, A. E. (2003), "Transient analysis of thick-walled piping under polynomial thermal loading", *Nuclear engineering and design*, No. 226, pp. 183-191.

Spyrakos, C. C. (1996), "Finite element modelling in engineering practice", Algor inc, USA, ISBN 0-9652806-0-8.

Snowberger, D. (2008), "Stress concentration factor convergence comparison study of a flat plate under elastic loading conditions", Rensselaer Polytechnic Institute Hartford, Connecticut.

Steele, C. R., Steele, M. L and Khathlan, A. (1986), "An efficient computational approach for a large opening in a cylindrical vessel", *journal of pressure vessel technology*, No. 108, pp.436-442.

Tan, C. L. and Fenner, R. T. (1980), “Boundary integral equation stress analysis of some problems in high pressure engineering, Proceeding 2nd international symposium on innovative numerical analysis in applied engineering sciences, Charlottesville, Virginia, University press of Virginia, pp787.

Timoshenko, S. (1940), “Strength of materials part II: Advanced theory and problem.”, Second edition, ninth printing, D. Van Nostrand Company, Inc.

Timoshenko, S. and Goodier, J. N. (1951), “Theory of elasticity”, Mcgraw-Hill, book Company, INC.

Xie, D. and Lu, L. (1985), “Prediction of stress concentration factors for cylindrical pressure vessels with nozzles”, *International journal of pressure vessels and piping,* No. 21, pp. 1-20.

Zhang, Q., Wang, Z. W., Tang, C. Y., Hu, D. P., Liu, P. Q. and Xia, L. Z. (2012), “Analytical solution of the thermo-mechanical stresses in a multilayered composite pressure vessel considering the influence of the closed ends”, *International journal of pressure vessels and piping,* No. 98, pp. 102-110.